Modeling and theoretical study of combustion of solid fuel over an inert porous medium

(多孔質体に付着した固体燃料の燃焼伝播に関する理論的研究)

Nepal Chandra Roy

Modeling and theoretical study of combustion of solid fuel over an inert porous medium

(多孔質体に付着した固体燃料の燃焼伝播に関する理論的研究)

By

Nepal Chandra Roy

A dissertation submitted to the Department of Mechanical and Space Engineering, Hokkaido University, Japan, in partial fulfilment of the requirements for the Degree of Doctor of Philosophy in Mechanical and Space Engineering

March 2014

Abstract

The efficient combustion of solid particulate matters (PMs) that are trapped in the porous channel walls of a diesel particulate filter (DPF) is recognized as the major technological challenge of the DPF regeneration process. Due to unknown aspects of the combustion of solid matters in the DPF, uncontrolled combustion occurs during the DPF regeneration process. Consequently, the DPF may encounter a loss of its mechanical integrity and sometimes uncontrolled regeneration process causes significant structural damage of the DPF, and therefore it fails to trap particulate matters efficiently from the exhaust gas. Thus the regeneration process poses a major technological challenge even to the state-of-the-art DPF. To tackle this challenge and for better understanding of the process, the role of mathematical model is widely recognized. But the modeling approaches used to date for understanding the regeneration process could not be able to serve the growing demand for engineering modeling tools to assist the diesel particulate filter and thereby for the development of system optimization because of the complexity of the models itself, lack of relevant mechanisms, many input data that are not usually available, computational cost, model consistency and reliability. For these reasons, this research has been motivated to develop a universal model as well as to provide analytical expressions of the combustion characters of solid fuel deposited over an inert porous medium.

Chapter 1 contains a brief overview of research works on combustion of solid fuel in porous medium occurring in various processes e.g., diesel particulate filter regeneration process, smoldering combustion, self-propagating high-temperature synthesis and sintering process. The literature review gives a clear idea of developing a model and its theoretical solution. At the end of this chapter, the objective and the structure of the thesis for achieving the target are presented through a flowchart.

In Chapter 2, a simple mathematical model has been proposed for the combustion of solid fuel over an inert porous medium. With a view to simplifying the model, only the thermal nonequilibrium between the porous medium and the gas, and a simple parameter “deposition of fuel” instead of fuel

mass fraction are introduced in the model. Large activation energy asymptotic is employed to obtain the analytical expressions of the temperature and species profiles as well as the moving speed of the reaction front. A numerical computation has also been performed to determine the sensitivity of the asymptotic analysis for variation of each of the physical parameters that provides a clear concept about the deviation of the asymptotic analysis from the numerical solution.

In Chapter 3, an advanced model is developed to examine the behavior of combustion wave observed in porous solid matters (e.g., smoldering, self-propagating high-temperature synthesis (SHS), DPF regeneration process). A detailed analysis of the opposed flow combustion of solid combustible (e.g., diesel particulate matters trapped in a DPF) deposited over an inert porous medium has been presented here. Analytical expressions of the combustion characters are obtained employing large activation energy asymptotic taking into account the sensible transport processes; namely, heat transfer between the porous medium and gas phases, radiation heat transfer from the porous medium, heat loss from the porous medium to the environment, mass transfer of oxygen from the gas stream to the surface of solid fuel and the effective diffusion in modeling the species diffusion. The applicability and adaptability of the model is then validated for predicting the characteristics of smoldering combustion and thus SHS process. In addition to, the governing equations are solved numerically and a comparison is made between the asymptotic analysis and the numerical solution.

It is well-known that one-dimensional propagation of a combustion wave is classified as forward and opposed. Both modes are jointly recognized not only in fire safety problems but also in technological applications. So a comparative study between the forward and opposed modes is the subject of Chapter 4. To accomplish this goal, firstly the analytical solutions of forward mode using the model developed in Chapter 3 have been derived and then a brief review of the solutions of opposed mode obtained in Chapter 3 is presented. The lines of demarcation of unsteady behaviors of the reaction fronts of forward and opposed modes are identified for a variety of conditions aiming at the control of fire safety and the development of new technology.

A practical application of forward and opposed modes is presented in Chapter 5. The problem has been constructed under the fact that a sample is ignited somewhere around the middle and after a short period of time, two reaction fronts separating from the ignition point propagate opposite to each other.

The effects of various physical parameters have not been fully uncovered yet and so it is discussed as ongoing research.

Finally, the concluding remarks of the thesis have been summarized in Chapter 6. In addition to, the direction of future works is also mentioned in this chapter.

Keywords: *Solid fuel, Porous medium, Diesel particulate filter, Smoldering, Heterogeneous combustion, Asymptotic Analysis, Moving speed of the reaction front, Unsteady behaviors, Ignite somewhere around the middle.*

Thesis Supervisor: Yuji NAKAMURA

Title: Associate Professor, Dr. Eng.

Acknowledgements

It is a matter of great pleasure to me to express my heartiest gratitude and profound respect to my supervisor, Professor Yuji Nakamura, Laboratory of Space Utilization, Division of Mechanical and Space Engineering, Hokkaido University, Japan for his valuable guidance, spontaneous encouragement, untiring efforts, keen interest and whole hearted supervision throughout the progress of my research without which this research would never have been materialized.

I would like to thank Professor Osamu Fujita, Laboratory of Space Utilization, Division of Mechanical and Space Engineering, Hokkaido University, Japan for his generous help and encouragement on my research, and for providing a congenial atmosphere, especially for the foreign students, in the lab seminar.

I would like to express my special thank to Professor Nobuyuki Oshima, Computational Fluid Mechanics Laboratory, Division of Mechanical and Space Engineering, Hokkaido University, Japan for his kind advice and comments on modeling the present problem and numerical calculation.

I would like to thank Professor Harunori Nagata, Laboratory of Space Systems, Division of Mechanical and Space Engineering, Hokkaido University, Japan for providing generous help and valuable comments on the improvement of the quality of the thesis.

I would like to thank Professor Longhua Hu, State Key Laboratory of Fire Science, University of Science and Technology of China for his kind help specially for making the structure of the thesis.

I wish to acknowledge my sincere gratitude to Dr. Akter Hossain for his well-thinking instructions and discussions about the research.

I would like to express my gratitude to the Ministry of Education, Culture, Sports, Science and Technology (MEXT), Japan for providing me with financial support as a Monbukagakusho scholarship. I would like to express my special thank once again to my supervisor Professor Yuji Nakamura for arranging this Japanese Government Scholarship.

Special thanks to my friends-Dr. Yangkyun Kim and Yan Hui for their encouragement, well wishes and technical and material supports in different stages of this research.

To my parents, Shanti Rani Roy and Bhupati Bhusion Roy

Table of Contents

Abstract i

Acknowledgements iv

Table of Contents vi

List of Figures x

List of Tables xiv

Nomenclature xv

1. Introduction and Background 1

1.1 Background and Motivation 1

1.2 Objective of the thesis 4

1.3 Literature review of combustion of solid fuel in porous medium 5

1.3.1 Modeling works of smoldering combustion 6

1.3.2 Modeling works of SHS process 9

1.3.3 Modeling works of DPF regeneration process 11

1.4 Feasibility of one-dimensional modeling of DPF regeneration process 13

1.5 Structure of the thesis 15

2. A Simple Model of Combustion of Solid Fuel over an Inert Porous Medium 17

2.1 Introduction 17

2.2 Mathematical formulation 19

2.2.1 Considerations and assumptions adopted in the model 19

2.2.2 Governing equations 21

2.2.3 Dimensionless form of governing equations 22
2.3 Asymptotic analysis 24
2.3.1 Outer solutions 24
2.3.2 Reaction-zone problem 26
2.4 Numerical method 28
2.5 Results and discussion 29
2.5.1 Validation of the asymptotic analysis 29
2.5.2 Sensitivity of the asymptotic analysis 32
2.5.3 Comparison and effects of parameters on the moving speed of the reaction front 34
2.6 Conclusions 37
3. An Upgraded Model of Combustion of Solid Fuel over an Inert Porous Medium **39**
3.1 Introduction 39
3.2 Mathematical formulation 41
3.2.1 Considerations and assumptions adopted in the model 41
3.2.2 Governing equations 43
3.2.3 Dimensionless form of governing equations 46
3.3 Asymptotic analysis 48
3.3.1 Outer solutions 48
3.3.2 Reaction zone 52
3.4 Numerical method 56
3.5 Results and discussion 58
3.5.1 Effect of radiation-conduction parameter 60
3.5.2 Effect of porosity 63
3.5.3 Effect of initial mass fraction of fuel 64
3.5.4 Effect of mass transfer coefficient 64

3.5.5 Effect of heat transfer coefficient 65

3.5.6 Effect of heat loss coefficient 66

3.5.7 Effect of Knudsen diffusion 67

3.5.8 Extinction limit diagram 68

3.5.9 Summary of the quantitative studies 69

3.6 Conclusions 70

4. Forward and Opposed Combustion of Solid Fuel over an Inert Porous Medium **72**

4.1 Introduction 72

4.2 Mathematical formulation 74

4.3 Forward mode 77

4.3.1 Asymptotic analysis 79

4.3.1.1 Combustion zone 79

4.3.1.2 Reaction zone 81

4.4 A brief of solutions of opposed mode 84

4.5 Results and discussion 84

4.6 Conclusions 91

5. Combustion of Solid Fuel over an Inert Porous Medium Ignited around the Middle **92**

5.1 Introduction 92

5.2 Mathematical formulation 94

5.3 Asymptotic analysis 96

5.3.1 Opposed mode 96

5.3.1.1 Outer solutions 99

5.3.1.2 Reaction zone 102

5.3.2 Forward mode 106

5.3.2.1 Combustion zone 106

5.3.2.2 Reaction zone 108

5.4 Results and discussion 114

5.5 Conclusions 118

6. Concluding Remarks and Future Works **119**

6.1 Concluding remarks 119

6.2 Future works 121

References **123**

Appendix **134**

Achievements

List of Figures

Figure 1.1	Geometric configuration of available particulate matter traps and the flow patterns [2].	2
Figure 1.2	Thermal image of PM regeneration by uniform combustion. Black arrow is direction of flow [4].	3
Figure 1.3	Example of massive melting on the downstream face of a DPF [4].	4
Figure 1.4	Snapshot showing the two regimes of combustion for solid fuels; flaming of the grass and smouldering of the organic soil (for scale reference, the flame is about 10 mm in height) [11].	7
Figure 1.5	A sequence of the advance of a combustion wave in the SHS process for Ti–C system; stoichiometric mixture without dilution; diameter is 18 mm and length is about 50 mm; the initial temperature is 300 K and radius of the carbon particle is 5 mm; the maximum temperature is about 3200 K and the burning velocity is 17 mm/s. (a) Just after the ignition; (b) 1 s; (c) 2 s; and (d) 3 s [23].	10
Figure 1.6	Schematic diagram of a fibrous particulate filter.	14
Figure 1.7	Flowchart of developing a model of the combustion of solid fuel over an inert porous medium.	16
Figure 2.1	Physical configuration of the model.	20
Figure 2.2	Schematic of initiation of a combustion reaction when $\tau = 0$ (opposed flow).	29
Figure 2.3	(a) Temperature and (b) species profiles in dimensional variables while $\lambda_m = 0.05$ W/(mK), $\varepsilon = 0.60$, $\phi = 0.70$ and $u_g = 0.30$ m/s.	31
Figure 2.4	Comparison of the moving speed of the burning front with the variation of u_g.	32

Figure 2.5	Absolute error between the solutions $((u_s)_{Asy} - (u_s)_{Num})$ as a function of λ_m while $\varepsilon = 0.60$, $\phi = 0.40$ and $u_g = 0.20$ m/s and $u_g = 0.30$ m/s.	33
Figure 2.6	Moving speed of the burning front as a function of λ_m while $\varepsilon = 0.60$, $\phi = 0.40$ and $u_g = 0.20$ m/s and 0.40 m/s.	34
Figure 2.7	Moving speed of the burning front as a function of ε while $\lambda_m = 0.40$ W/(mK), $\phi = 0.65$ and $u_g = 0.40$ m/s.	35
Figure 2.8	Moving speed of the burning front as a function of ϕ while $\lambda_m = 0.40$ W/(mK), $\varepsilon = 0.60$ and $u_g = 0.40$ m/s.	36
Figure 2.9	Moving speed of the burning front and amount of thermal nonequilibrium between the phases (dash-dot line) as a function of h while $\lambda_m = 0.40$ W/(mK), $\varepsilon = 0.60$, $\phi = 0.65$ and $u_g = 0.40$ m/s.	37
Figure 3.1	Physical configuration of the model.	42
Figure 3.2	Schematic of initiation of a combustion reaction when $\tau = 0$ (opposed flow).	57
Figure 3.3	Comparison between the numerical and asymptotic solution.	58
Figure 3.4	Variation of the moving speed of the reaction front with the gas flow velocity. Experimental data are taken from Torero et al. [112] and numerical data are from Ohlemiller et al. [12].	59
Figure 3.5	(a) Moving speed of the reaction front and (b) the amount of fuel leakage, f_0^*, through the reaction front as a function of N_R while $\lambda_m = 0.40$ W/(mK), $\varepsilon = 0.80$, $Y_{F,u} = 0.30$, $h_{ex} = 10^4$ W/(m^{3}K).	61
Figure 3.6	Temperature and species profiles in dimensional variables for $\lambda_m = 0.4$ W/(mK), $\varepsilon = 0.8$, $Y_{F,u} = 0.3$, $u_g = 0.5$ m/s, $h_{ex} = 3 \times 10^4$ W/(m^{3}K) when $N_R = 0.0$ (without radiation) and $N_R = 0.005$ (with radiation).	62
Figure 3.7	(a) Moving speed of the reaction front and (b) the amount of fuel leakage, f_0^*, through the reaction front as a function of ε while $\lambda_m =$	63

0.40 W/(mK), $N_R = 0.01$, $Y_{F,u} = 0.30$, $h_{ex} = 10^4$ W/(m^{3}K).

Figure 3.8 Moving speed of the reaction front as a function of $Y_{F,u}$ for $\lambda_m = 0.40$ W/(mK), $\varepsilon = 0.80$, $u_g = 0.60$ m/s, $Y_{O,u} = 0.154$ m/s, $h_{ex} = 10^4$ W/(m^{3}K) and $N_R = 0.01$. 64

Figure 3.9 Moving speed of the reaction front and the amount of fuel leakage, f_0^*, through the reaction front as a function of h_m for $\lambda_m = 0.4$ W/(mK), $\varepsilon = 0.8$, $Y_{F,u} = 0.3$, $h_{ex} = 10^4$ W/(m^{3}K) and $N_R = 0.01$. 65

Figure 3.10 Moving speed of the reaction front as a function of volumetric heat transfer coefficient, h, for $\lambda_m = 0.4$ W/(mK), $\varepsilon = 0.8$, $Y_{F,u} = 0.3$, $u_g = 0.40$ m/s and $h_{ex} = 10^4$ W/(m^{3}K). 66

Figure 3.11 Moving speed of the reaction front as a function of heat loss coefficient, h_{ex}, for $\lambda_m = 0.4$ W/(mK), $\varepsilon = 0.8$, $Y_{F,u} = 0.3$ and $N_R = 0.01$. 67

Figure 3.12 Temperature and species profiles for the effect of including Knudsen diffusion with molecular diffusion for $\lambda_m = 0.4$ W/(mK), $\varepsilon = 0.8$, $Y_{F,u} = 0.3$, $u_g = 0.6$ m/s, $h_{ex} = 2\times10^4$ W/(m^{3}K) and $N_R = 0.005$ while D_{eff} with Knudsen and molecular diffusion and D with molecular diffusion only. 68

Figure 3.13 Extinction limit diagram as a function of radiation-conduction parameter and gas flow velocity for $\lambda_m = 0.4$ W/(mK), $\varepsilon = 0.8$ and $Y_{F,u} = 0.3$. 69

Figure 4.1 Physical configuration of the model. 74

Figure 4.2 Variation of the moving speed of the reaction front with the gas flow velocity. Experimental data are taken from Torero and Fernandez-Pello [123] and numerical data are from Leach et al. [18]. 85

Figure 4.3 Temperature profiles of forward and opposed modes while $h_{ex} = 10^4$ W/(m^{3}K), $N_R = 0.01$ and $u_g = 0.4$ m/s. 86

Figure 4.4	Moving speed of the reaction front as a function of thermal conductivity of the porous medium, λ_m, while $h_{ex} = 10^4$ W/(m^{3}K), u_g = 0.3 m/s and N_R = 0.01.	87
Figure 4.5	Moving speed of the reaction front as a function of initial oxygen mass fraction, $Y_{O,u}$, while $h_{ex} = 10^4$ W/(m^{3}K), u_g = 0.4 m/s and N_R = 0.01.	88
Figure 4.6	Moving speed of the reaction front as a function of volumetric heat transfer coefficient, h, for $h_{ex} = 10^4$ W/(m^{3}K) when (i) u_g = 0.30 m/s, N_R = 0.01 and (ii) u_g = 0.40 m/s, N_R = 0.02.	90
Figure 4.7	Moving speed of the reaction front as a function of gas flow velocity while $h_{ex} = 10^4$ W/(m^{3}K) and N_R = 0.01.	91
Figure 5.1	Physical configuration of ignition at the middle.	94
Figure 5.2	Temperature profiles of forward and opposed modes of Case 1 while $h_{ex} = 10^4$ W/(m^{3}K), N_R = 0.01 and u_g = 0.4 m/s.	115
Figure 5.3	Temperature profiles of forward and opposed modes of Case 2 while $h_{ex} = 10^4$ W/(m^{3}K), N_R = 0.01 and u_g = 0.4 m/s.	115
Figure 5.4	Species profiles of forward and opposed modes of Case 1 while $h_{ex} = 10^4$ W/(m^{3}K), N_R = 0.01 and u_g = 0.4 m/s.	116
Figure 5.5	Species profiles of forward and opposed modes of Case 2 while $h_{ex} = 10^4$ W/(m^{3}K), N_R = 0.01 and u_g = 0.4 m/s.	116
Figure 5.6	Moving speed of the reaction front of forward and opposed modes of Case 1 as a function of the heat transfer coefficient, h, for $h_{ex} = 10^4$ W/(m^{3}K), u_g = 0.40 m/s and N_R = 0.01.	117
Figure 5.7	Moving speed of the reaction front of opposed mode of Case 1 and Case 2 as a function of the heat transfer coefficient, h, for $h_{ex} = 10^4$ W/(m^{3}K), u_g = 0.40 m/s and N_R = 0.01.	117

List of Tables

Table 2. 1	Thermophysical properties used in the analysis and numerical computation	30
Table 3. 1	Thermophysical properties used in the analysis and numerical computation	57

Nomenclature

a	Rosseland extinction coefficient, 1/m
A	Frequency factor, m^3 /(kg s)
c_m	Specific heat of porous medium, J/(kg K)
c_g	Specific heat of gas, J/(kg K)
d	Pore diameter, m
D	Mass diffusivity, m^2/s
D_{eff}	Effective diffusivity, m^2/s
D_K	Knudsen diffusion coefficient, m^2/s
E	Activation energy, J/kg
h	Volumetric heat transfer coefficient, W/(m^3K)
h_{ex}	Heat loss coefficient from the porous medium to the environment, W/(m^3K)
h_m	Mass transfer coefficient from the gas stream to the surface of fuel, m/s
K	Heat transfer parameter
K_{ex}	Heat loss parameter
K_m	Mass transfer parameter
Le	Lewis number
n	Mass of oxygen per mass of fuel ratio
N_R	Radiation-conduction parameter
Nu	Interstitial Nusselt number
Pr	Prandtl number
q_r	Radiative heat flux, W/m^2
Q	Fuel mass based heat of reaction, J/kg
R	Universal gas constant, J/(kg K)
Re	Reynolds number

S	Dimensionless temperature of the porous medium
Sc	Schmidt number
Sh	Sherwood number
t	Time, s
T_{ad}	Adiabatic temperature, K
T_m	Temperature of the porous medium, K
T_g	Temperature of the gas, K
T_u	Unburned temperature, K
u_g	Gas flow velocity, m/s
u_s	Moving speed of the reaction front, m/s
V	Total volume of the porous medium, m^3
V_f	Volume of fuel, m^3
V_g	volume of gas, m^3
V_V	Volume of voids, m^3
W	Rate of the chemical reaction, kg/(m^3s)
X	Distance along the DPF, m
Y_F	Mass fraction of fuel
$Y_{F,u}$	Initial mass fraction of fuel
Y_O	Mass fraction of oxidizer
$Y_{O,u}$	Initial mass fraction of oxidizer

Greek symbols

α	Dimensionless heat of combustion
β	Zel'dovich number
γ	Dimensionless heat release
δ	Thermal excursion during the burning process
ε	Porosity of the porous medium

ζ	Dimensionless distance along the DPF
θ	Dimensionless gas temperature
λ_g	Thermal conductivity of the gas, W/(m K)
λ_m	Thermal conductivity of the porous medium, W/(m K)
v_g	Kinematic viscosity, m^2/s
ξ	Dimensionless distance along the DPF
ρ_f	Density of fuel, kg/m^3
ρ_g	Density of the gas, kg/m^3
ρ_m	Density of the porous medium, kg/m^3
σ	Stefan-Boltzmann constant, $J/(m^2 K^4 s)$
τ	Dimensionless time
ϕ	Deposition of fuel

Subscripts

ex	External
f	Fuel or Reaction front
g	Gas
m	Porous medium
u	Unburned or ambient

Superscripts

f	Forward
in	Inner solution
~	Dimensional
^	Dimensionless

Chapter 1

Introduction and Background

1.1 Background and motivation

A diesel engine is widely used in passenger cars, heavy-duty trucks and off-road vehicles throughout the world due to not only its higher efficiency but also its longer durability. The main drawback of diesel engines is that they emit about 10 times more particulate matter (PM) than gasoline engines. These emissions are probably carcinogenic to humans that pose serious threat to the public health and the known sources of hazardous environmental contamination [1]. As a result, the Environmental Protection Agency (EPA) imposes stricter emission control legislations for diesel engine to reduce its 90% PM emission. Due to these regulations, intensive efforts have been employed to develop a proper technology for the reduction of PM emission.

To reduce the PM emission from the diesel engines, there have been developed a variety of ceramic and sintered metal-based diesel particulate filters (DPFs). Geometric configurations of different types of filters are schematically illustrated in Figure 1.1. A wall-flow monolith DPF consists of many square parallel channels of which successive channels are blocked with cement at the opposite end. The exhaust gas enters into the open end of a channel. Since it is being plugged at opposite end, gas is forced to flow through the porous channel walls that allows the exhaust gas to escape through the neighboring channel. In this way, more than 95% of PM accumulates on the filter. As long as, accumulation of PM is continued to increase, the back-pressure across the filter also raises that therefore reduces engine performance. If the accumulating PMs are not removed, the engine will ultimately cease to function. The most commonly used way of removing PMs from the DPF is to oxidize the PMs through a process which is referred to as regeneration (see Figure 1.2). The regeneration process is initiated by changing the ongoing conditions to heat the DPF and igniting the PMs. However, the oxidation of PMs requires quite a high temperature generally more than 500 °C [3].

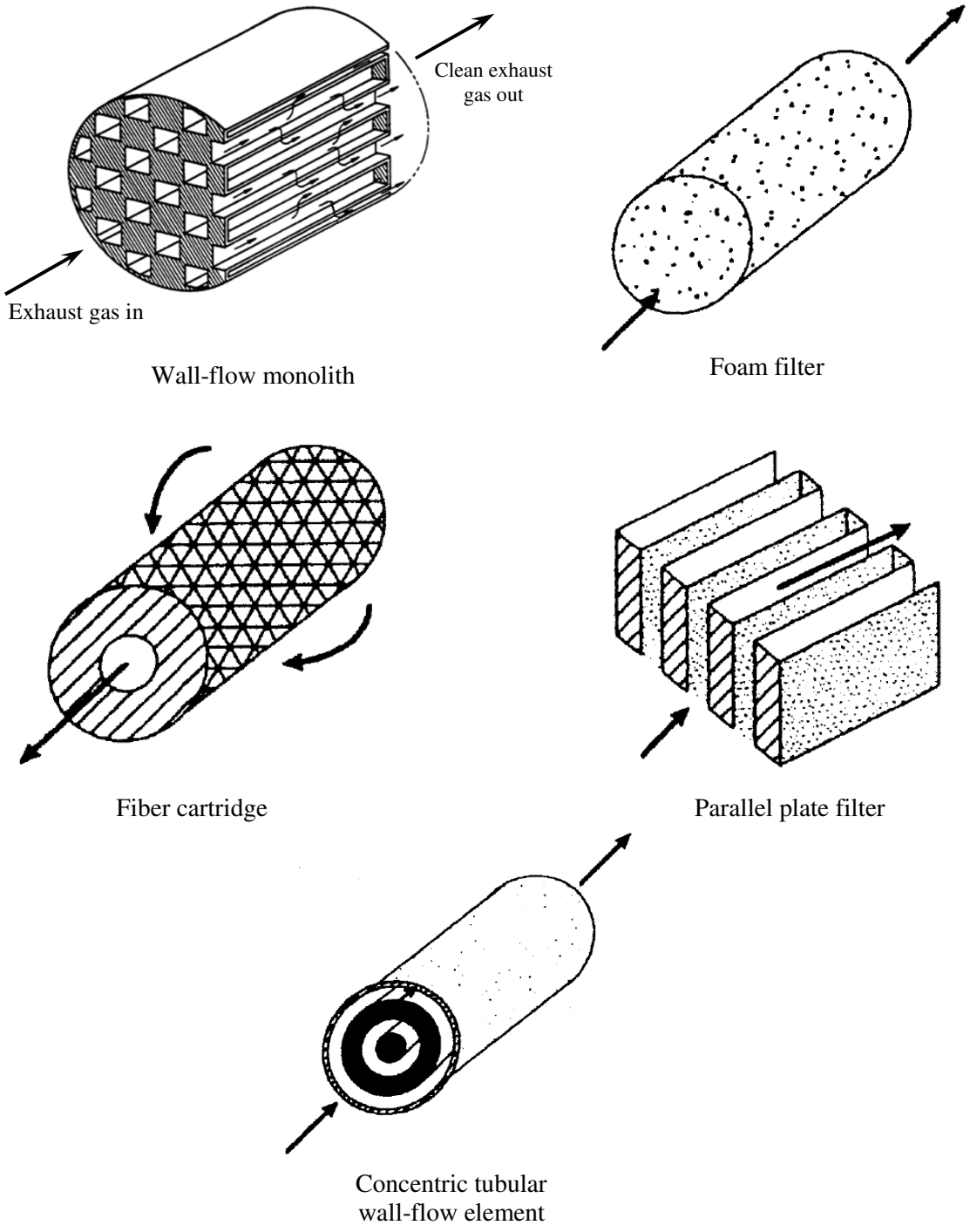

Figure 1.1: Geometric configuration of available particulate matter traps and the flow patterns [2].

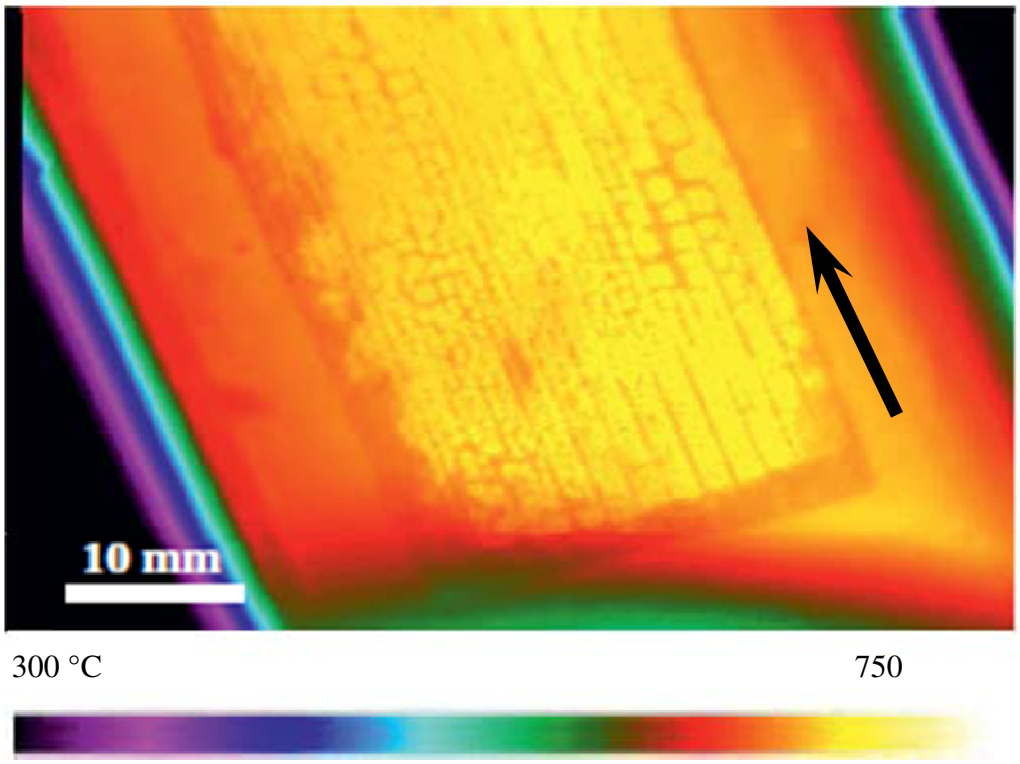

Figure 1.2: Thermal image of PM regeneration by uniform combustion. Black arrow is direction of flow [4].

The efficient combustion of the PMs trapped in the channel walls of a DPF is recognized as the most challenging aspects of the PM removal technology. It is due to the fact that a high temperature combustion wave is generated during the combustion of PMs, the temperature of which may exceed in some cases the melting temperature of the DPF material [5]. This causes a massive damage to the filter material. Consequently, it fails to trap efficiently the PMs from the exhaust gas and the replacement of the damaged DPF has to be made. Figure 1.3 exhibits the melting condition of a DPF during the regeneration process.

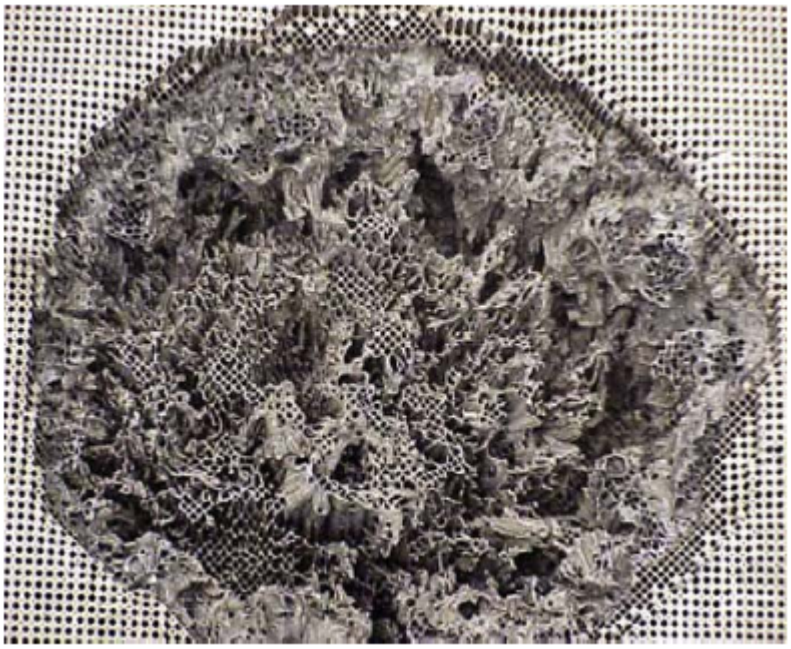

Figure 1.3: Example of massive melting on the downstream face of a DPF [4].

1.2 Objective of the thesis

To date, the main difficulty for the widespread applications of particulate traps is to control the DPF regeneration rate in an efficient way. Hence the design of regeneration control systems must be supported by reliable mathematical modeling of the DPF regeneration process. In addition to, the determination of proper size of a DPF and the general design optimization of PM trap systems is such a task that requires extensive modeling work [6]. Over last few decades, a significant number of works focused on modeling the DPF regeneration process. Since the problem is very complicated and significant difficulties exist in exploiting laboratory results in the estimation of kinetics parameters applicable to full-scale models [7, 8], from engineering point of view special modeling approaches have proven its effectiveness for the better understanding of the regeneration process and thereby for the development of system optimization.

Diesel particulate emissions standards are becoming stringent day by day. To meet those standards, the development of an efficient DPF is highly demanded. On the contrary, for the development of a reliable and durable trapping system, the role of mathematical model is widely recognized. Thus the objective of this work is to develop a mathematical model for the combustion of solid fuel over an

inert porous medium and to provide analytical expressions of the combustion characteristics of solid combustible deposited over the inert porous medium.

1.3 Literature review of combustion of solid fuel in porous medium

Over decades, combustion of solid fuel in porous medium has been the focus of research because of its ever-increasing applications along with new sorts of technological problems. In some of the applications, the porous medium actively takes part in the combustion as a fuel (e.g., smoldering combustion and high temperature material synthesis known as self-propagating high temperature synthesis (SHS)), while in some applications the porous medium might contain solid fuel (e.g., DPF regeneration process) or fuel could be generated in the porous medium just preceding the combustion zone (e.g., in situ combustion for the recovery of oil, coal gasification) and it acts as an inert in the combustion. These can be different in scale, in context and from technological point of view but in all processes combustion occurs in a stationary fuel. Moreover, when a sample is ignited at one end, a high-temperature combustion wave starts to propagate and under appropriate conditions, it moves through the sample using the heat released by the exothermic reaction and converting the reactants into desired products. Since the underlying mechanisms of these processes are believed to be identical, hence the same mathematical model could be applied to illustrate these applications [9, 10]. However, all of the processes of combustion of solid fuel in porous medium can be categorized into the following two groups:

(i) a process in which porous solid fuel that apparently acts as a unique solid matrix directly involves in the combustion; and

(ii) a process in which porous solid matrix containing solid fuel remains inert during the combustion but indirectly supports the combustion.

Due to these two different types of contributions of the porous medium, the models developed to date for one process cannot be used effectively in other processes and vice versa. As a result, any model of these processes cannot be used to examine the characteristics of combustion of solid combustible over an inert porous medium. Even, the models of corresponding processes are lack of their essential

transport mechanisms and thereby not complete and universal.

Below, a review of the most important studies of smoldering combustion, SHS and DPF regeneration process that are relevant to the objective of this thesis, has been carried out in order to identify the fundamental mechanisms of these processes. This is due to the fact that SHS and DPF regeneration are useful technological processes and the main demand in these processes is to control the propagation of the combustion wave without having any unsteady behavior. On the other hand, in spite of being unwanted to several scientific disciplines specially in fire safety problems, nowadays smoldering combustion is noticeably used for the development of new environmental and energy technologies [11]. So, in these particular interests the main target is to obtain the steady propagation of the combustion wave. Thus the background knowledge of these processes might be useful to develop a universal model of the combustion of solid fuel over an inert porous medium.

1.3.1 Modeling works of smoldering combustion

There are many solid fuels that can sustain smoldering combustion such as: coal, cotton, tobacco, dust, paper, peat, duff and hummus (see Figure 1.4), wood, board of organic fibres, synthetic foams and charring polymers including polyurethane foams [11]. Generally, these types of solid fuels consist of particulates, grains, fibres or a porous matrix. As a result, smoldering fuels are itself a porous medium that allow oxygen to penetrate into the reaction zone. These features bring about slow but continuous combustion of solid fuels. When the ignition at one end of a smoldering solid fuel initiates the propagation of a combustion wave, it moves to the other end of the fuel.

A lot of theoretical and numerical models have been developed with the aim of identifying the important mechanisms of the propagation of the reaction front of smoldering combustion. Ohlemiller et al. [12] presented a detailed numerical model of reverse smolder combustion to provide useful insights of the controlling phenomena of the process. Analytical models [13, 14] for forced cocurrent and opposed smoldering combustion, respectively, have been investigated in terms of the propagation velocity and flame temperature with the variation of physical parameters. They observed that extinction is occurred when all of the energy released in the reaction zone is used to heat the incoming gas. The above studies presumed the thermal and chemical equilibrium between the solid and gas

phases based on the assumption that the contact time between them is extremely high. On the contrary, when the residence time of contact between the moving gas and the solid becomes short for thermal equilibration; the assumption of local thermal equilibrium between the phases is inappropriate [15]. Leach et al. [16, 17] observed by the numerical simulation that the volumetric heat transfer coefficient, introduced to measure the intensity of the thermal nonequilibrium between the phases, demonstrates a significant impact on smolder velocity and even extinction is experienced owing to the high value of it. However, there is no theoretical works that could confirm this finding.

Figure 1.4: Snapshot showing the two regimes of combustion for solid fuels; flaming of the grass and smouldering of the organic soil (for scale reference, the flame is about 10 mm in height) [11].

Not only the heat transfer between solid and flowing gas, other heat transfer processes are also necessary to consider for better prediction of propagation and extinction features in the present system. In fact, smolder wave propagates supported by heat released from the exothermic reaction. This heat released in the reaction zone is transferred not only to the gas but also toward the un-reacted material

by conduction and radiation; and at the same time it is partially lost to the environment. Dosanjh et al. [13] and Leach et al. [17, 18] observed that the radiative heat transfer significantly affects the reaction front structure and it becomes strong when pore diameters are large. Moreover, Leach et al. [17, 18] solved their problems numerically taking only with and without radiation effect, regardless of changing the intensity of radiative heat transfer; while Dosanjh et al. [13] investigated just for two limiting values. Thus, for predicting the influence of radiation over a wide range of conditions, further study is required. Now, as mentioned above that heat is lost from the reaction zone to the surrounding environment. It has a large effect on the propagation of the reaction front and even it can cause extinction or quenching of the reaction front [11, 13]. Nevertheless, any of the studies of Leach et al. [16-18] did not take into account the heat loss to the surrounding environment. In this regard, Rein et al. [19] extended the model of Leach et al. [18] including the heat losses to the surrounding environment. In a recent study, Rein et al. [20] proposed a novel model for both forward and opposed smoldering combustion. But they eventually neglected the chemical nonequilibrium effect in this model. Similar to other works of smoldering combustion, the models developed by Rein et al. [19, 20] are only for the combustion of polyurethane foam. In addition to, their target was for better understanding of the controlling mechanisms of smolder combustion for the purpose of fire safety, yet they presented only the effect of inlet gas velocity over a range for microgravity. Furthermore, the models are solved numerically which is generally difficult to carry out for anybody to investigate the effects of other physical parameters. So, this demands further study with a model that includes the heat loss to the environment. As heat transfer from the solid to the gas is important when thermal nonequilibrium exists between the phases, mass transfer from the gas stream to the surface of fuel is also essential in case of chemical nonequilibrium between the phases. Although one should not straightforwardly take the chemical equilibrium between the phases without being certain of its validity [10], most of the theoretical studies published to date ignored the chemical nonequilibrium due to the complexity of the model or presuming the chemical equilibrium between the phases. The effect of the chemical nonequilibrium is considered in [16, 18-21] through the mass transfer coefficient. But it has not been investigated in any of these studies except Wang et al. [21]. They found that the smolder propagation velocity increases with the increase of the mass transfer coefficient.

It is noted that one feature that is generally ignored in traditional modeling approaches in modeling the species diffusion through the porous medium is the effective diffusivity. Regarding the importance of effective diffusivity in smoldering combustion, Ohlemiller [22] used the more conventional approach for the effective diffusivity due to the lack of evidence on the pore structure developed in smoldering and emphasized that a better description has to be used. It has been ignored taking the highly porous medium so that oxygen diffusion is independent of porosity. Thus, the scope of using an advanced definition of effective diffusivity remains untouched in the field of smoldering combustion.

The above literature review shows that the key transport mechanisms in smoldering combustion are the heat transfer from the solid to the gas, radiative heat transfer, heat loss to the environment, mass transfer from the bulk gas to the surface of fuel and effective diffusivity.

1.3.2 Modeling works of SHS process

As like as the smoldering combustion, the reaction front of SHS process also self-propagates through the virgin solid fuel from one end to other end in the form of a combustion wave (see Figure 1.5). With a view to identifying the essential mechanisms of SHS process, the modeling studies in the field of SHS process are concisely presented here. Particularly, SHS process was investigated theoretically as condensed phase combustion [24-26] or gasless combustion [27-29] in which solid-solid reaction is occurred. On the other hand, SHS process can occur even with solid-gas interactions [26, 30, 31]. A review of the method of SHS involving solid-solid and solid-gas reactions has been performed by Munir and Anselmi-Tumburini [31]. In almost all of SHS process, solid materials are lumped together and synthesized by igniting. However, when preparing nitrides, the reaction is commonly between a solid and nitrogen gas. In such case, continuous supply of gaseous nitrogen to the surface of metal by penetrating through the pores or diffusion through a product layer plays a major role in the overall combustion reaction. Munir and Holt [30] presented a theoretical analysis on nitride synthesis through solid-gas reactions and utilized the analysis results for predicting the combustion characters of nitrides.

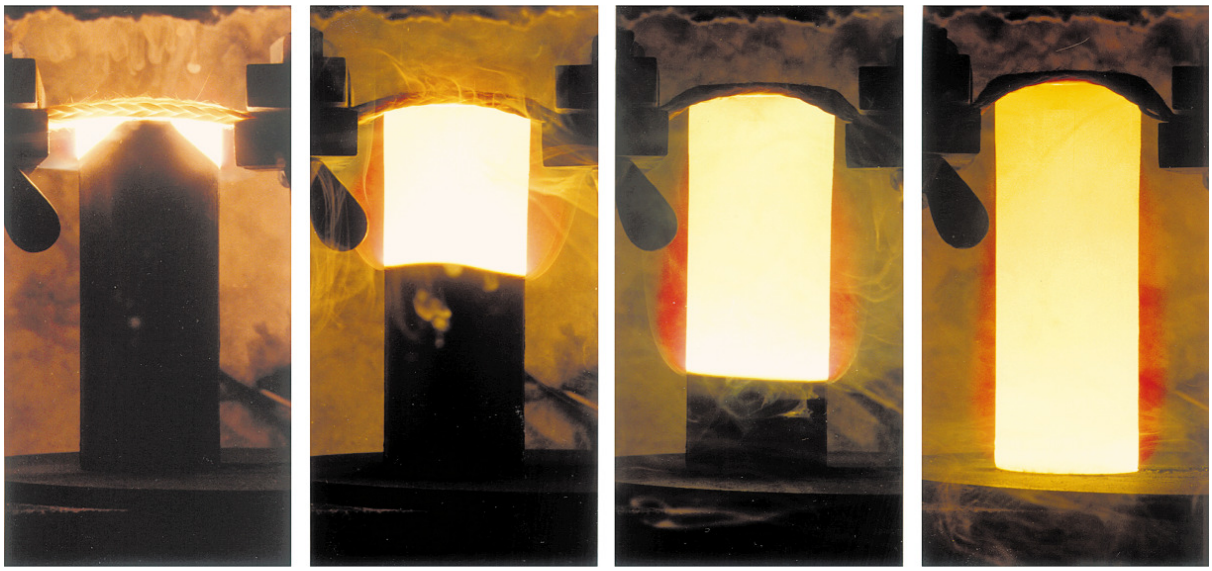

(a) (b) (c) (d)

Figure 1.5: A sequence of the advance of a combustion wave in the SHS process for Ti–C system; stoichiometric mixture without dilution; diameter is 18 mm and length is about 50 mm; the initial temperature is 300 K and radius of the carbon particle is 5 mm; the maximum temperature is about 3200 K and the burning velocity is 17 mm/s. (a) Just after the ignition; (b) 1 s; (c) 2 s; and (d) 3 s [23].

To investigate the combustion behavior in the SHS process, there have been numerous modeling studies formulated by considering only ambient heat loss [25, 28, 32, 33] and both radiative and ambient heat loss [23, 34, 35]. Makino and Law [36] developed a one-dimensional and adiabatic model to examine the heterogeneous reaction front propagation in the SHS process, based on a premixed mode of propagation for the bulk reaction front supported by the nonpremixed reaction of dispersed nonmetal particles in the liquid metal. Later, they have extended this work allowing the heat loss to the ambient environment to analyze the nonadiabatic heterogeneous reaction front propagation and extinction behavior in SHS [32, 33]. They found that the reaction front propagation decreases with increasing heat loss and the reaction front extinguishes at a critical heat loss rate. Furthermore, Makino [23] conducted an extensive review to expose the fundamental aspects of the heterogeneous reaction front in the SHS process. He focused on the theoretical description of the heterogeneous features of the combustion wave and concluded that these have not been captured by the conventional premixed-flame theory for a homogeneous medium. Since combustion wave possesses micro-heterogeneous

characteristics that results in thermal heterogeneity, hence some studies [37-39] considered the heat transfer between two reactants and heat transfer coefficient is used to define a decisive parameter for the combustion wave propagation. On the other hand, it has been realized that there are no comprehensive mathematical models to date that can describe the complex mechanisms of heat and mass transfer occurring at the scale of reactant particles [37]. In this regard, mass transfer could play a vital role in the SHS process [37, 39]. But they did not take any attempt to include the mass transfer mechanism into their model.

In summary, it can be concluded that the important transport mechanisms in SHS process are radiative heat transfer, heat loss to the environment, heat transfer from a reactant to its neighboring reactant and mass transfer between the reactant particles. Also, the further modeling of SHS process incorporating all of the above transport mechanisms is needed to describe the complex mechanisms of heat and mass transfer occurring in the process.

1.3.3 Modeling works of DPF regeneration process

Under the framework of finding the important mechanisms of smoldering, DPF regeneration process and SHS, a survey has been conducted on the modeling works of DPF regeneration process. Mathematical modeling is commonly used for the better understanding of the DPF regeneration process and thereby for the development of system optimization. A detailed mathematical formulation of the regeneration process of PM layer was first described by Bissett and Shadman [40]. This was a zero-dimensional model dealing with PM combustion in one point of a filter channel which was then extended to one-dimensional accounting for the axial heat conduction, and the PM layer and flow distribution along the channel [41]. In addition to, Bissett [42] made an attempt to describe the process in a somewhat general setting with an aim to provide the interesting physical and mathematical features of the process. All of these models have been developed presuming only the thermal nonequilibrium between the solid and the exhaust gas temperature. The chemical nonequilibrium and heat loss from the solid phase are neglected. But in recent years chemical nonequilibrium between the solid and gas phases [43-45] and both the thermal and chemical nonequilibrium between them [46-49] are taken into account in the models. The effect of heat transfer coefficient related to the thermal

nonequilibrium has been investigated by Flytzani-Stephanopoulos et al. [50]. They observed that the large value of heat transfer coefficient reduces the heat conduction through the solid resulting in lower DPF temperature. During the regeneration process the DPF temperature becomes high, so the radiative heat transfer could have significant effect. Haralampous and Koltsakis [51] and Dardiotis et al. [46] developed models incorporating the radiative heat transfer along with the thermal and chemical nonequilibrium. Koltsakis and Stamatelos [52] formulated a model considering only the thermal and chemical nonequilibrium between the phases while Depcik and Assanis [49] presented a variety of models including not only the thermal and chemical nonequilibrium but also the radiative and external heat losses from the solid. But they did not examine the effect of these transport mechanisms except external heat loss. Kostoglou et al. [53] employed a computational tool to solve a simple one-dimensional model of DPF regeneration process including the heat losses from the DPF to the environment by radiation, natural and forced convection. They found that the heat losses are detrimental to the effectiveness of the regeneration process. To account for the effect of species diffusion within the DPF, the regeneration process is now investigated by a coupled reaction-diffusion model [43, 46, 51] in which effective diffusion is incorporated into the traditional one-dimensional models. It is because the traditional models fail to predict the maximum temperatures during uncontrolled regeneration with moderate to high particle deposition in the DPF. Haralampous and Koltsakis [43] numerically observed that the consequences of various physical parameters are very sensitive to the effective diffusivities of the species. Also, diffusion of oxygen plays a crucial role in uncontrolled regeneration conditions that are significant for filter thermal failure [51]. To this end, a conclusion can be drawn that the key transport mechanisms for DPF regeneration process are recognized as that of the smoldering combustion. Nevertheless, no study is found in the field of DPF regeneration process that has included all of these transport mechanisms into a model. Even though many studies considered the chemical nonequilibrium into their models, but none of them examined the effect of this mechanism.

From the above literature review of smoldering combustion, SHS and DPF regeneration process, it can be concluded that a model corresponding to any of the processes must include all of the transport mechanisms which are indispensable to the process. To develop a universal model applicable for all of

the processes, one must take into account the primary elements directly involved in the processes. For example, it is easily understood that inert porous medium, solid fuel and oxygen are the primary elements for DPF regeneration; while, in case of SHS and smoldering, it is difficult to identify a priori that what types of primary elements are to be involved there. They can be either porous solid fuel as well as oxygen, or similar to the DPF regeneration. During the propagation of the reaction front of SHS and smoldering, there is also a possibility to encounter the similar type of characteristic as seen in DPF regeneration. That is, the solid product may act as an inert porous medium when there exits solid fuel and gas as primary elements. For these reasons, the models to date in the field of smoldering cannot be used efficiently in other processes and vice versa. Thus, a universal model applicable for all of these processes is highly admired owing to gain a deep knowledge about the problems of the corresponding processes.

1.4 Feasibility of one-dimensional modeling of DPF regeneration process

Over decades, mathematical modeling of regeneration process is being used as a predictive tool in determining a promising technique for the efficient combustion of diesel particulate matters and for the development of a reliable and durable trapping system. Depending upon the geometric and flow configurations of diesel particulate filters, mathematical models are different or necessary modifications are made of a previously-developed model during the model formulation.

To study the regeneration process of a wall-flow monolith filter, a zero-dimensional mathematical model of the regeneration process of the soot layer was developed by Bissett and Shadman [40]. This model was later extended to one-dimensional accounting for the axial heat conduction and the soot layer and flow distribution along the channel [41]. Koltsakis and Stamatelos [54] considered the zero-dimensional model as a starting point and formulated a new model capable of representing real-world trap regeneration behavior. It was then extended to zero-dimensional [6] and one-dimensional [55] catalytic regeneration models.

Oh and Cavendish [56] developed a transient, one-dimensional model to study the transient behavior of automobile monolithic converters. The radial variations of the gas-phase temperature,

concentration, and velocity within the individual channels are assumed to be negligible so that these variables can be interpreted as cross-sectional averages. Moreover, the model was formulated considering the negligible temperature gradients in the solid phase in the transverse direction, the negligible axial diffusion of mass and heat in the gas phase, and the occurrence of chemical reactions only on the external surface of the catalytic wall. However the axial heat conduction in the solid phase was included in the model owing to its significant effect on the wall temperature profile. Later, Oh et al. [57] extended this model for describing the thermal response and conversion performance of an electrically heated monolith converter during warm-up. The model presumed a uniform flow distribution at the monolith face and adiabatic operation of the converter. These assumptions confirm that all the channels would behave the same and hence the channel-to-channel variations or interactions can be ignored in the calculations (i.e., single-passage one-dimensional monolith model).

Shadman and Bissett [58] considered a cylindrical casing as a fibrous diesel particulate filter (see Figure 1.6). The axial dispersion in the gas phase was neglected owing to the large convective flow rate along the filter. In addition to, the radial variations in temperature and concentration are ignored and average values over a cross section are used to model axial variations. The overall reaction mechanism involved in the burning of diesel particulates was assumed to be represented by the heterogeneous non-catalytic oxidation of carbon to CO_2.

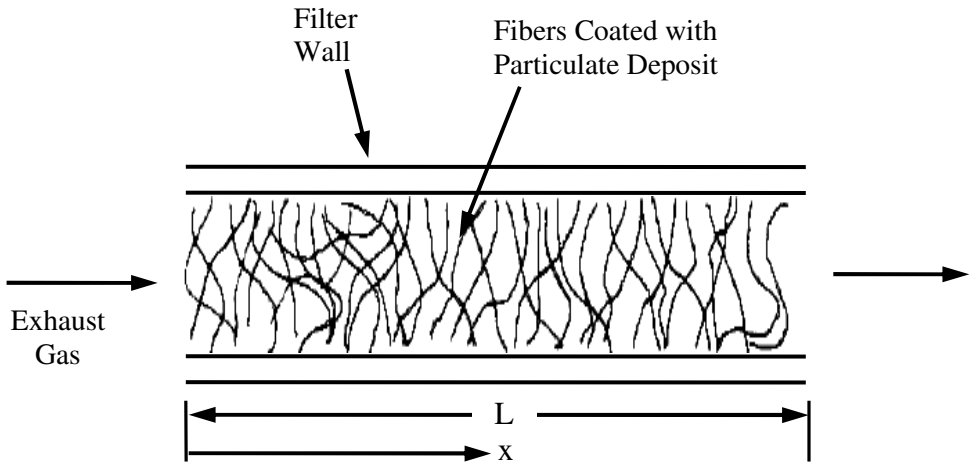

Figure 1.6: Schematic diagram of a fibrous particulate filter.

Even though the DPF regeneration process is, in fact, three-dimensional, this can be accurately considered as (perimeter averaged) one-dimensional. Konstandopoulos et al. [59] carried out a three-dimensional calculation using a state-of-the-art Computational Fluid Dynamics (CFD) code and observed that the analytical solutions of a one-dimensional single channel flow model demonstrate an excellent agreement with the three-dimensional results as well as with many experiments [52]. On the other hand, it has been widely accepted that catalytic regeneration can be modeled as one-dimensional configuration during the high flow-rate regeneration [60]. Depcik and Assanis [48] reviewed the history of one-dimensional catalyst modeling to illustrate the physical phenomena that take place in the catalyst. Even they showed that the one-dimensional models with simplified representation of the fluid flow through the device have been used effectively in designing catalyst systems that met the emission standards to date.

Thus the combustion of diesel particulate matters trapped within a DPF can be modeled as one-dimensional configuration under some assumptions. With a view to formulating a one-dimensional model, the following assumptions are made throughout the thesis:

(i) the flow distribution at the face of the diesel particulate filter is uniform;

(ii) the radial variations of the gas-phase and solid-phase temperatures, concentrations of gas and solid particulate matters, and velocity within the individual channels are assumed to be negligible so that these variables can be interpreted as cross-sectional averages; and

(iii) the temperature gradients in the solid-phase in the transverse direction are negligible.

1.5 Structure of the thesis

Figure 1.7 shows the step-by-step attempts aiming at achieving the objective of this study. At first, a simple model has been proposed considering only the thermal nonequilibrium between the solid and gas phases that successfully conserves the fundamental physics of the combustion of solid fuel over an inert porous medium. A simple parameter “deposition of fuel” is introduced instead of fuel mass fraction to simplify the model. Then an advanced model has been developed by taking into account the important transport mechanisms that are identified in the above literature review; namely, the heat

transfer between the porous medium and gas phases, radiation heat transfer from the porous medium, heat loss from the porous medium to the environment, mass transfer of oxygen from the gas stream to the surface of solid fuel and the effective diffusion in modeling the species diffusion. Using this model, the opposed flow of the propagation of a combustion wave has been investigated first, then a comparative study between forward and opposed modes is presented. Finally, a practical application of forward and opposed modes has been elucidated in which a sample is ignited somewhere around the middle and after a short period of time, two reaction fronts separating from the ignition source propagate opposite to each other.

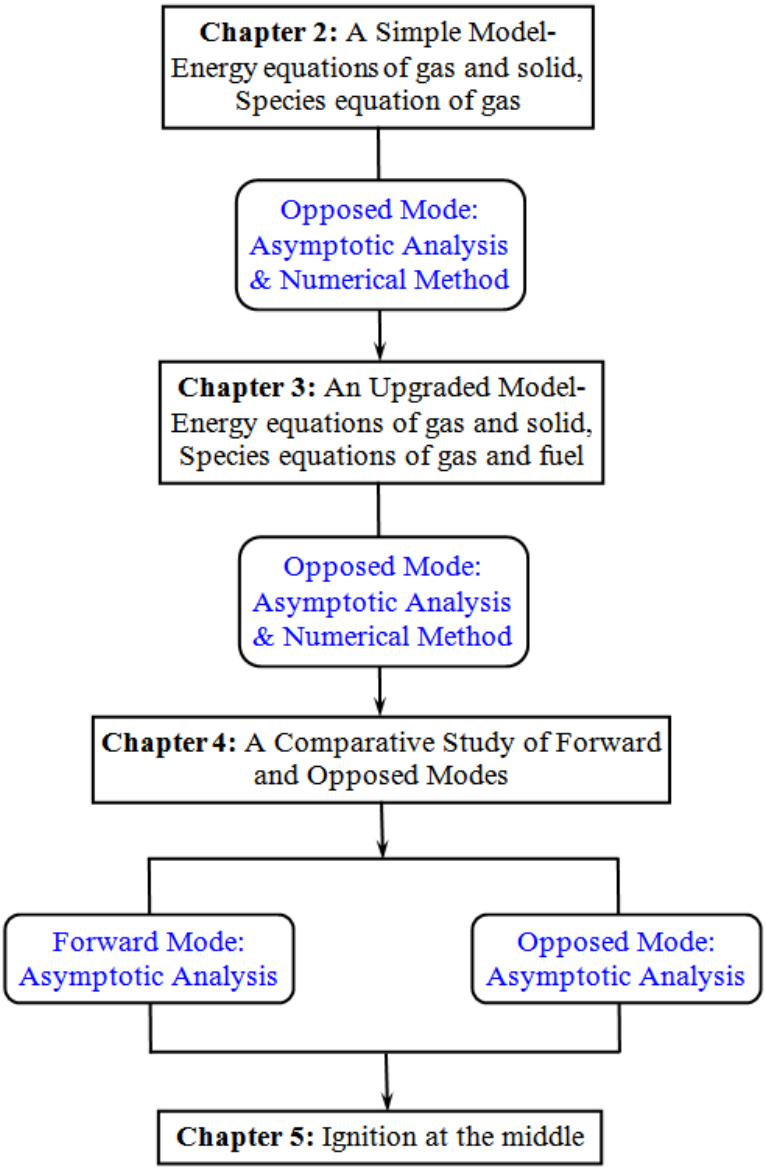

Figure 1.7: Flowchart of developing a model of the combustion of solid fuel over an inert porous medium.

Chapter 2

A Simple Model of Combustion of Solid Fuel over an Inert Porous Medium

2.1 Introduction

Combustion of solid fuel in porous medium is involved in a variety of processes because porous medium is used in some processes for its several significant advantages that facilitate the combustion to occur effectively, and some processes itself occur in a porous medium, for example, diesel particulate filter regeneration process [61], in situ combustion for the recovery of oil, coal gasification, catalytic combustion, high temperature material synthesis known as self-propagating high temperature synthesis (SHS), incineration of solid waste, biomass combustion, smoldering combustion and sintering process [62, 63]. These processes can be different depending upon the role of porous medium, in context or from technological point of view. Nevertheless, without any exception exothermic heterogeneous combustion that occurs with two (solid fuel and gaseous oxidizer) or more different phases, is the main chemical reaction mechanism of all these processes.

There are many studies on heterogeneous combustion in various aspects, on application as well as fundamental viewpoints [62-85]. Fatehi and Kaviany [62] carry out numerical simulation to examine the reverse combustion in a packed bed of wood particles including the local thermal nonequilibrium between the gas and solid phases. Debenest et al. [64-66] numerically investigate the forward smoldering process in fixed beds of solid fuels taking into account the thermal nonequilibrium between the phases, while the computational studies [67-73] deal with sintering process where coke is widely used as an ideal fuel. Venkataramana et al. [67] develop a one-dimensional two-temperature model of iron ore sintering and solve it using an explicit finite difference method. Even though Yang and his group [68-71] propose a one-dimensional model which includes various processes in the bed

of particles considering the thermal nonequilibrium between the solid fuel and gas, it requires a large number of input data and is solved numerically. Kasai et al. [72] and Hayashi et al. [73] develop two- and three-dimensional simulation models in order to simulate the heat transfer occurring in the sintering bed. Schult et al. [14, 74, 75] introduce a single temperature model of smoldering combustion and employ the asymptotic analysis assuming both the gas-deficient and solid-deficient for forward and opposed smoldering combustion. Rabinovich and Gurevich [76] examine the counter- and co-moving oxygen-deficient smoldering combustion considering the thermal equilibrium between the phases. Aldushin et al. [77] employ two-temperature model to analyze coflow filtration combustion waves and Wahle et al. [10] extend it including heat loss to the environment, energy accumulation, and net gas production in the reaction. The ignition, extinction and sustained moving of a combustion front are investigated for the recovery of oil from subsurface porous medium by Akkutlu and Yortsos [63]. Zheng and Keith [78] and Boshoff-Mostert and Viljoen [79] use asymptotic analysis for the regeneration of a diesel particulate filter considering single temperature of gas and solid. In fact, the above studies [10, 14, 74-79] employ analytical method to solve their problems presuming the heterogeneous combustion as homogeneous combustion and consider the same temperature of the phases or, use numerical computations to present their final results. On the other hand, numerous computational studies [41, 42, 80-85] have been published to understand the regeneration process of diesel particulate filters. Even though the models are sophisticated with many degrees of freedom but they require detailed input data such as exhaust gas velocity profiles or complex reaction kinetics. Pontikakis and Stamatelos [84] reported that with regard to the chemical reactions submodel and the basic assumptions, the majority of the models in use today could be considered as extension of [41, 42].

In this chapter, (i) a simple one-dimensional model for combustion of solid fuel over an inert porous medium has been proposed; (ii) two energy equations are considered with different density, thermal conductivity and specific heat capacity for the porous medium and gas; (iii) the thermal nonequilibrium between the porous medium and gas is included; (iv) to simplify the model, a simple parameter “deposition of fuel” is introduced instead of fuel mass fraction; (v) the system of equations is solved analytically and during the analysis, any of the transport terms was not neglected from the

energy equations which has not been accomplished yet in the literature of heterogeneous combustion in an inert porous medium.

Large activation energy asymptotic is employed to obtain the analytical expressions of the moving speed of the reaction front, temperature profiles of porous medium and gas, and the species profile of gas. Then the effects of the physical parameters such as the gas flow velocity, the porosity of the porous medium, the thermal conductivity of the porous medium, the deposition of solid fuel and the heat transfer coefficient between the porous medium and gas have been investigated on the moving speed of the reaction front. Moreover, numerical simulation has been carried out in order to make sure the accuracy of the analysis with the variation of each of the parameters. The acceptable ranges of the variation of the parameters are determined by verifying the sensitivity of the asymptotic analysis and also by comparing with the numerical solution in each figure.

2.2 Mathematical formulation

2.2.1 Considerations and assumptions adopted in the model

Before going to the model formulation, the general approach to modeling this system has been elucidated first. The physical configuration of the model is illustrated in Figure 2.1. It shows a typical fibrous cylindrical DPF. When a slice (red part) is cut parallel to the axial direction of the DPF and is viewed from its top, it seems like a flat porous medium covered with solid fuels. So, an infinitely long flat porous medium is considered as a sample over which solid fuels of diameter of the scale of nanometer to micrometer are attached. The sample is taken long enough for the combustion wave to be completely contained within it and can capture a steady-state solution. Oxidizer is flowing from left to right through the porous medium and adjacent to the surface of fuel. The rate of oxygen diffusion to the surface of fuel is high so that the difference between the concentration of the oxygen at the gas/solid interface and the gas within the porous medium is small. The reaction front propagates from the right to left in the direction of fresh fuel and opposite to the direction of gas flow velocity which is referred to as opposed flow combustion. Since the gas flow velocity is sufficiently larger than the

variations of the transport properties, all variations perpendicular to the gas flow velocity become negligible.

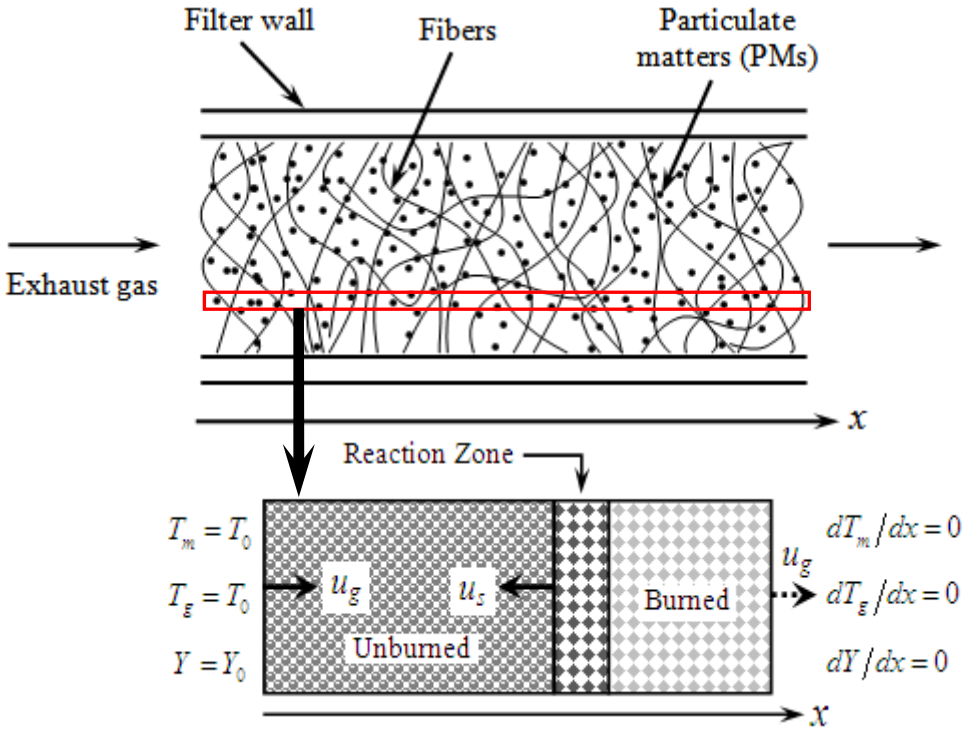

Figure 2.1: Physical configuration of the model.

Moreover, the deposited fuel layer is assumed to be thin enough so that the temperature gradient across the fuel can be neglected. Then the resulting phenomena might be treated essentially a one-dimensional and the axial distance is measured by x in the direction of gas flow velocity. The temperatures of the porous medium and fuel are presumed to be equal along the x direction. The difference of pressure along the porous medium is almost constant. The system has been considered as adiabatic so that the heat loss from the system to the external atmosphere arising only in near proximity to cold sides is taken to be negligible. A two-temperature model is employed where thermal nonequilibrium between the porous medium and gas is allowed to occur within the reaction front. For simplicity reasons, a single-step exothermic heterogeneous reaction is considered by which solid fuel is converted (oxidized) directly to the gaseous product following:

[solid fuel] (s) + n [O_2] (g) → (1+ n) [gaseous product] (g),

where n is the mass of oxygen per mass of fuel ratio (stoichiometric).

The present phenomena has been formulated by introducing a new constant parameter, ϕ, termed as deposition of fuel. It is defined by $\phi = V_f/V_V$ in which V_V (= V_f + V_g), V_f and V_g are respectively the volume of voids, volume of fuel and volume of gas. This is although taken to be constant but informative. As a result the species equation of fuel is circumvented from the model and yields a simplified model.

Furthermore, some assumptions are made: (i) the volumetric effective conductivities of porous medium [$(1-\varepsilon)\lambda_m$] and that for the gas [$\varepsilon(1-\phi)\lambda_g$] are constant, where ε (= V_V/V) is the porosity of the porous medium and V is the total volume of the porous medium, λ_m and λ_g are the thermal conductivities of the porous medium and gas; (ii) the specific heat capacities for the gas, c_g and porous medium, c_m are constants; and (iii) the effective mass diffusivity of gas [$\varepsilon(1-\phi)D$] remains constant, where D denotes the mass diffusivity of gas.

2.2.2 Governing equations

Following [62, 86], the volume-averaged energy equations for porous medium and gas, and species equation for gas (dropping the volume-averaging notation for simplicity) can be written as

$$(1-\varepsilon)\rho_m c_m \frac{\partial T_m}{\partial t} = (1-\varepsilon)\lambda_m \frac{\partial^2 T_m}{\partial x^2} + QW - h(T_m - T_g), \tag{2.1}$$

$$\varepsilon(1-\phi)\rho_g c_g \frac{\partial T_g}{\partial t} + \varepsilon(1-\phi)\rho_g c_g u_g \frac{\partial T_g}{\partial x} = \varepsilon(1-\phi)\lambda_g \frac{\partial^2 T_g}{\partial x^2} + h(T_m - T_g), \tag{2.2}$$

$$\varepsilon(1-\phi)\rho_g \frac{\partial Y}{\partial t} + \varepsilon(1-\phi)\rho_g u_g \frac{\partial Y}{\partial x} = \varepsilon(1-\phi)\rho_g D \frac{\partial^2 Y}{\partial x^2} - nW. \tag{2.3}$$

Here T_m, ρ_m and T_g, ρ_g are the temperature and density of porous medium and gas, respectively, Y is the oxidizer mass fraction, u_g is the velocity at which the gas is flowing into the reaction zone where a heterogeneous exothermic reaction occurs between fuel and gas, Q is the fuel mass based heat of reaction and h is the volumetric heat transfer coefficient from the porous medium to gas.

The surface (i.e., heterogeneous) reaction rate, W, is given by the Arrhenius law

$$W = \varepsilon\phi AY \exp\left[-E/RT_m\right], \tag{2.4}$$

where A is a pre-exponential factor, taken to be constant, R is the universal gas constant, and E is the activation energy.

The boundary conditions to be satisfied by equations (2.1)–(2.3) are

$$x = -\infty:\ Y = Y_0, \quad T_m = T_0, \quad T_g = T_0, \tag{2.5}$$

$$x = +\infty:\ \frac{\partial Y}{\partial x} = 0, \quad \frac{\partial T_m}{\partial x} = 0, \quad \frac{\partial T_g}{\partial x} = 0. \tag{2.6}$$

In this study, the volumetric heat transfer coefficient, h, [62] is expressed by

$$h = \frac{6(1-\varepsilon)Nu\lambda_g}{d^2}, \tag{2.7}$$

where Nu is the interstitial Nusselt number based on the porosity, the pore diameter and gas properties. Equation (2.7) uses the specific interfacial gas/solid surface area of a porous medium $A_{sg}/V = 6(1-\varepsilon)/d$, where A_{sg} is the solid-gas surface area and d is the pore diameter. The correlation for Nu is given by Wakao and Kaguei [87] as

$$Nu = 2 + 1.1\,\mathrm{Pr}^{1/3}\,\mathrm{Re}^{0.6}, \quad 15 < \mathrm{Re} < 8500. \tag{2.8}$$

Here, the Prandtl and Reynolds numbers are defined as $\mathrm{Pr} = \nu_g/\kappa$ and $\mathrm{Re} = \varepsilon u_g d/\nu_g$, respectively, and ν_g and κ are respectively the kinematic viscosity and the thermal diffusivity of the gas.

2.2.3 Dimensionless form of governing equations

In this study the primary quantity of interest is to find the steady moving speed of the reaction front u_s. Taking into account u_s as a characteristic speed; it is convenient to render the problem in dimensionless form by introducing the following group of dimensionless variables [88, 89]:

$$\zeta = \frac{\rho_m c_m u_s}{\lambda_m} x, \quad \tau = \frac{\rho_m c_m u_s^2}{\lambda_m} t, \quad y = \frac{Y}{Y_0}, \quad S = \frac{T_m - T_0}{T_{ad} - T_0}, \quad \theta = \frac{T_g - T_0}{T_{ad} - T_0}. \tag{2.9}$$

Thus the conservation equations (2.1)–(2.3) take the form

$$\frac{\partial S}{\partial \tau}=\frac{\partial^2 S}{\partial \zeta^2}+\frac{\Lambda\varepsilon\phi\gamma}{1-\varepsilon}\,y\exp\left[-\frac{\beta(1-S)}{1-\alpha(1-S)}\right]-\frac{K}{1-\varepsilon}(S-\theta), \tag{2.10}$$

$$\frac{l}{rb}\frac{\partial\theta}{\partial\tau}+\frac{l}{rbu}\frac{\partial\theta}{\partial\zeta}=\frac{\partial^2\theta}{\partial\zeta^2}+\frac{Kl}{\varepsilon(1-\phi)}(S-\theta), \tag{2.11}$$

$$\frac{Lel}{rb}\frac{\partial y}{\partial\tau}+\frac{Lel}{rbu}\frac{\partial y}{\partial\zeta}=\frac{\partial^2 y}{\partial\zeta^2}-\frac{nLel\phi}{(1-\phi)b}\Lambda y\exp\left[-\frac{\beta(1-S)}{1-\alpha(1-S)}\right]. \tag{2.12}$$

The corresponding boundary conditions are

$$\zeta=-\infty:\ S=0,\quad \theta=0,\quad y=1, \tag{2.13}$$

$$\zeta=+\infty:\ \frac{\partial S}{\partial\zeta}=0,\quad \frac{\partial\theta}{\partial\zeta}=0,\quad \frac{\partial y}{\partial\zeta}=0. \tag{2.14}$$

The nondimensional parameters introduced in equations (2.1)–(2.3) are

$$\begin{aligned}&\beta=\frac{E(T_{ad}-T_0)}{RT_{ad}^2},\ \gamma=\frac{QY_0}{c_m(T_{ad}-T_0)},\ \alpha=\frac{T_{ad}-T_0}{T_{ad}},\ K=\frac{h\lambda_m}{\rho_m^2u_s^2c_m^2},\\ &Le=\frac{\lambda_g}{\rho_g Dc_g},\ \Lambda=\frac{A\lambda_m e^{-\beta/\alpha}}{\rho_m^2u_s^2c_m},\ r=\frac{\rho_m}{\rho_g},\ l=\frac{\lambda_m}{\lambda_g},\ u=\frac{u_s}{u_g}\ \text{ and }\ b=\frac{c_m}{c_g},\end{aligned} \tag{2.15}$$

where β is the Zel'dovich number, α is the dimensionless heat of combustion, γ is the dimensionless heat release, K is the heat transfer parameter, Le is a Lewis number which is assumed to be unity and Λ is the reaction rate eigenvalue, the determination of which will yield the dimensional moving speed of the reaction front, u_s, according to its definition.

Finally, a moving coordinate $X = \zeta + \tau$ is introduced attached to the flame front. In this coordinate system, the steadily moving speed of the reaction front is time-independent. Thus, the conservation equations take the form

$$\frac{dS}{dX}=\frac{d^2S}{dX^2}+\frac{\Lambda\varepsilon\phi\gamma}{1-\varepsilon}\,y\exp\left[-\frac{\beta(1-S)}{1-\alpha(1-S)}\right]-\frac{K}{1-\varepsilon}(S-\theta), \tag{2.16}$$

$$\frac{l(1+u)}{rbu}\frac{d\theta}{dX}=\frac{d^2\theta}{dX^2}+\frac{Kl}{\varepsilon(1-\phi)}(S-\theta), \tag{2.17}$$

$$\frac{Lel\left(1+u\right)}{rbu}\frac{dy}{dX}=\frac{d^2y}{dX^2}-\frac{nLel\phi}{\left(1-\phi\right)b}\Lambda y\exp\left[-\frac{\beta\left(1-S\right)}{1-\alpha\left(1-S\right)}\right]. \tag{2.18}$$

The associated boundary conditions become

$$X=-\infty:\ \ S=0,\quad \theta=0,\quad y=1, \tag{2.19}$$

$$X=+\infty:\ \ S'=0,\quad \theta'=0,\quad y'=0. \tag{2.20}$$

The following is the details of the asymptotic analysis employed to solve the system of steady equations (2.16)–(2.18) subject to the boundary conditions (2.19)–(2.20).

2.3 Asymptotic analysis

2.3.1 Outer solutions

Due to large activation energy, the nondimensional activation energy, β, appeared in the reaction-rate expression is very large. This results the reaction rate to be concentrated to a thin $O(\beta^{-1})$ reaction zone. Then the solutions on either side of the reaction zone are obtained in the form of asymptotic expansions in powers of β^{-1}. In the preheat region $X < 0$, the source terms in the conservation equations are exponentially small and in the burned region $X > 0$, the reaction rate ceases to increase (It is presumed that oxidizer is completely consumed at the reaction front, that is, at $X = 0$). So the source terms in these regions can be neglected and hence the equations to be solved are

$$\frac{dS}{dX}=\frac{d^2S}{dX^2}-\frac{K}{1-\varepsilon}\left(S-\theta\right), \tag{2.21}$$

$$\frac{l\left(1+u\right)}{rbu}\frac{d\theta}{dX}=\frac{d^2\theta}{dX^2}+\frac{Kl}{\varepsilon\left(1-\phi\right)}\left(S-\theta\right), \tag{2.22}$$

$$\frac{Lel\left(1+u\right)}{rbu}\frac{dy}{dX}=\frac{d^2y}{dX^2}, \tag{2.23}$$

with the boundary conditions

$$X=-\infty:\ \ S=\theta=0,\ \ y=1, \tag{2.24}$$

$$X=+\infty:\ \ S'=\theta'=0,\ \ y'=0. \tag{2.25}$$

Now since activation energy is very large, the flame temperature will be very high. As a consequence, the assumption of complete consumption of oxidizer at the reaction front (i.e., $y = 0$ at $X = 0$) suggests that the system is controlled by the oxidizer, then the solutions of (2.23) are

$$y\left(X<0\right)=1-\exp\left[\frac{Lel\left(1+u\right)}{rbu}X\right]\ \text{ and }\ \ y\left(X>0\right)=0. \tag{2.26}$$

A relation between the temperatures of the porous medium, S, and gas, θ, can be found by combining equations (2.21) and (2.22) and upon integration gives

$$S'=S-\frac{\varepsilon\left(1-\phi\right)}{\left(1-\varepsilon\right)l}\theta'+\frac{\varepsilon\left(1-\phi\right)\left(1+u\right)}{\left(1-\varepsilon\right)rbu}\theta+A, \tag{2.27}$$

where

$$A=\begin{cases}0, & X<0\\ -C\left[1+\dfrac{\varepsilon\left(1-\phi\right)\left(1+u\right)}{\left(1-\varepsilon\right)rbu}\right], & X>0\end{cases}. \tag{2.28}$$

Here, the boundary condition $S(+\infty) = \theta(+\infty) = C$, and C is to be determined later.

Differentiating (2.22) with respect to X and then applying (2.22) and (2.27)

$$\begin{aligned}&\theta'''-\left\{1+\frac{l\left(1+u\right)}{rbu}\right\}\theta''-\left\{\frac{Kl}{\varepsilon\left(1-\phi\right)}+\frac{K}{1-\varepsilon}-\frac{l\left(1+u\right)}{rbu}\right\}\theta'\\&+\left\{\frac{Kl}{\varepsilon\left(1-\phi\right)}+\frac{Kl\left(1+u\right)}{\left(1-\varepsilon\right)rbu}\right\}\theta=-\frac{Kl}{\varepsilon\left(1-\phi\right)}A.\end{aligned} \tag{2.29}$$

To find the solutions of (2.29), it needs to obtain the solutions of the corresponding characteristic polynomial:

$$m^3-\left\{1+\frac{l\left(1+u\right)}{rbu}\right\}m^2-\left\{\frac{Kl}{\varepsilon\left(1-\phi\right)}+\frac{K}{\varepsilon\phi}-\frac{l\left(1+u\right)}{rbu}\right\}m+\left\{\frac{Kl}{\varepsilon\left(1-\phi\right)}+\frac{Kl\left(1+u\right)}{\left(1-\varepsilon\right)rbu}\right\}=0. \tag{2.30}$$

Considering the appropriate values of the parameters, it can be shown that equation (2.30) must have one negative root, m_1 and two positive roots, m_2 and m_3, to define the finite solutions of the equation (2.29).

Once equation (2.29) is solved, the temperature of the porous medium, S, is determined from the equation (2.22). Then the temperatures of the porous medium and gas are given by

$$S\left(X<0\right)=p_2a_2\exp\left[m_2X\right]+p_3a_3\exp\left[m_3X\right], \tag{2.31}$$

$$\theta\left(X<0\right)=a_2\exp\left[m_2X\right]+a_3\exp\left[m_3X\right], \tag{2.32}$$

$$S\left(X>0\right)=C+p_1a_1\exp\left[m_1X\right], \tag{2.33}$$

$$\theta\left(X>0\right)=C+a_1\exp\left[m_1X\right], \tag{2.34}$$

where

$$p_i=1+\frac{\varepsilon\left(1-\phi\right)}{Kl}\left\{\frac{l\left(1+u\right)}{rbu}m_i-m_i^2\right\},\quad i=1,2,3. \tag{2.35}$$

The constants a_1, a_2 and a_3 are found later.

Therefore, the temperatures of the porous medium and the gas at the reaction front (i.e., $X = 0$) are given by equations (2.31) and (2.32), respectively, as

$$s_f^*=S\left(0\right)=p_2a_2+p_3a_3, \tag{2.36}$$

$$\theta_f^*=\theta\left(0\right)=a_2+a_3. \tag{2.37}$$

2.3.2 Reaction-zone problem

Since the reaction zone becomes very thin owing to high activation energy, a stretched inner variable $\eta = \beta X$ is introduced to measure the jumps of temperature and oxygen across the reaction front. Inner solutions for the dependent variables are sought as expansions of the form [90, 91]:

$$S=s_f^*+\beta^{-1}S_1^{in}+\cdots, \tag{2.38}$$

$$\theta = \theta_f^* + \beta^{-1}\Theta_1^{in} + \cdots, \tag{2.39}$$

$$y = \beta^{-1}Y_1^{in} + \cdots, \tag{2.40}$$

$$\Lambda = \beta^2\left(\Lambda_0 + \beta^{-1}\Lambda_1 + \cdots\right). \tag{2.41}$$

Substituting equations (2.38)–(2.41) into the conservation equations (2.16)–(2.18) and taking the limit $\beta \to \infty$, the leading order reaction zone problem is obtained as

$$\frac{d^2S_1^{in}}{d\eta^2} + \frac{\Lambda_0\varepsilon\phi\gamma}{1-\varepsilon}Y_1^{in}\exp\left[-\frac{\beta\left(1-s_f^*\right)}{1-\alpha\left(1-s_f^*\right)}\right]\exp\left[\frac{S_1^{in}}{\left\{1-\alpha\left(1-s_f^*\right)\right\}^2}\right] = 0, \tag{2.42}$$

$$\frac{d^2\Theta_1^{in}}{d\eta^2} = 0, \tag{2.43}$$

$$\frac{d^2Y_1^{in}}{d\eta^2} - \frac{nLel\phi\Lambda_0}{(1-\phi)b}Y_1^{in}\exp\left[-\frac{\beta\left(1-s_f^*\right)}{1-\alpha\left(1-s_f^*\right)}\right]\exp\left[\frac{S_1^{in}}{\left\{1-\alpha\left(1-s_f^*\right)\right\}^2}\right] = 0. \tag{2.44}$$

From the equations (2.42) and (2.44), one can easily find

$$\frac{d^2S_1^{in}}{d\eta^2} + \frac{\varepsilon\gamma(1-\phi)b}{nLel(1-\varepsilon)}\frac{d^2Y_1^{in}}{d\eta^2} = 0 \tag{2.45}$$

Integrating the equation (2.45) and using the matching conditions between the inner and outer solutions give the energy balance

$$\left(\frac{dS}{dX}\right)_{X=0^-} - \left(\frac{dS}{dX}\right)_{X=0^+} = \frac{\varepsilon\gamma(1-\phi)(1+u)}{n(1-\varepsilon)ru}. \tag{2.46}$$

Similarly, the jump relation obtained from (2.43) and matching conditions at the reaction front (i.e., at $X = 0$) give the following three constraints:

$$\theta'\left(0^-\right) = \theta'\left(0^+\right),\ S\left(0^-\right) = S\left(0^+\right) \text{ and } \theta\left(0^-\right) = \theta\left(0^+\right). \tag{2.47}$$

The unknown constants a_1, a_2, a_3 and C are found from (2.46) and (2.47).

Moreover, integrating the equation (2.45) twice and matching yields

$$Y_1^{in} = -\frac{nLel\left(1-\varepsilon\right)}{\varepsilon\gamma\left(1-\phi\right)b}\left[S_1^{in} - \left(\frac{dS}{dX}\right)_{X=0^+}\eta\right]. \tag{2.48}$$

Upon substitution of equation (2.48) into (2.42) yields

$$\frac{d^2S_1^{in}}{d\eta^2} - \frac{nLel\phi\Lambda_0}{\left(1-\phi\right)b}\exp\left[-\frac{\beta\left(1-s_f^*\right)}{1-\alpha\left(1-s_f^*\right)}\right]\left[S_1^{in} - \left(\frac{dS}{dX}\right)_{X=0^+}\eta\right]\exp\left[\frac{S_1^{in}}{\left\{1-\alpha\left(1-s_f^*\right)\right\}^2}\right] = 0. \tag{2.49}$$

Following [92, 93] and doing some tedious analysis, it is found from the solution of (2.49) that the moving speed of the reaction front is implicitly related to the other parameters by the expression

$$2\left[\frac{n\left(1-\varepsilon\right)ru\left\{1-\alpha\left(1-s_f^*\right)\right\}^2}{\varepsilon\gamma\left(1-\phi\right)\left(1+u\right)}\right]^2\frac{nLel\phi A\lambda_m e^{-\beta/\alpha}}{\left(1-\phi\right)b\rho_m^2u_s^2c_m\beta^2} = \exp\left[\frac{\beta\left(1-s_f^*\right)}{1-\alpha\left(1-s_f^*\right)} - p\chi\right], \tag{2.50}$$

in which

$$p\chi = 1.344\chi - 4\chi^2\left(1-\chi\right)/\left(1-2\chi\right) + 3\chi^3 - \ln\left[1-4\chi^2\right] \quad \text{for } -0.2 < \chi < 0.5. \tag{2.51}$$

Having obtained the maximum temperature of the porous medium, s_f^*, the moving speed of the reaction front, u_s, can be readily determined from Eq. (2.50). The value of χ used in (2.50) can also be found as follows [94]:

$$\chi = \frac{p_1\left(m_2-m_3\right)}{p_1\left(m_2-m_3\right) + p_2\left(m_3-m_1\right) + p_3\left(m_1-m_2\right)}. \tag{2.52}$$

2.4 Numerical method

A computational procedure is performed to compare the results obtained by the asymptotic analysis. The unsteady set of equations is discretized using the implicit finite difference formula in which first-order backward difference for time-derivative terms, forward-difference for the convection terms and

central-difference for diffusion terms are used. Thus it becomes a system of tri-diagonal algebraic equations which is then solved employing Thomas Algorithm.

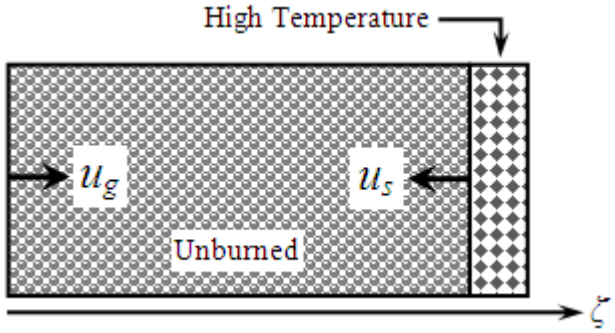

Figure 2.2: Schematic of initiation of a combustion reaction when $\tau = 0$ (opposed flow).

The numerical simulation has been performed by setting a high-temperature profile for the porous medium temperature and at the end of the computational domain (see Figure 2.2) so that the reaction front propagates opposite to the direction of gas flow velocity. The reaction front is assumed to be planar and propagates at a constant speed. The species and temperature distributions, as well as the moving speed of the reaction front, are solved iteratively, prescribing a front speed for a set of constant properties. Here the moving speed of the reaction front is determined following the method described in [62, 95]. The nondimensional mesh sizes along the space and time are chosen as $\Delta\zeta = 0.005$ and $\Delta\tau = 10^{-5}$, respectively, so that the solutions are grid independent.

2.5 Results and discussion

2.5.1 Validation of the asymptotic analysis

The temperature and species profiles obtained by the asymptotic analysis and the numerical solution are shown in Figure 2.3 for $\beta = 16$, $\lambda_m = 0.05$ W/(mK), $\varepsilon = 0.60$, $\phi = 0.70$ and $u_g = 0.30$ m/s and other properties are listed in Table 2.1. It is evident from the figure that the asymptotic analysis gives an excellent agreement with the numerical solution. The moving speed of the reaction front in numerical simulation is found $u_s = 0.11386$ mm/s while in asymptotic analysis $u_s = 0.11763$ mm/s. Since in the asymptotic analysis the final burned gas temperature is a function of u_s, it deviates slightly

from the numerical solution. It is note that λ_m is chosen here very small. In the following sections, the results are elaborately discussed with the aim of determining the acceptable range of the parameters in which the asymptotic analysis is found to be satisfactory. In addition to, the temperature profiles show that there exist thermal nonequilibrium between the porous medium and gas that persists in the pre-heat and post-flame regions.

Table 2.1: Thermophysical properties used in the analysis and numerical computation

Specific heat of porous medium	: c_m (J/kg K)	1100 [83]
Specific heat of gas	: c_g (J/kg K)	1007 [21]
Thermal conductivity of the gas	: λ_g (W/m K)	0.026 [21]
Density of the porous medium	: ρ_m (kg/m^3)	1300 [83]
Density of the gas	: ρ_g (kg/m^3)	1.187 [21]
Fuel mass based heat of reaction	: Q (J/kg)	3.0×10^{7} [83]
Frequency factor	: A (kg/m^3 s)	1.2×10^{11} [84]
Pore diameter	: d (m)	6.4×10^{-3} [62]
Kinematic viscosity	: v_g (m^2/s)	1.517×10^{-5} [21]
Porosity of the porous medium	: ε	0.60 [44]
Zel'dovich number	: β	16
Ambient temperature	: T_0 (K)	300
Adiabatic temperature	: T_{ad} (K)	2000

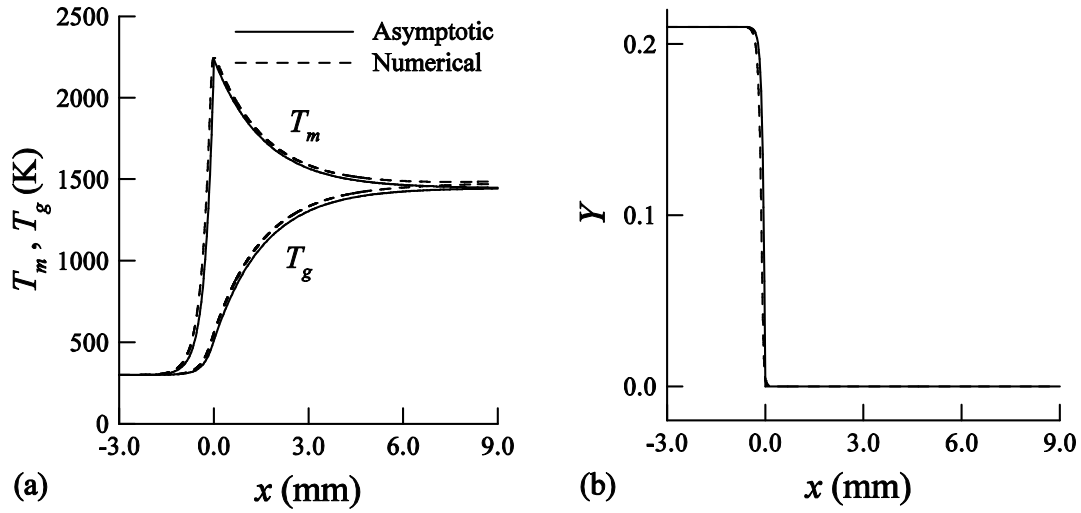

Figure 2.3: (a) Temperature and (b) species profiles in dimensional variables while λ_m = 0.05 W/(mK), ε = 0.60, ϕ = 0.70 and u_g = 0.30 m/s.

In Figure 2.4, the moving speed of the reaction front, u_s, with the variation of the gas flow velocity, u_g, is compared with Fatehi and Kaviany [62]. For the validation purpose, the parameters are used as in [62] except T_{ad} = 1400 K, ϕ = 0.83. In [62], adiabatic temperature is a function of the gas flow velocity while it is a constant in the present analysis. So it is better to pick up a nearly intermediate value as an adiabatic temperature. In addition to, since the present model is different from [62] due to the factors ϕ and $(1-\phi)$ appearing in the governing equations, the value of the deposition of fuel, ϕ, is taken as 0.83 so that the present model apparently reduces to [62]. Nevertheless there are differences in the reaction and heat transfer terms of the models. By observing the models of the present paper and [62], it is clear that for a set of parameters and any value of the deposition of fuel heat production will be lower and heat transfer rate from the porous medium to gas will be higher in case of the present model than in [62]. Consequently, the moving speed of the reaction front could be lower compared to [62] owing to the foregoing effects. It is thus evident that there must have discrepancy between the results obtained by the present model and Fatehi and Kaviany [62]. In spite of the differences between the models, there is a fairly good agreement between the asymptotic solution of the present study and Fatehi and Kaviany [62]. Also the asymptotic solution predicts well the numerical solution.

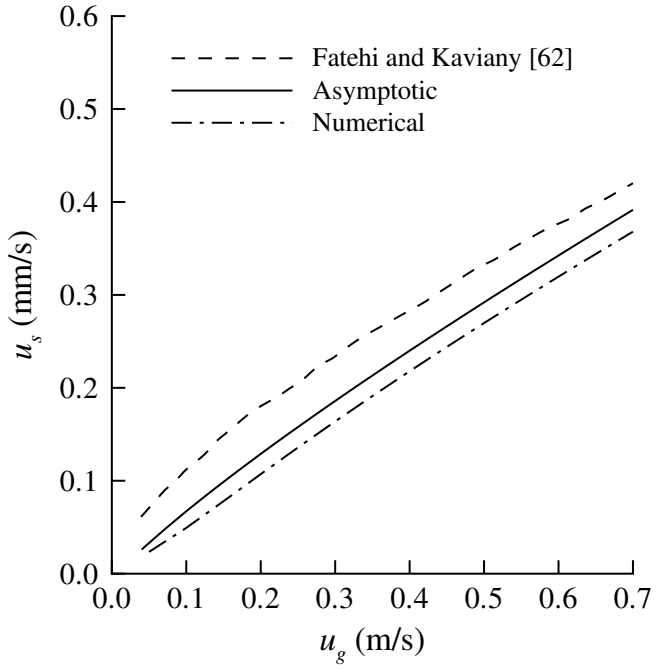

Figure 2.4: Comparison of the moving speed of the reaction front with the variation of u_g.

2.5.2 Sensitivity of the asymptotic analysis

First it should be mentioned that the analysis can predict accurately when the coefficients of the terms of the dimensionless governing equations $l/(rbu)$, $K/(1-\varepsilon)$, $Kl/\varepsilon(1-\phi)$ and $l\phi/(1-\phi)$ be order of unity. Once the values of the thermophysical properties are set for which any of the above mentioned coefficients is different from unity, then the results will be deviated from the actual value.

Here the value of ε varies from from 0.4 to 0.9, since the porosity of silicon carbide (SiC) foam can be in the range 70-90% while it is possible to produce the high strength Al_2O_3 foam with porosity over 85% [96]. Also, Adler [97] mentioned that wall flow filters using fuel borne additive for regeneration consists of ceramics with an open pore volume of about 50%.

The absolute error between the numerical and asymptotic solution of the moving speed of the reaction front ($(u_s)_{Asy} - (u_s)_{Num}$) owing to the increase of the thermal conductivity of the porous medium is presented in Figure 2.5. It shows that the absolute error monotonically increases with an increase of the thermal conductivity of the porous medium. It is evident that the absolute error increases, since the orders of the coefficients of the terms of the dimensionless governing equations become higher than unity. As the dimensionless parameter, l, is defined by the thermal conductivity, λ_m, and it is with most

of the coefficients of the terms of the governing equations, hence its value is very important for the orders of the coefficients. Now it is seen from the curves (i) and (ii) for u_g = 0.30 m/s and u_g = 0.20 m/s, respectively, that the difference between the curves is comparatively small and almost constant when λ_m < 0.5 W/(mK). Thus it can be concluded that the asymptotic solution will give a good agreement with the numerical solution provided that the thermal conductivity of the porous medium is less than 0.5 W/(mK). Interestingly, for λ_m = 0.5 W/(mK), the value of l = 19 which is nearly equal to β. Hence the asymptotic solution will predict well the numerical solution if l is less than or equal to the order of β. In the following section, λ_m is taken as 0.4 W/(mK) for the reference only which turns l (≈ 15) into an order of β. So, for the figures presented below it is expected to have a good accuracy between the results obtained by the asymptotic analysis and numerical solution. The other physical properties and parameters are chosen from practical point of view and listed in Table 2.1. Since the Reynolds number, Re, is defined by porosity, gas flow velocity and the pore diameter, the values of these parameters must be chosen in such a way so that the value of Re maintains the restriction of equation (2.8).

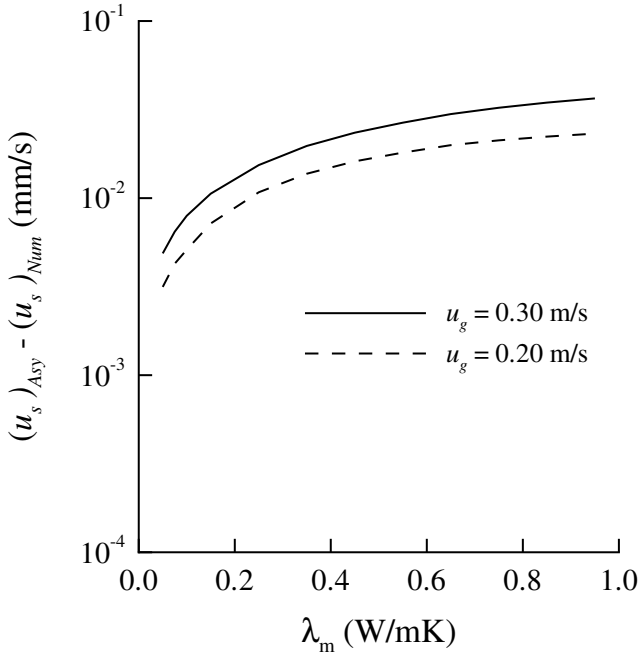

Figure 2.5: Absolute error between the solutions ($(u_s)_{Asy}$– $(u_s)_{Num}$) as a function of λ_m while ε = 0.60, ϕ = 0.40 and u_g = 0.20 m/s and u_g = 0.30 m/s.

2.5.3 Comparison and effects of parameters on the moving speed of the reaction front

Figure 2.6 shows the moving speed of the reaction front with the variation of the thermal conductivity of the porous medium. It is obvious that heat release due to the reaction is increased with the increase of gas flow velocity. On the other hand, it is clear from the Figure 2.6 that the peak of the increasing trend of the moving speed of the reaction front moves to the higher thermal conductivity of the porous medium while gas flow velocity is increased. For higher thermal conductivity, more heat is dissipated in the outer regions through conduction and it is transferred to the gas. On the other hand, for smaller thermal conductivity, heat is being accumulated at the reaction front and its temperature is high enough. This condition favors the reaction rate up to a certain thermal conductivity of the porous medium when the gas velocity is fixed (i.e., heat release due to the reaction is fixed). For this reason, the moving speed of the reaction front first increases then decreases as the thermal conductivity increases. This figure also validates the condition that the asymptotic solution gives a good agreement with the numerical solution when $\lambda_m < 0.5$ W/(mK).

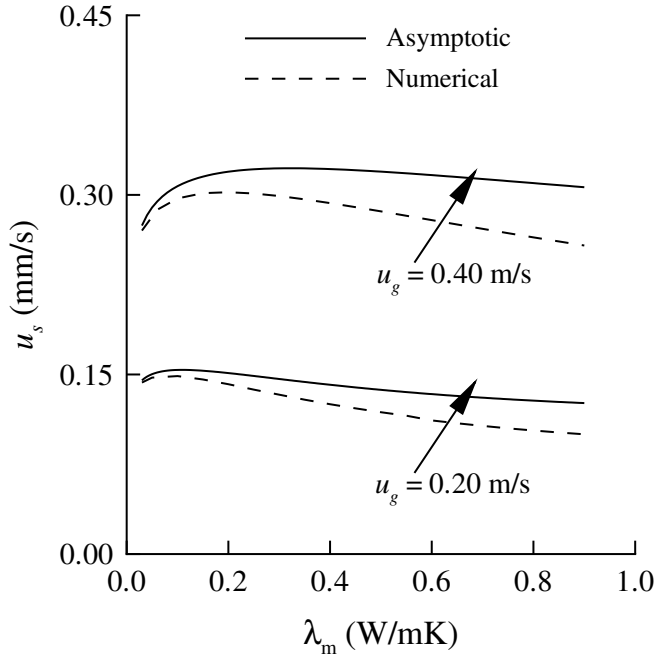

Figure 2.6: Moving speed of the reaction front as a function of λ_m while $\varepsilon = 0.60$, $\phi = 0.40$ and u_g = 0.20 m/s and 0.40 m/s.

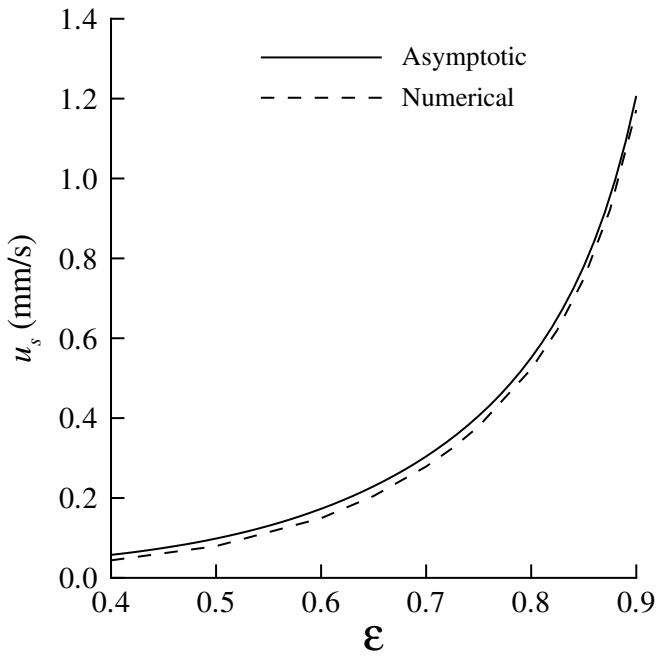

Figure 2.7: Moving speed of the reaction front as a function of ε while λ_m = 0.40 W/(mK), ϕ = 0.65 and u_g = 0.40 m/s.

The moving speed of the reaction front as a function of porosity is presented in Figure 2.7. It is evident from the figure that the moving speed of the reaction front increases when the porosity of the porous medium is increased. This happens due to the fact that the specific surface area of the porous medium increases with the increase of porosity which favors the surface reaction. Moreover there is an excellent agreement between the numerical and asymptotic solution in the entire range of the porosity of the porous medium.

Figure 2.8 exhibits the moving speed of the reaction front in terms of fuel deposition, ϕ. When the deposition of fuel is increased, the moving speed of the reaction front decreases. In case of higher deposition the reaction front propagates by oxidizing more fuel particle in its movement but for lower deposition it propagates by oxidizing less fuel particle. For this reason, the moving speed of the reaction front of fuel becomes lower for large deposition and becomes higher for small deposition. It is found that the asymptotic analysis gives a fairly good agreement with the numerical solution. The discrepancy between the solutions decreases with the increase of deposition of fuel.

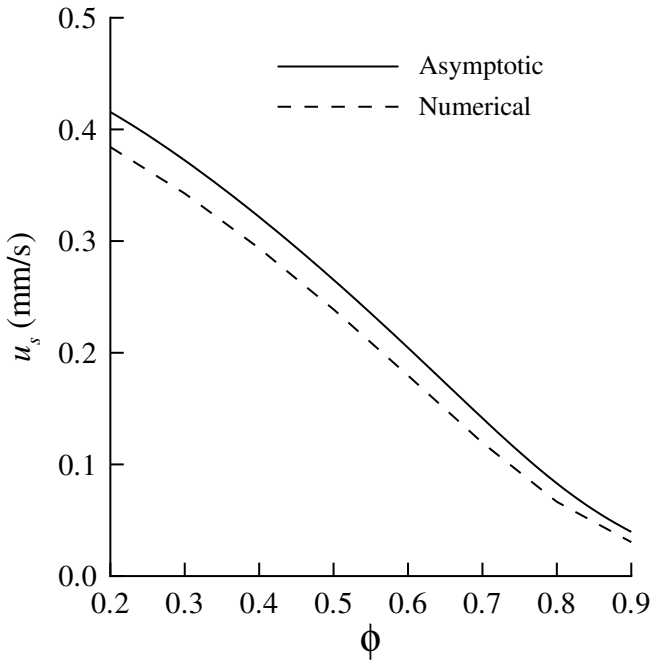

Figure 2.8: Moving speed of the reaction front as a function of ϕ while λ_m = 0.40 W/(mK), ε = 0.60 and u_g = 0.40 m/s.

The effect of volumetric heat transfer coefficient, h, on the moving speed of the reaction front is illustrated in Figure 2.9. From the figure, it is clear that the moving speed of the reaction front becomes lower for higher heat transfer rate. Because more heat is transferred to the gas for high heat transfer rate, consequently the flame temperature of the porous medium becomes lower and fuel reaction rate is relatively less in the lower flame temperature. Also, the asymptotic solution is found to be satisfactory with the numerical solution. Moreover, the difference between the maximum and downstream temperatures ($s_f - S(+\infty)$) (dash-dot line) obtained by the numerical simulation which measures the amount of thermal nonequilibrium between the phases is presented also in Figure 2.9. This shows that the thermal nonequilibrium between the phases decreases with the increase of volumetric heat transfer rate. As a consequence, when the thermal nonequilibrium between the phases decreases the moving speed of the reaction front also decreases.

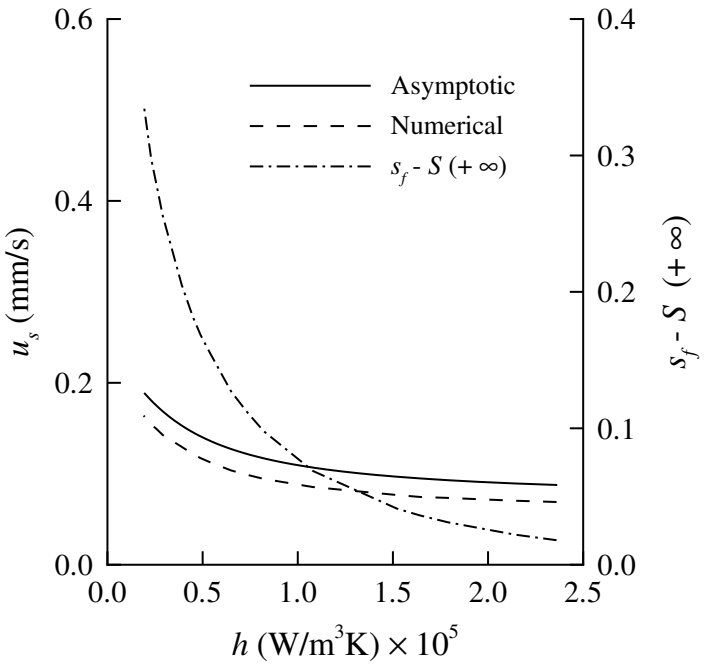

Figure 2.9: Moving speed of the reaction front and amount of thermal nonequilibrium between the phases (dash-dot line) as a function of h while $\lambda_m = 0.40$ W/(mK), $\varepsilon = 0.60$, $\phi = 0.65$ and $u_g = 0.40$ m/s.

2.6 Conclusions

A one-dimensional mathematical model has been proposed in response to the need for computational tools and academic interest. It can be used for the development of particulate matter trap design and in the engineering of the regeneration process, sintering process or in any kind of solid fuel combustion attached over an inert porous medium. A two-temperature model having two energy equations with different density, thermal conductivity and specific heat capacity for the porous medium and gas is employed to determine the effect of the thermal nonequilibrium between the porous medium and gas. To simplify the model, a simple parameter "deposition of fuel" is introduced into the model instead of fuel mass fraction. Without neglecting any of the transport terms of the model, large activation energy asymptotic is employed to solve the problem. Results demonstrate the variation of the moving speed of the reaction front in terms of porosity of the porous medium, thermal conductivity of the porous medium, deposition of solid fuel, gas flow velocity and volumetric heat transfer coefficient from the porous medium to gas. An increase of porosity of the porous medium, thermal conductivity of the porous medium and gas flow velocity cause to increase the moving speed

of the reaction front. But it decreases owing to the increase of deposition of solid fuel as well as the heat transfer coefficient. A numerical computation has also been performed to determine the sensitivity of the asymptotic analysis for variation of each of the parameters that give a clear concept about the deviation of the asymptotic analysis from the numerical solution. It is observed that the asymptotic solution gives a good agreement with the numerical solution when the ratio of the thermal conductivity of the porous medium to gas, l, is of order of β.

Chapter 3

An Upgraded Model of Combustion of Solid Fuel over an Inert Porous Medium

3.1 Introduction

In the first instance and on trial, a very simplified model for the combustion of solid fuel over an inert porous medium is developed in Chapter 2. One of the simplifications of the model was the use of "deposition of fuel" instead of the fuel mass fraction. It is assumed to be a constant throughout the sample. Moreover, the model includes only the thermal nonequilibrium between the porous medium and gas. As a result, the model has some limitations: (i) it fails to predict the fuel distribution along the porous medium; (ii) it cannot be used to investigate the forward flow combustion of solid fuel over an inert porous medium; and (iii) it cannot provide the effects of the key transport mechanisms such as: heat loss from the porous medium to the environment, radiative heat transfer from the porous medium and mass transfer from the bulk gas to the surface of fuel. So, the lack of important transport mechanisms and other limitations of the simple model necessitate further modeling of diesel particulate filter (DPF) regeneration process which is the problem of this thesis.

When the essential transport mechanisms of DPF regeneration process are included into a model, it should be kept in mind that the same type of phenomena is observed in smoldering combustion and SHS and all of these processes occur as a result of combustion of solid fuel in porous medium. In addition to, the fundamental mechanisms of smoldering combustion, self-propagating high-temperature synthesis (SHS) and DPF regeneration process seem to be identical. On the other hand, Wahle and Matkowsky [9] and Wahle et al. [10] reported that when the fundamental mechanisms of some processes are similar, the same mathematical model can be used to elucidate those applications. Based on this ground, smoldering combustion, SHS and DPF regeneration process can be described by

the same mathematical model. But, in smoldering and SHS process, porous solid fuel takes part in the reaction while porous medium remains inert in DPF regeneration process. As a result, the models developed to date in the field of smoldering combustion cannot be used effectively in other processes and vice versa. Hence, the formulation of an upgraded model has become inevitable so that it can be applicable for all of the above mentioned processes.

In this chapter, an upgraded model for the combustion of solid fuel over an inert porous medium has been formulated taking into account the thermal nonequilibrium between the porous medium and gas phases, radiative heat transfer from the porous medium, heat loss from the porous medium to the environment, the mass transfer of oxygen from the gas stream to the surface of solid fuel and the effective diffusion in modeling the species diffusion. Thus the model includes all of the transport mechanisms identified in Chapter 1 which are the controlling factors of smolder propagation, SHS and DPF regeneration process or which can have significant effect to modify the controlling factors of these processes.

Large activation energy asymptotic is employed to obtain the analytical expressions of the moving speed of the reaction front as well as the temperatures and species distributions. The effects of the pertinent physical parameters, such as, the radiation-conduction parameter, initial mass fraction of fuel, porosity of the porous medium, mass transfer coefficient, heat transfer coefficient between the phases, heat loss coefficient and the Knudsen diffusion have been investigated in terms of the moving speed of the reaction front and the fuel leakage through the reaction front. The results are presented to justify the universality of the present model by comparing with the findings available in the literature of smoldering combustion and SHS process. Since the present model can be used to describe the smoldering combustion and SHS process, hence the behavior of combustion wave of the present phenomena has been investigated over a wide range of conditions that can be useful to apprehend not only the present phenomena but also other processes as well.

3.2 Mathematical formulation

3.2.1 Considerations and assumptions adopted in the model

The model configuration employed here is illustrated in Figure 3.1. An infinitely long porous medium is considered over which solid fuels are deposited. Also, it is assumed that oxidizer enters into the reaction zone from left to right through the porous medium. In the reaction zone, oxidizer reacts with solid fuels and generates heat. Accumulating enough heat from the heterogeneous exothermic oxidation of solid fuel, the self-sustained reaction front propagates in the direction of fresh fuel and opposite to the direction of gas flow velocity. During the propagation, the heat released by the reaction is partially transferred toward the fresh fuel through the conduction and radiation and partially lost to the environment [11]. The radiative heat transfer has a significant consequence on the flame structure of smoldering combustion [13, 17, 18] and its effect becomes prominent for larger pore diameters [17, 18]. Besides, the heat loss to the environment is recognized as one of the controlling factors of the smolder propagation [11, 13, 98]. As a result, these are included into the present model. Now, the reaction front can sustain if the net heat lost from the reaction zone is balanced by the heat released from the oxidation of fuel. Again, the generation of heat directly depends upon the availability of oxygen into the reaction zone. Here, oxidizer comes into the reaction zone by diffusion and convection. When the rate of oxygen diffusion from the gas stream to the surface of solid fuel is not so high, there occurs concentration gradient between the gas stream and the solid-gas interface. In other words, when reaction happens there is an increase of local temperature and hence the local reaction rate until all of the neighboring oxygen is consumed. Consequently, the reaction front starts to consume oxygen when it reaches just ahead of the reaction front. Thus, there occurs a very low oxygen level locally [99]. The effect of this chemical nonequilibrium must be taken into account into the model. Because it is well known that the two controlling mechanisms of the propagation of smoldering combustion are the oxygen transport to, and the heat loss from, the reaction zone [11, 13, 98]. Moreover, as the molecular diameters of gas are short and mean free paths are long compared to the characteristic dimensions of the pores, it is important that the effect of porosity can be accurately reflected in modeling the species diffusion process. In addition to, mass transport within the fuel

particles depends on the structure of the free volume within them and in all models it is implicitly or explicitly presumed that the pores are highly interconnected. In this case, it is usual to define an effective diffusivity applicable for throughout the bulk of the fuel particles [22]. Accordingly, the diffusion of gas has been modeled in this study by effective diffusivity instead of using only the molecular diffusivity. Here, the temperatures of the porous medium and fuel are assumed to be equal along the x direction. Since the temperature of the porous medium is quite high and that of the gas is comparatively low, there will be a significant heat transfer from the porous medium to the gas. This effect cannot be neglected since it has substantial impact on smolder propagation [16, 17]. Hence this is incorporated into the model. In this study, a single-step exothermic heterogeneous reaction is used for simplicity reasons with the consideration that solid fuel is converted (oxidized) directly to the gaseous product:

1 g (unburned solid fuel) + n O_2 → (1+ n) (gaseous product),

where n is the mass of oxygen per mass of fuel ratio.

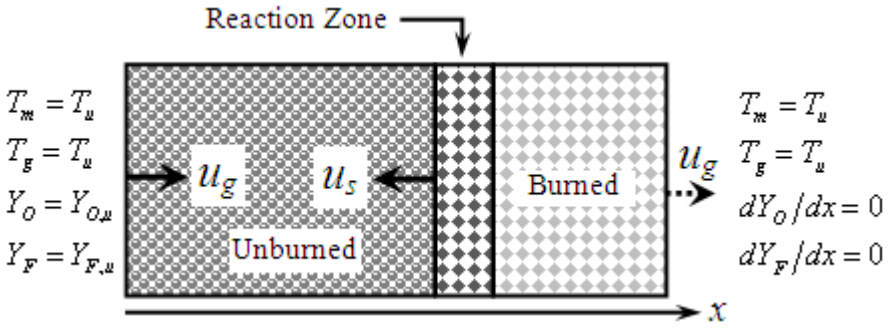

Figure 3.1: Physical configuration of the model.

Moreover, it is assumed that (i) the volumetric effective conductivities of porous medium $[(1-\varepsilon)\lambda_m]$ and that for the gas $[\varepsilon\lambda_g]$ are constant, where ε (= V_V/V) is the porosity of the porous medium and V_V and V are, respectively, the volume of voids and the total volume of the porous medium, λ_m and λ_g are the thermal conductivities of the porous medium and gas; (ii) the specific heat capacities for the gas, c_g

and porous medium, c_m are constants; and (iii) the effective mass diffusivity of gas [εD] remains constant, where D denotes the molecular diffusivity of gas.

3.2.2 Governing equations

An upgraded model is formulated including all essential transport mechanisms for the combustion of solid fuel deposited over an inert porous medium which can be applicable for all of the processes. Following [86, 100 101], the volume-averaged energy equations for porous medium and gas, and species equation for fuel and gas (dropping the volume-averaging notation for the sake of simplicity) can be written as

$$(1-\varepsilon)\rho_m c_m \frac{\partial T_m}{\partial t} = (1-\varepsilon)\lambda_m \frac{\partial^2 T_m}{\partial x^2} + QW - h\left(T_m - T_g\right) - \frac{\partial q_r}{\partial x} - h_{ex}\left(T_m - T_u\right), \tag{3.1}$$

$$\varepsilon\rho_g c_g \frac{\partial T_g}{\partial t} + \varepsilon\rho_g c_g u_g \frac{\partial T_g}{\partial x} = \varepsilon\lambda_g \frac{\partial^2 T_g}{\partial x^2} + h\left(T_m - T_g\right), \tag{3.2}$$

$$\varepsilon\rho_g \frac{\partial Y_O}{\partial t} + \varepsilon\rho_g u_g \frac{\partial Y_O}{\partial x} = \varepsilon\rho_g \frac{\partial}{\partial x}\left(D_{eff} \frac{\partial Y_O}{\partial x}\right) - nW - \frac{h_m \rho_g}{d}\left(Y_O - Y_{O,u}\right), \tag{3.3}$$

$$\varepsilon\rho_f \frac{\partial Y_F}{\partial t} = -W. \tag{3.4}$$

Here T_m, ρ_m and T_g, ρ_g are the volume-averaged temperature and the density of the porous medium and gas, respectively, ρ_f is the density of fuel, Y_O and Y_F are the volume-averaged oxidizer and fuel mass fractions, u_g is the gas flow velocity, Q is the fuel mass based heat of reaction, h is the volumetric heat transfer coefficient from the porous medium to gas, q_r represents the radiative heat flux, h_{ex} is the heat loss coefficient from the porous medium to the environment and h_m is the mass transfer coefficient from the gas stream to the surface of fuel and W is the rate of the chemical reaction, given by an Arrhenius law

$$W = \varepsilon(1-\varepsilon) A \rho_g \rho_f Y_O Y_F \exp\left[-E/RT_m\right], \tag{3.5}$$

where A is a pre-exponential factor, taken to be constant, R is the universal gas constant, and E is the activation energy.

The boundary conditions to be satisfied by equations (3.1)–(3.4) are

$$x = -\infty: \; T_m = T_u, \; T_g = T_u, \; Y = Y_{O,u}, \; Y = Y_{F,u}, \tag{3.6}$$

$$x = +\infty: \; T_m = T_u, \quad T_g = T_u, \quad \frac{\partial Y_O}{\partial x} = 0, \quad \frac{\partial Y_F}{\partial x} = 0. \tag{3.7}$$

The volumetric heat transfer coefficient, h, appeared in equations (3.1) and (3.2) is assumed as Fatehi and Kaviany [62] and is expressed by

$$h = \frac{6(1-\varepsilon) Nu \lambda_g}{d^2}, \tag{3.8}$$

where Nu is the interstitial Nusselt number based on the pore diameter and gas properties. In equation (3.8), the interfacial solid-gas surface area of the porous medium is used as $A_{sg}/V = 6(1-\varepsilon)/d$, where A_{sg} is the solid-gas surface area and d is the pore diameter. The correlation for Nu is given by Wakao and Kaguei [87] as

$$Nu = 2 + 1.1 \mathrm{Pr}^{1/3} \mathrm{Re}^{0.6}, \quad 15 < \mathrm{Re} < 8500. \tag{3.9}$$

In equation (3.9), the Prandtl and Reynolds numbers are defined as $\mathrm{Pr} = \nu_g/\kappa$ and $\mathrm{Re} = \varepsilon u_g d/\nu_g$, respectively, and ν_g and κ are respectively the kinematic viscosity and the thermal diffusivity of the gas.

Again the last term of equation (3.3) which indicates the mass diffusion of oxygen from the gas stream to the surface of fuel is included in the model according to [21] and modeled using the solid-gas mass transfer coefficient, h_m, defined by Fatehi and Kaviany [62] as,

$$h_m = \frac{6(1-\varepsilon) ShD}{\varepsilon d}, \tag{3.10}$$

where the interstitial mass transfer Sherwood number is correlated by Wakao and Kaguei [87],

$$Sh = 2 + 1.1 Sc^{1/3} \mathrm{Re}^{0.6}, \quad 3 < Sc < 10000. \tag{3.11}$$

The Schmidt number *Sc* is defined as $Sc = v_g/D$.

The gas is assumed to be transparent (i.e., no absorption and radiation) within the porous medium. On the contrary, the radiation heat transfer from the solid is taken into account, since the temperature of the porous medium is quite high due to exothermic reaction between the gas and solid fuel on the porous medium. Here, the radiant heat flux term which is valid for an optical thick medium is expressed by the Rosseland diffusion approximation [102]:

$$q_r = -\frac{4\sigma}{3a}\frac{\partial T_m^4}{\partial x}, \tag{3.12}$$

where σ is the Stefan-Boltzmann constant and a is the Rosseland extinction coefficient.

The diffusion coefficient of the gas in the porous medium, D_ε, can be written as the inverse average of the molecular diffusion coefficient, D, and Knudsen diffusion coefficient, D_K, and given by [43]

$$\frac{1}{D_\varepsilon} = \frac{1}{D} + \frac{1}{D_K}, \tag{3.13}$$

where D_K is defined as [103]

$$D_K = \frac{4}{3} d \sqrt{\frac{RT_g}{2\pi M}}. \tag{3.14}$$

Here M is the molar mass of the gas. In this study, the 'effective' diffusivity is defined by [104]

$$D_{eff} = \left(\frac{\varepsilon}{\Omega}\right) D_\varepsilon, \tag{3.15}$$

where Ω is a tortuosity factor which accounts for the extension of the path that a gas must pass through the porous medium. The tortuosity factor typically depends on the structure of the porous medium and it is normally determined experimentally. The value of Ω is assumed here to be 2 [105].

3.2.3 Dimensionless form of governing equations

The primary quantity of interest in the present problem is the steady moving speed of the reaction front u_s. Considering u_s as a characteristic speed; it is convenient to cast the problem in dimensionless form by introducing the following group of dimensionless variables [88, 89]:

$$\xi = \frac{\rho_m c_m u_s}{\lambda_m} x, \quad \tau = \frac{\rho_m c_m u_s^2}{\lambda_m} t, \quad y_O = \frac{Y_O}{Y_{O,u}}, \quad y_F = \frac{Y_F}{Y_{F,u}}, \quad S = \frac{T_m - T_u}{T_{ad} - T_u}, \quad \theta = \frac{T_g - T_u}{T_{ad} - T_u}. \tag{3.16}$$

Thus the conservation equations (3.1)–(3.4) reduce to

$$(1-\varepsilon)\frac{\partial S}{\partial \tau} = \frac{\partial}{\partial \xi}\left[\left\{1-\varepsilon+N_R(1+\delta S)^3\right\}\frac{\partial S}{\partial \xi}\right] + \Lambda\gamma\omega - K(S-\theta) - K_{ex}S, \tag{3.17}$$

$$\frac{l}{rb}\frac{\partial \theta}{\partial \tau} + \frac{l}{rbu}\frac{\partial \theta}{\partial \xi} = \frac{\partial^2 \theta}{\partial \xi^2} + \frac{Kl}{\varepsilon}(S-\theta), \tag{3.18}$$

$$\begin{aligned} &\frac{Lel}{rb}\frac{\partial y_O}{\partial \tau} + \left[\frac{Lel}{rbu} - \frac{\varepsilon\Pi\delta}{2\Omega\sqrt{1+\delta\theta}\left(1+\Pi\sqrt{1+\delta\theta}\right)^2}\frac{\partial \theta}{\partial \xi}\right]\frac{\partial y_O}{\partial \xi} \\ &= \frac{\varepsilon\Pi\sqrt{1+\delta\theta}}{\Omega\left(1+\Pi\sqrt{1+\delta\theta}\right)}\frac{\partial^2 y_O}{\partial \xi^2} - \frac{\Lambda n Lel \Omega_{st}}{\varepsilon b}\omega - \frac{LelK_m}{\varepsilon rb}(y_O - 1), \end{aligned} \tag{3.19}$$

$$\frac{\partial y_F}{\partial \tau} = -\frac{\Lambda r_f}{\varepsilon}\omega. \tag{3.20}$$

The associated boundary conditions become

$$\xi = -\infty: \; S = 0, \quad \theta = 0, \quad y_O = 1, \quad y_F = 1, \tag{3.21}$$

$$\xi = +\infty: \; S = 0, \quad \theta = 0, \quad \frac{\partial y_O}{\partial \xi} = 0, \quad \frac{\partial y_F}{\partial \xi} = 0. \tag{3.22}$$

Here the nondimensional parameters

$$\gamma \equiv \frac{QY_{F,u}}{c_m\left(T_{ad}-T_u\right)},\quad \delta \equiv \frac{T_{ad}-T_u}{T_u},\quad K \equiv \frac{h\lambda_m}{\rho_m^2 u_s^2 c_m^2},\quad N_R \equiv \frac{16\sigma T_u^3}{3\lambda_m a},\quad \Pi \equiv \frac{4}{3}\frac{d}{D}\sqrt{\frac{RT_u}{2\pi M}},$$
$$K_{ex} \equiv \frac{h_{ex}\lambda_m}{\rho_m^2 u_s^2 c_m^2},\quad K_m \equiv \frac{h_m\lambda_m}{\rho_m u_s^2 c_m d},\quad \Omega_{st} \equiv \frac{Y_{F,u}}{Y_{O,u}},\quad Le \equiv \frac{\lambda_g}{\rho_g D c_g},\quad \Lambda \equiv \frac{A\lambda_m\rho_g\rho_f Y_{O,u}e^{-\beta/\alpha}}{\rho_m^2 u_s^2 c_m}, \tag{3.23}$$

where γ is the dimensionless heat release, δ represents the thermal excursion during the burning process, K is the heat transfer parameter, N_R is the radiation-conduction parameter, K_{ex} is the heat loss parameter, K_m is the mass transfer parameter, Le is a Lewis number which is assumed to be unity and Λ is the burning rate eigenvalue, the determination of which will yield the dimensional moving speed of the reaction front, u_s, according to its definition.

The nondimensional reaction rate, ω, is given by

$$\omega \equiv \varepsilon\left(1-\varepsilon\right) y_O y_F \exp\left[-\frac{\beta\left(1-S\right)}{1-\alpha\left(1-S\right)}\right], \tag{3.24}$$

where

$$\alpha \equiv \frac{T_{ad}-T_u}{T_{ad}} \quad \text{and} \quad \beta \equiv \frac{E\left(T_{ad}-T_u\right)}{RT_{ad}^2}, \tag{3.25}$$

are the dimensionless heat of combustion and the Zel'dovich number, respectively. The other additional parameters are defined by

$$r \equiv \frac{\rho_m}{\rho_g},\ r_f \equiv \frac{\rho_m}{\rho_f},\ l \equiv \frac{\lambda_m}{\lambda_g},\ u \equiv \frac{u_s}{u_g} \text{ and } b \equiv \frac{c_m}{c_g}. \tag{3.26}$$

According to the definitions of the foregoing quantities, the nondimensional moving speed of the reaction front is equal to unity. It is thus useful to analyze the problem in the moving coordinate $X = \xi - \tau$ attached to the reaction front. Consequently, the steadily moving speed of the reaction front is time-independent. Introducing this transformation into the equations (3.17)–(3.20), the system of equations take the form

$$\left(1-\varepsilon\right)\frac{dS}{dX} = \frac{d}{dX}\left[\left\{1-\varepsilon+N_R\left(1+\delta S\right)^3\right\}\frac{dS}{dX}\right] + \Lambda\gamma\omega - K\left(S-\theta\right) - K_{ex}S, \tag{3.27}$$

$$\frac{l(1-u)}{rbu}\frac{d\theta}{dX}=\frac{d^2\theta}{dX^2}+\frac{Kl}{\varepsilon}(S-\theta), \tag{3.28}$$

$$\left[\frac{Lel(1-u)}{rbu}-\frac{\varepsilon\Pi\delta}{2\Omega\sqrt{1+\delta\theta}\left(1+\Pi\sqrt{1+\delta\theta}\right)^2}\frac{d\theta}{dX}\right]\frac{dy_O}{dX}$$
$$=\frac{\varepsilon\Pi\sqrt{1+\delta\theta}}{\Omega\left(1+\Pi\sqrt{1+\delta\theta}\right)}\frac{d^2y_O}{dX^2}-\frac{\Lambda nLel\Omega_{st}}{\varepsilon b}\omega-\frac{LelK_m}{\varepsilon rb}(y_O-1), \tag{3.29}$$

$$\frac{dy_F}{dX}=-\frac{\Lambda r_f}{\varepsilon}\omega. \tag{3.30}$$

The corresponding boundary conditions become

$$X=-\infty:\ \ S=\theta=0,\ \ y_O=1,\ \ y_F=1, \tag{3.31}$$

$$X=+\infty:\ \ S=\theta=0,\ \ \ y_O'=y_F'=0. \tag{3.32}$$

Our purpose is to solve the steady problem given by equations (3.27)–(3.30) subject to the boundary conditions (3.31)–(3.32) and thus to determine the burning rate eigenvalue Λ by carrying out an asymptotic analysis. This can then be used to find the dimensional moving speed of the reaction front u_s, according to its definition (3.23).

3.3 Asymptotic analysis

3.3.1 Outer solutions

Since the nondimensional activation energy, β that appears in the reaction-rate expression is assumed to be large, this implies that all chemical activity is confined to a thin $O(\beta^{-1})$ reaction zone. Then the solutions on either side of the reaction zone can be obtained in the form of asymptotic expansions in powers of β^{-1}. In the preheat region $X < 0$, the source terms in the conservation equations are exponentially small and in the burned region $X > 0$, all the chemical reaction has gone to completion. So the source terms become negligible in these regions.

To analyze the problem theoretically, the difficulty arises due to the nonlinear radiation term of the coefficient $1-\varepsilon+N_R(1+\delta S)^3$ of equation (3.27). Most of the studies avoided this difficulty by solving

their problem numerically. Consequently, there are a few theoretical works that dealt with radiation effect. A long time before, Dosanjh et al. [13] and Schult et al. [14] solved a simple one temperature model taking into account the effect of the nonlinear radiation term. Also, authors [106-108] solve their problems for gaseous fuel combustion taking the radiation heat transfer as a constant with the definition of effective thermal conductivity which includes thermal conductivity of the porous medium and the radiation heat transfer. But it is difficult to measure the thermal conductivity of the porous medium and an effective conductivity depends to a great extent upon the specifics of the porous medium [106], so there is an uncertainty of the appropriateness of the data values. Since it is difficult to make the problem tractable for analytical solution considering the nonlinear effect of the radiation term, hence it is better to use a linear approximation of the term. Although our motivation is based on the concept of constant radiation heat transfer but approach is different. Thus, to investigate the problem analytically it is presumed that

$$1-\varepsilon+N_R\left(1+\delta S\right)^3 \approx \Gamma, \tag{3.33}$$

where

$$\Gamma=\begin{cases}1-\varepsilon+N_R\left(1+\delta\right)^3, & X\le 0\\ 1-\varepsilon+\dfrac{N_R}{2}\left\{1+\left(1+\delta\right)^3\right\}, & X>0\end{cases}. \tag{3.34}$$

To derive the approximation of the relation defined in (3.34), firstly it is roughly set the possible value $S = 1$ in (3.33) for all $X \le 0$.

In the downstream region i.e., for $X > 0$, depending on the heat loss to the environment and heat transfer rate, S can vary between 0 and 1. So, two possible values $S = 0$ and $S = 1$ are set in (3.33) which gives $\Gamma = 1- \varepsilon + N_R$ and $\Gamma = 1- \varepsilon + N_R(1 + \delta)^3$. Then the values of Γ are summed up and divided by 2 that yields $\Gamma = 1- \varepsilon + N_R\{1 + (1 + \delta)^3\}/2$.

Moreover, equation (3.29) cannot be solved analytically because of the variable coefficients of y_O' and y_O'' of the equation that are accounted for the effective diffusion. It is noteworthy that any study didn't solve a model theoretically which assumed the effective diffusivity for modeling the diffusion

of oxidizer through the porous medium. As a first attempt, such a problem has been taken to solve. To circumvent the difficulty, the largest effect of the coefficients is considered. Since Π is very large, the value of $\varepsilon\Pi\sqrt{1+\delta\theta}\Big/\left\{\Omega\left(1+\Pi\sqrt{1+\delta\theta}\right)\right\}$ tends to ε/Ω when θ attains its maximum value, $\theta_f^* = \theta\left(X_f\right)$, at $X = X_f$. Hence, $\theta = \theta_f^*$ has been set in this term so that

$$B_1 = \frac{\varepsilon\Pi\sqrt{1+\delta\theta_f^*}}{\Omega\left(1+\Pi\sqrt{1+\delta\theta_f^*}\right)}, \tag{3.35}$$

gives the maximum effect on the diffusion term.

Again, $\varepsilon\Pi\delta\Big/\left(2\Omega\sqrt{1+\delta\theta}\left(1+\Pi\sqrt{1+\delta\theta}\right)^2\right)$ tends to $\varepsilon\delta/\left(2\Omega\Pi\right)$ as $\theta \to 0$. Also $d\theta/dx$ attains its maximum just ahead or behind the maximum value of θ. Thus it can de deduced that the highest effect of $\varepsilon\Pi\delta\left(d\theta/dX\right)\Big/\left(2\Omega\sqrt{1+\delta\theta}\left(1+\Pi\sqrt{1+\delta\theta}\right)^2\right)$ on the convection of gas is accounted for by taking it as

$$B_2 = \frac{\varepsilon\delta}{2\Omega\Pi}\left(\frac{d\theta}{dX}\right)_{X=X_f^{\pm}}. \tag{3.36}$$

Therefore, the equations to be solved for the outer regions are

$$\left(1-\varepsilon\right)\frac{dS}{dX} = \Gamma\frac{d^2S}{dX^2} - K\left(S-\theta\right) - K_{ex}S, \tag{3.37}$$

$$\frac{l\left(1-u\right)}{rbu}\frac{d\theta}{dX} = \frac{d^2\theta}{dX^2} + \frac{Kl}{\varepsilon}\left(S-\theta\right), \tag{3.38}$$

$$\left[\frac{Lel\left(1-u\right)}{rbu} - B_2\right]\frac{dy_O}{dX} = B_1\frac{d^2y_O}{dX^2} - \frac{LelK_m}{\varepsilon rb}\left(y_O - 1\right), \tag{3.39}$$

$$\frac{dy_F}{dX} = 0, \tag{3.40}$$

with the boundary conditions

$$X=-\infty:\ \ S=\theta=0,\ \ y_O=y_F=1, \tag{3.41}$$

$$X=-\infty:\ \ S=\theta=0,\ \ y_O=y_F=1, \tag{3.42}$$

Now from (3.38), one obtains

$$S=\theta+\frac{\varepsilon(1-u)}{rbuK}\theta'-\frac{\varepsilon}{Kl}\theta''. \tag{3.43}$$

Upon substitution of (3.43) into (3.37) gives

$$\begin{aligned}&\theta^{(iv)}-\left\{\frac{1-\varepsilon}{\Gamma}+\frac{l(1-u)}{rbu}\right\}\theta'''-\left\{\frac{Kl}{\varepsilon}+\frac{K+K_{ex}}{\Gamma}-\frac{(1-\varepsilon)l(1-u)}{rbu\Gamma}\right\}\theta''\\&+\frac{1}{\Gamma}\left\{\frac{Kl(1-\varepsilon)}{\varepsilon}+\frac{Kl(1-u)}{rbu}+\frac{K_{ex}l(1-u)}{rbu}\right\}\theta'+\frac{KlK_{ex}}{\varepsilon\Gamma}\theta=0.\end{aligned} \tag{3.44}$$

The analytical solutions of fourth order differential equation (3.44) are not available in the literature. For obtaining the solutions of Eq. (3.44), it is required to find the roots of the corresponding characteristic polynomial:

$$\begin{aligned}&m^4-\left\{\frac{1-\varepsilon}{\Gamma}+\frac{l(1-u)}{rbu}\right\}m^3-\left\{\frac{Kl}{\varepsilon}+\frac{K+K_{ex}}{\Gamma}-\frac{(1-\varepsilon)l(1-u)}{rbu\Gamma}\right\}m^2\\&+\frac{1}{\Gamma}\left\{\frac{Kl(1-\varepsilon)}{\varepsilon}+\frac{Kl(1-u)}{rbu}+\frac{K_{ex}l(1-u)}{rbu}\right\}m+\frac{KlK_{ex}}{\varepsilon\Gamma}=0.\end{aligned} \tag{3.45}$$

Considering the appropriate values of the parameters, it can be shown by Descartes' rule of signs that Eq. (3.45) must have two positive roots, m_1 and m_2; and two negative roots, m_3 and m_4, to define the finite solutions of the Eq. (3.44).

Once Eq. (3.44) is solved, the temperature of the porous medium, S, is determined from Eq. (3.43). Then the temperatures of the porous medium and gas are given by

$$S(X<0)=p_1a_1\exp[m_1X]+p_2a_2\exp[m_2X], \tag{3.46}$$

$$\theta(X<0)=a_1\exp[m_1X]+a_2\exp[m_2X], \tag{3.47}$$

$$S(X>0)=p_3a_3\exp[m_3X]+p_4a_4\exp[m_4X], \tag{3.48}$$

$$\theta(X>0) = a_3 \exp[m_3 X] + a_4 \exp[m_4 X], \tag{3.49}$$

where

$$p_i = 1 - \frac{\varepsilon}{Kl}\left\{ m_i^2 - \frac{l(1-u)}{rbu} m_i \right\}, \quad i = 1,2,3,4, \tag{3.50}$$

and the constants a_1, a_2, a_3 and a_4 are found later.

Thus the temperature of the porous medium at the reaction front (i.e., X = 0) can be expressed as follows:

$$S(0) = s_f^* = p_1 a_1 + p_2 a_2. \tag{3.51}$$

As the activation energy is assumed to be large, the reaction front temperature will be very high. Consequently, one of the reactants (fuel and oxidizer) must be depleted after passing through the reaction front. Here it is considered that oxidizer is fully consumed at the reaction front (i.e., y_O = 0 at X = 0) [12, 109] suggesting that the system is controlled by oxidizer. Therefore, the solutions of Eq. (3.39) becomes

$$y_O(X<0) = 1 - \exp[\mu_1 X] \quad \text{and} \quad y_O(X>0) = 0, \tag{3.52}$$

where

$$\mu_{1,2} = \left[\frac{Lel(1-u)}{rbuB_1} - \frac{B_2}{B_1} \pm \sqrt{\left\{ \frac{Lel(1-u)}{rbuB_1} - \frac{B_2}{B_1} \right\}^2 + \frac{4LelK_m}{\varepsilon rbB_1}} \right] \Big/ 2.$$

Also, if f_0^* is the remained fuel mass fraction at the reaction front, then the solutions of (3.40) can be written as

$$y_F(X<0) = 1 \quad \text{and} \quad y_F(X>0) = f_0^*. \tag{3.53}$$

3.3.2 Reaction zone

In the asymptotic limit $\beta \to \infty$, the reaction zone becomes very thin which acts as a heat source and a sink of oxygen that cause jumps in the heat flux as well as oxygen. For this reason, a stretched inner

variable $\eta = \beta X$ is introduced to measure the jumps of temperature and oxygen across the reaction front. Inner solutions for the dependent variables S, θ and y, and the burning rate eigenvalue Λ are now sought as expansions of the form [90, 91]:

$$S = s_f^* + \beta^{-1} S_1^{in} + \cdots, \tag{3.54}$$

$$\theta = \theta_f^* + \beta^{-1} \Theta_1^{in} + \cdots, \tag{3.55}$$

$$y_O = \beta^{-1} G_1^{in} + \cdots, \tag{3.56}$$

$$y_F = F_0^{in} + \beta^{-1} F_1^{in} + \cdots, \tag{3.57}$$

$$\Lambda = \beta^2 \left(\Lambda_0 + \beta^{-1} \Lambda_1 + \cdots \right), \tag{3.58}$$

$$\eta = \beta X. \tag{3.59}$$

Thus the reaction zone problem become

$$\Gamma^{in} \frac{d^2 S_1^{in}}{d\eta^2} + \varepsilon\gamma\Lambda_0 F_0^{in} G_1^{in} \exp\left[-\frac{\beta\left(1 - s_f^*\right)}{1 - \alpha\left(1 - s_f^*\right)} \right] \exp\left[\frac{S_1}{\left\{1 - \alpha\left(1 - s_f^*\right)\right\}^2} \right] = 0, \tag{3.60}$$

$$\frac{d^2 \Theta_1^{in}}{d\eta^2} = 0, \tag{3.61}$$

$$B_1 \frac{d^2 G_1^{in}}{d\eta^2} - \frac{nLel\Omega_{st}}{b} \left(1 - \varepsilon\right) \Lambda_0 F_0^{in} G_1^{in} \exp\left[-\frac{\beta\left(1 - s_f^*\right)}{1 - \alpha\left(1 - s_f^*\right)} \right] \exp\left[\frac{S_1^{in}}{\left\{1 - \alpha\left(1 - s_f^*\right)\right\}^2} \right] = 0, \tag{3.62}$$

$$\frac{dF_0^{in}}{d\eta} + \Lambda_0 r_f \left(1 - \varepsilon\right) F_0^{in} G_1^{in} \exp\left[-\frac{\beta\left(1 - s_f^*\right)}{1 - \alpha\left(1 - s_f^*\right)} \right] \exp\left[\frac{S_1^{in}}{\left\{1 - \alpha\left(1 - s_f^*\right)\right\}^2} \right] = 0. \tag{3.63}$$

The matching conditions are:

as $\eta \rightarrow -\infty$,

$$\frac{dS_1^{in}}{d\eta} \rightarrow \left(\frac{dS}{dX} \right)_{X=0^-}, \tag{3.64}$$

$$\frac{d\Theta_1^{in}}{d\eta} \to \left(\frac{d\theta}{dX}\right)_{X=0^-}, \tag{3.65}$$

$$\frac{dG_1^{in}}{d\eta} \to \left(\frac{dy_O}{dX}\right)_{X=0^-} = -\mu_1, \tag{3.66}$$

$$\frac{dF_0^{in}}{d\eta} \to \frac{1}{\beta}\left(\frac{dy_F}{dX}\right)_{X=0^-} = 0, \tag{3.67}$$

as $\eta \to +\infty$,

$$\frac{dS_1^{in}}{d\eta} \to \left(\frac{dS}{dX}\right)_{X=0^+}, \tag{3.68}$$

$$\frac{d\Theta_1^{in}}{d\eta} \to \left(\frac{d\theta}{dX}\right)_{X=0^+}, \tag{3.69}$$

$$\frac{dG_1^{in}}{d\eta} \to 0, \tag{3.70}$$

$$\frac{dF_0^{in}}{d\eta} \to 0. \tag{3.71}$$

Combining Eqs. (3.62) and (3.63) and using the matching conditions, one obtains

$$\left[y_F\right]_-^+ = -\frac{bB_1 r_f}{nLel\Omega_{st}}\left[\frac{dy_O}{dX}\right]_-^+,$$

which gives

$$f_0^* = 1 - \frac{bB_1 r_f \mu_1}{nLel\Omega_{st}}. \tag{3.72}$$

From the Eqs. (3.60) and (3.62), it can be found that

$$\frac{\Gamma^{in}}{\varepsilon\gamma}\frac{d^2S_1^{in}}{d\eta^2} + \frac{bB_1}{nLel\left(1-\varepsilon\right)\Omega_{st}}\frac{d^2G_1^{in}}{d\eta^2} = 0. \tag{3.73}$$

Integrating the Eq. (3.73) and matching yields the energy balance

$$\left(\frac{dS_1^{in}}{d\eta}\right)_{\eta\to-\infty}-\left(\frac{dS_1^{in}}{d\eta}\right)_{\eta\to+\infty}=-\frac{\varepsilon\gamma bB_1}{nLel\left(1-\varepsilon\right)\Omega_{st}\Gamma^{in}}\left[\left(\frac{dG_1^{in}}{d\eta}\right)_{\eta\to-\infty}-\left(\frac{dG_1^{in}}{d\eta}\right)_{\eta\to+\infty}\right],$$

That is, $$\left(\frac{dS}{dX}\right)_{X=0^-}-\left(\frac{dS}{dX}\right)_{X=0^+}=\frac{\varepsilon\gamma bB_1\mu_1}{nLel\left(1-\varepsilon\right)\Omega_{st}\Gamma^{in}}. \tag{3.74}$$

Similarly, the jump relation obtained from Eq. (3.61) and matching conditions at the reaction front (i.e., $X = 0$) gives the following three constraints:

$$\theta'\left(0^-\right)=\theta'\left(0^+\right),\ S\left(0^-\right)=S\left(0^+\right)\ \text{ and }\ \theta\left(0^-\right)=\theta\left(0^+\right). \tag{3.75}$$

Now using Eqs. (3.46)–(3.49) into (3.74) and (3.75), one can easily find the constants a_1, a_2, a_3 and a_4. Integrating Eq. (3.73) twice and matching yields

$$G_1^{in}=-\frac{nLel\left(1-\varepsilon\right)\Omega_{st}\Gamma^{in}}{\varepsilon\gamma bB_1}\left[S_1^{in}-\left(\frac{dS}{dX}\right)_{X=0^+}\eta\right]. \tag{3.76}$$

Therefore, Eq. (3.60) takes the form

$$\begin{aligned}\frac{d^2S_1^{in}}{d\eta^2}&=\frac{nLel\left(1-\varepsilon\right)\Omega_{st}\Gamma^{in}}{bB_1}\Lambda_0 f_0^*\exp\left[-\frac{\beta\left(1-s_f^*\right)}{1-\alpha\left(1-s_f^*\right)}\right]\\&\times\left[S_1^{in}-\left(\frac{dS}{dX}\right)_{X=0^+}\eta\right]\exp\left[\frac{S_1^{in}}{\left\{1-\alpha\left(1-s_f^*\right)\right\}^2}\right].\end{aligned} \tag{3.77}$$

Equation (3.77) is solved by Liñán [92]. According to the relation between Λ and Λ_0 given by (3.58) along with the definition of Λ given in Eq. (3.23), the moving speed of the reaction front is implicitly related to the other parameters by the expression

$$\begin{aligned}&2\left[\frac{nLel\left(1-\varepsilon\right)\Omega_{st}\Gamma^{in}\left\{1-\alpha\left(1-s_f^*\right)\right\}^2}{\varepsilon\gamma bB_1\mu_1}\right]^2\frac{nLel\left(1-\varepsilon\right)\Omega_{st}f_0^*A\lambda_m\rho_g\rho_fY_{O,u}e^{-\beta/\alpha}}{bB_1\rho_m^2u_s^2c_m\beta^2}\\&=\exp\left[\frac{\beta\left(1-s_f^*\right)}{1-\alpha\left(1-s_f^*\right)}-\psi\chi\right],\end{aligned} \tag{3.78}$$

in which

$$\psi\chi = 1.344\psi - 4\psi^2(1-\psi)/(1-2\psi) + 3\psi^3 - \ln\left[1-4\psi^2\right] \quad \text{for } -0.2 < \psi < 0.5. \tag{3.79}$$

Having obtained the maximum temperature of the porous medium s_f^* by Eq. (3.51), one can readily determine the moving speed of the reaction front u_s from (3.78). The value of ψ can also be found by [94] as

$$\psi = \frac{S'(0^+)}{S'(0^+) - S'(0^-)}. \tag{3.80}$$

3.4 Numerical method

In this study, a numerical simulation is also carried out to validate the results obtained by the asymptotic analysis. The nondimensional governing equations (3.17)–(3.20) with boundary conditions (3.21)–(3.22) are discretized using the implicit finite difference formula in which first-order backward difference for time-derivative terms and central-difference for the convection and diffusion terms are used. Thus it reduces to a system of tri-diagonal algebraic equations. Finally, this system is solved employing Gaussian elimination method.

To simulate the initiation of a combustion reaction, a high-temperature profile is set in the porous medium and at the end of the computational domain (see Figure 3.2) so that the reaction front propagates opposite to the direction of gas flow velocity. The reaction front is assumed to be planar and propagates at a constant speed. The species and temperature distributions, as well as the moving speed of the reaction front, are solved iteratively, prescribing a front speed for a set of constant properties. Here the moving speed of the reaction front is determined following the method described in [62, 95]. The calculation is performed setting $\Delta\xi = 0.01$ and $\Delta\tau = 10^{-4}$, so that the solutions are grid independent.

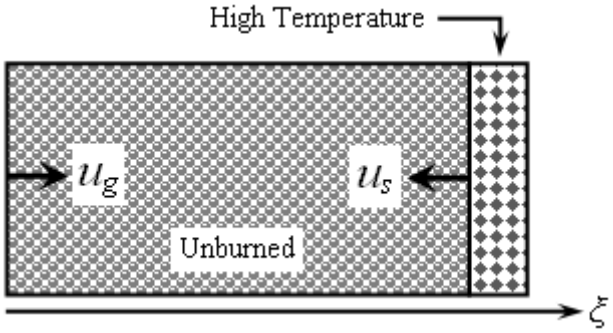

Figure 3.2: Schematic of initiation of a combustion reaction when $\tau = 0$ (opposed flow).

Table 3.1: Thermophysical properties used in the analysis and numerical computation

Specific heat of porous medium	: c_m (J/kg K)	1100 [83]
Specific heat of gas	: c_g (J/kg K)	1007 [21]
Thermal conductivity of the gas	: λ_g (W/m K)	0.026 [21]
Density of the porous medium	: ρ_m (kg/m^3)	1300 [83]
Density of the gas	: ρ_g (kg/m^3)	1.187 [21]
Density of fuel	: ρ_f (kg/m^3)	550 [41]
Fuel mass based heat of reaction	: Q (J/kg)	3.0×10^7 [83]
Frequency factor	: A (m^3/kg s)	1.0×10^{10} [13]
Pore diameter	: d (m)	1.0×10^{-3}
Kinematic viscosity	: v_g (m^2/s)	1.517×10^{-5} [21]
Porosity of the porous medium	: ε	0.80
Zel'dovich number	: β	15
Initial mass fraction of oxidizer	: $Y_{O,u}$	0.154 [41]
Ambient temperature	: T_0 (K)	300 [100]
Adiabatic temperature	: T_{ad} (K)	1800

3.5 Results and discussion

Before going to the details of the effects of the key parameters, it should be noted that Schnitzlein and Löwe [110] use 0.83 as the mean porosity of ceramic fiber coil diesel particulate traps while Hoffmann et al. [111] measured the porosity of a diesel particulate filter to be 0.77. So, in the present study the average value 0.80 of 0.83 and 0.77 is used as the porosity of the porous medium and other thermophysical properties are listed in Table 3.1. In this study, solid fuels deposited over the porous medium are assumed to be carbon which is the main particle deposit trapped in the diesel particulate filter.

At first, a comparison between the numerical and asymptotic solutions in terms of the moving speed of the reaction front, u_s, is depicted in Figure 3.3. From the figure, it is evident that for the moving speed of the reaction front the asymptotic solutions show a better agreement with the numerical solution.

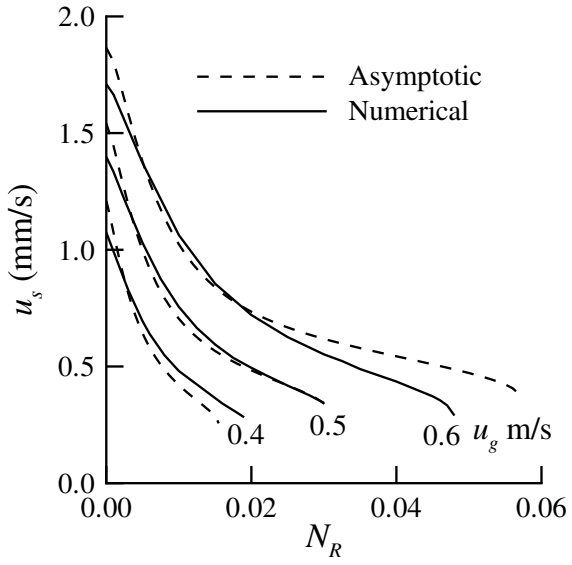

Figure 3.3: Comparison between the numerical and asymptotic solution.

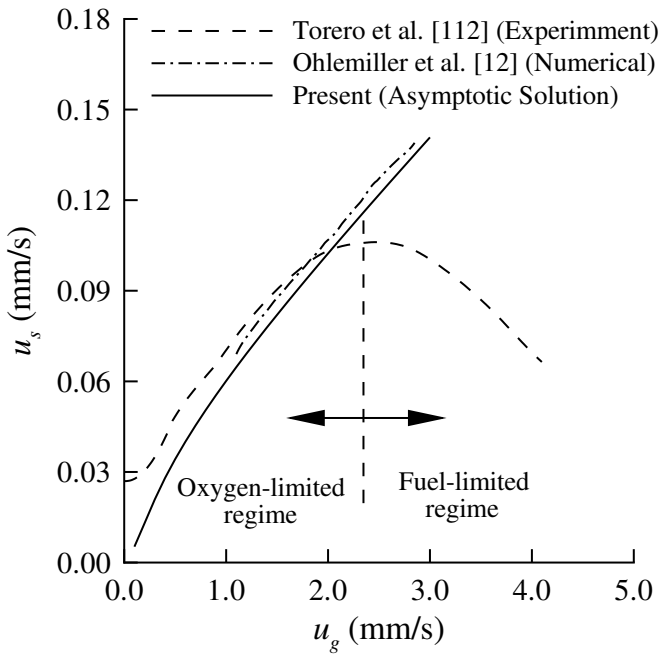

Figure 3.4: Variation of the moving speed of the reaction front with the gas flow velocity. Experimental data are taken from Torero et al. [112] and numerical data are from Ohlemiller et al. [12].

In Figure 3.4, a comparison is made between the experimental data of Torero et al. [112] and the asymptotic solutions of the present model. Since the properties of Ohlemiller et al. [12] are almost equal to or of the order of Torero et al. [112], the numerical data of Ohlemiller et al. [12] is also presented for being certain up to the mark. In this figure, the solutions of the present model are obtained using the thermophysical properties of Torero et al. [112] and others required data are chosen from Table 3.1. Evidently, the present model can predict correctly the numerical data of Ohlemiller et al. [12]. On the other hand, the model shows a good qualitative agreement with the experimental data of Torero et al. [112] which correspond to the solutions of oxygen-limited regime [113]. Even the simplified model of [13] used by Torero et al. [112] fails to predict the solution of the fuel-limited regime. This is mainly due to the fact that in the present study, it is assumed that the oxidizer is fully consumed at the reaction front which often occurs for reverse smoldering combustion as observed by Ohlemiller et al. [12] and Ohlemiller and Lucca [109]. That is, the solutions of the present model as well as Ohlemiller et al. [12] are for the oxygen-limited regime. Therefore, it can be concluded that the

present model predicts very well the qualitative trend of behavior of the moving speed of the reaction front with the variation of the gas flow velocity within the oxygen-limited regime. In addition to, as the present model demonstrates a good qualitative agreement with the experimental and numerical data of smolder combustion, it can be concluded that the present model also works well for predicting the characteristics of smoldering combustion.

Below, the effects of the key parameters such as the radiation-conduction parameter, N_R, porosity of the porous medium, ε, initial mass fraction of fuel, $Y_{F,u}$, mass transfer coefficient, h_m, heat transfer coefficient, h, heat loss coefficient, h_{ex}, and the effective diffusion, D_{eff}, have been investigated on the moving speed of the reaction front, the amount of fuel leakage through the reaction front, temperature and species distributions. Since the asymptotic solutions are found to agree well with the numerical solution as presented in Figure 3.3, the following results and discussion are made on the basis of asymptotic solutions.

3.5.1 Effect of radiation-conduction parameter

The moving speed of the reaction front, u_s, and the amount of fuel leakage, f_0^*, through the reaction front with the variation of the radiation-conduction parameter, N_R, is presented in Figures 3.5(a) and (b), respectively, for $\lambda_m = 0.4$ W/(mK), $\varepsilon = 0.80$, $Y_{F,u} = 0.30$ and $h_{ex} = 10^4$ W/(m^{3}K) with different value of u_g. In the figures, the upper branch (dashed line) of the curves lying above the turning point usually called quenching point corresponds to stable solutions while the lower branch (solid line) of the curves corresponds to unstable solutions [91]. As the unstable solutions are not of great physical interest [91], the main concern of this study will be concentrated on stable solutions. From the Figure 3.5(a), it is observed that the moving speed of the reaction front monotonically decreases with an increase of N_R. Using the definition of the parameter N_R given by (3.23), it can infer that when the value of N_R increases, the Rosseland extinction coefficient decreases. Also it is known that the pore diameter increases with the decrease of the Rosseland extinction coefficient. Since the radiative heat transfer effect becomes prominent for larger diameters [17], the net heat lost from the reaction zone will be higher that results to decrease the moving speed of the reaction front; and for further increase of N_R, the reaction front extinguishes. It happens because with the increase of N_R the heat loss from the

porous medium has surmounted the critical value to be sustained the reaction front. Since the heat generation increases owing to the increase of gas flow velocity, the critical value of heat loss through the radiation for the reaction front extinguishment is increased. Figure 3.5(b) shows that the amount of fuel leakage through the reaction front decreases when the value of N_R is increased. This is due to the fact that the reaction zone broadens with the increase of N_R that enhances the consumption of fuel. Moreover, the fuel leakage increases with an increase of the gas flow velocity, u_g. It is note that gas deficient case is considered in this study. Consequently, although the moving speed of the reaction front increases as the gas comes faster to the reaction zone with larger gas flow velocity, the reaction front with thin pre-heat region moves to the fresh fuel leaving more un-reacted fuel behind. Interestingly, though the radiative heat transfer has significant effect on the moving speed of the reaction front and the fuel leakage through the reaction front; and extinction could be occurred due to higher value of it, these facts are not reported to date in the open literature of DPF regeneration process, SHS and smoldering combustion.

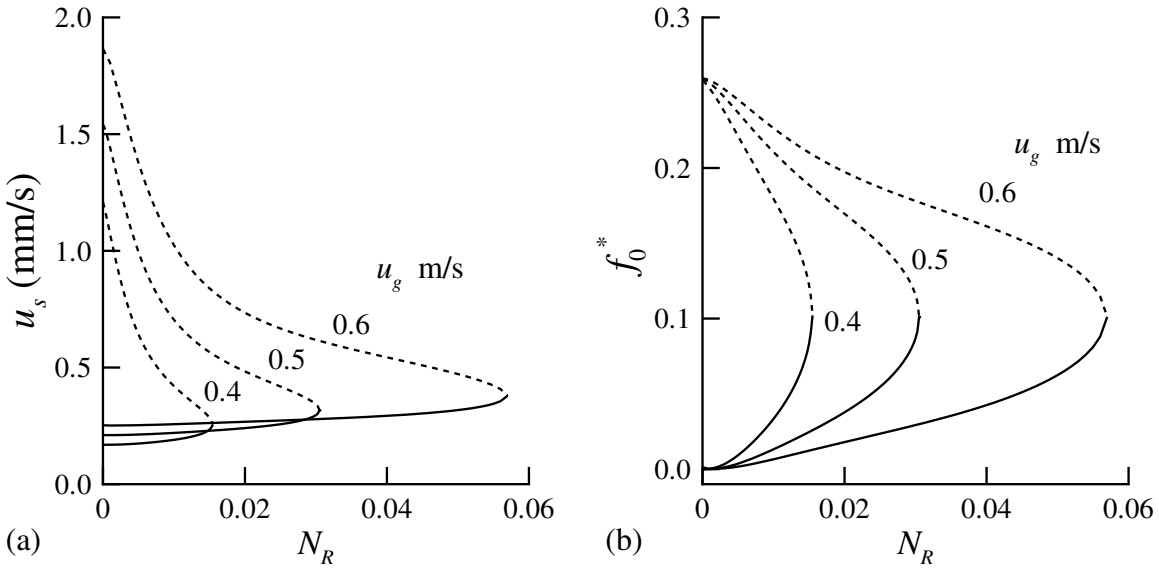

Figure 3.5: (a) Moving speed of the reaction front and (b) the amount of fuel leakage, f_0^*, through the reaction front as a function of N_R while λ_m = 0.40 W/(mK), ε = 0.80, $Y_{F,u}$ = 0.30, h_{ex} = 10^4 W/(m^3K).

The effect of the radiation heat transfer on the temperature (T_m = porous medium, T_g = gas) and species profiles is shown in Figures 3.6(a) and (b), respectively, for λ_m = 0.4 W/(mK), ε = 0.80, h_{ex} = 3

$\times 10^4$ W/(m^{3}K), $Y_{F,u} = 0.30$ and $u_g = 0.50$ m/s. In Figure 3.6(a), the value of the radiation-conduction parameter $N_R = 0.0$ indicates that there is no radiation effect while $N_R = 0.005$ represents an effect of radiation in the phenomena. It is seen that the maximum temperature increases when radiative heat transfer is not considered. This confirms that the suppression of radiative heat transfer caused a large increase in the peak reaction zone temperature [13, 17]. Also, it is clear that the pre-heat region becomes wider owing to the increase of radiative heat transfer through the porous medium and accordingly the reaction zone becomes thicker and thermal nonequilibrium between the porous medium and gas increases. In addition to, the maximum temperature of the gas increases with an increase of the radiative heat transfer. It is understandable because the heat loss due to radiation from the porous medium and the wider pre-heat region give rise to increase the temperature of the gas. The results provide one striking phenomena alike to [62, 92, 114] that although oxidizer is exhausted just after the reaction front, fuel can leak through the reaction front. The species profiles shown in Figure 3.6(b) reveal that the amount of fuel leakage through the reaction front decreases with the radiation heat transfer. This happens because the thick reaction zone developed by the radiation heat transfer facilitates to burn out more fuel but reduces the moving speed of the reaction front.

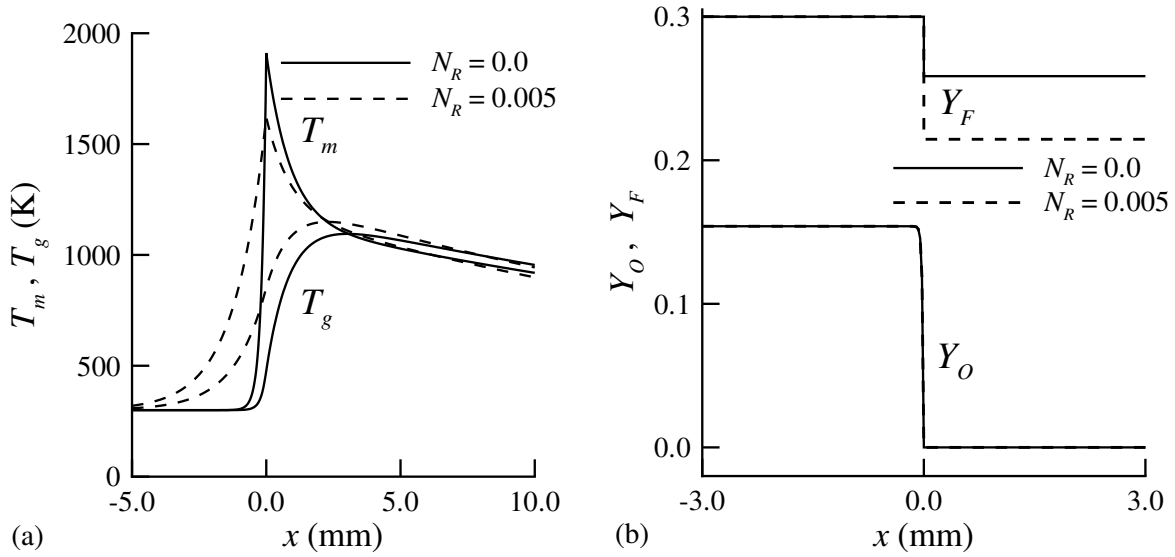

Figure 3.6: (a) Temperature and (b) species profiles in dimensional variables for $\lambda_m = 0.4$ W/(mK), $\varepsilon = 0.8$, $Y_{F,u} = 0.3$, $u_g = 0.5$ m/s, $h_{ex} = 3 \times 10^4$ W/(m^{3}K) when $N_R = 0.0$ (without radiation) and $N_R = 0.005$ (with radiation).

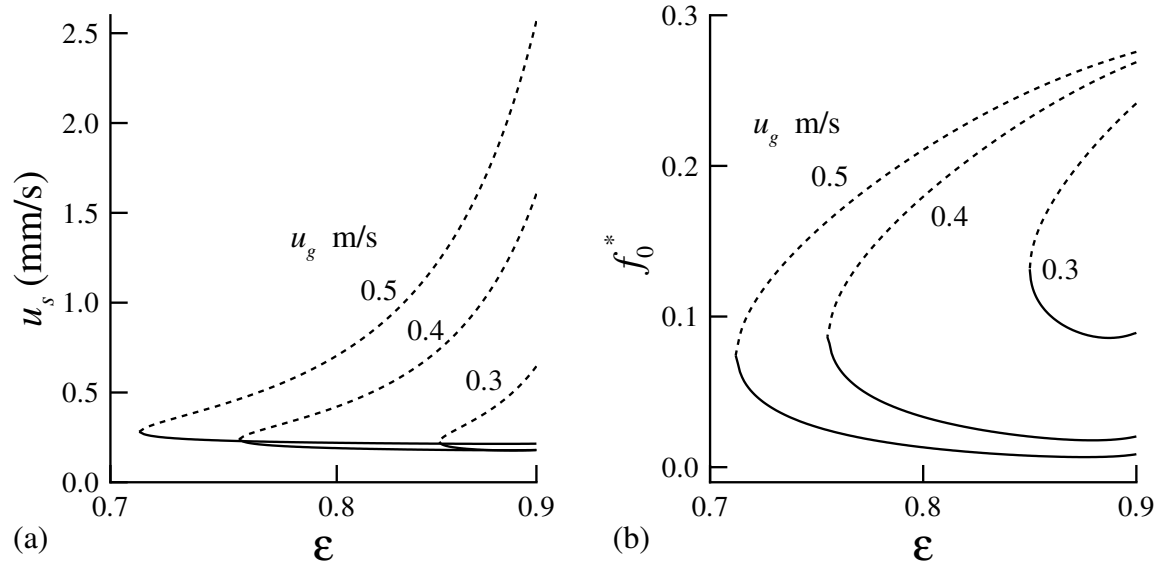

Figure 3.7: (a) Moving speed of the reaction front and (b) the amount of fuel leakage, f_0^*, through the reaction front as a function of ε while $\lambda_m = 0.40$ W/(mK), $N_R = 0.01$, $Y_{F,u} = 0.30$, $h_{ex} = 10^4$ W/(m^{3}K).

3.5.2 Effect of porosity

The effect of porosity on the moving speed of the reaction front, u_s, and the amount of fuel leakage, f_0^*, through the reaction front is shown in Figures 3.7(a) and (b), respectively, for $\lambda_m = 0.4$ W/(mK), $N_R = 0.01$, $Y_{F,u} = 0.30$ and $h_{ex} = 10^4$ W/(m^{3}K) with different value of u_g. From the Figure 3.7(a), it is evident that the moving speed of the reaction front decreases with the decrease of ε. The decrease of porosity of the porous medium results in a decrease of the surface area of the porous medium. Consequently, the reaction rate and hence the moving speed of the reaction front decreases owing to the decrease of porosity. With further decrease of porosity, the reaction front extinguishes. Figure 3.7(b) shows that the amount of fuel leakage through the reaction front decreases due to the decrease of ε. This is because the effective thermal conductivity of the porous medium increases with the decrease of porosity for which the reaction zone becomes thicker along with the wider pre-heat zone and hence the fuel consumption increases. In addition to, the fuel leakage increases as the gas flow velocity, u_g, increases. It is worthwhile to mention that the extinction of the reaction front and the aspect of fuel leakage through the reaction front with the variation of porosity of the porous medium have not been investigated in any literature of DPF regeneration process, SHS and smoldering combustion.

3.5.3 Effect of initial mass fraction of fuel

Figure 3.8 exhibits the moving speed of the reaction front, u_s, with the variation of the initial mass fraction of fuel, $Y_{F,u}$. Evidently, the moving speed of the reaction front gradually increases with an increase of the initial mass fraction of fuel. It is well established that the rate of the moving speed of the reaction front is primarily determined by a balance between the rate of heat released by the reaction and the energy required to heat the solid fuel and gaseous oxidizer to the reaction temperature [109, 115]. In this case, since the gas flow rate is fixed and the amount of fuel increases, hence the energy required to heat the fuel to the reaction temperature gradually increases. For this reason, the initial mass fraction of fuel gradually accelerates the moving speed of the reaction front.

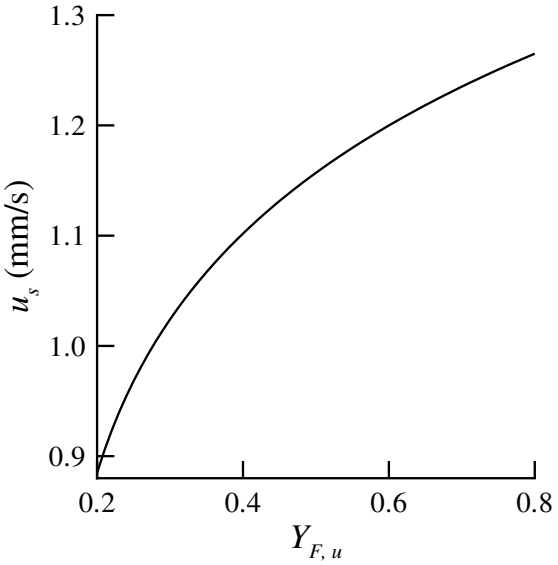

Figure 3.8: Moving speed of the reaction front as a function of $Y_{F,u}$ for λ_m = 0.40 W/(mK), ε = 0.80, u_g = 0.60 m/s, $Y_{O,u}$ = 0.154 m/s, h_{ex} = 10^4 W/(m^{3}K) and N_R = 0.01.

3.5.4 Effect of mass transfer coefficient

The moving speed of the reaction front, u_s, against the mass transfer coefficient, h_m, is depicted in Figure 3.9. It is found that when the mass transfer coefficient is increased, the moving speed of the reaction front increases. This is because the relations (3.10) and (3.11) give that the mass transfer coefficient becomes larger due to the increase of the gas flow velocity (or gas diffusivity) that enhances the amount of oxygen to the surface of fuel at the reaction front. This agrees with the

observation of Wang et al. [21] for smoldering combustion. Hence the present model could affirm the similar trend of the moving speed of the reaction front with mass transfer rate as predicted in smoldering combustion. It is also clear from the figure that the amount of fuel leakage through the reaction front increases as the mass transfer coefficient increases. This is due to the fact that since the system is gas deficient and the gas flow velocity (or gas diffusivity) is high for larger mass transfer rate, so the reaction front with thin pre-heat zone moves fast to the fresh solid fuel leaving the larger amount of fuel unburned

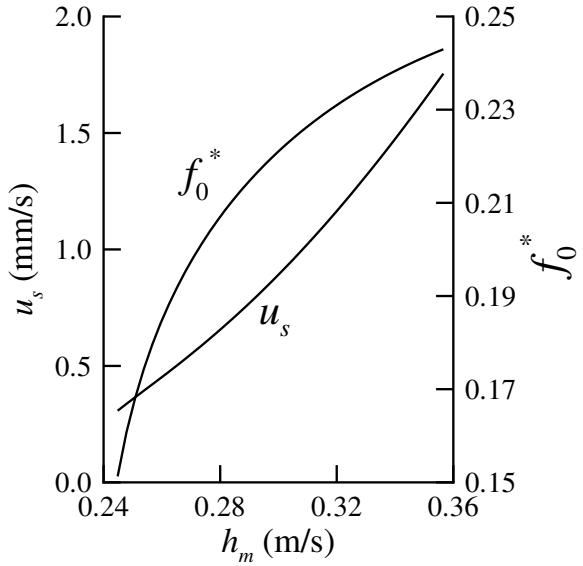

Figure 3.9: Moving speed of the reaction front and the amount of fuel leakage, f_0^*, through the reaction front as a function of h_m for $\lambda_m = 0.4$ W/(mK), $\varepsilon = 0.8$, $Y_{F,u} = 0.3$, $h_{ex} = 10^4$ W/(m^{3}K) and $N_R = 0.01$.

3.5.5 Effect of heat transfer coefficient

For different values of the radiation-conduction parameter, the moving speed of the reaction front with the variation of the heat transfer coefficient is presented in Figure 3.10. From the figure, it is seen that the moving speed of the reaction front monotonically decreases owing to the increase of the heat transfer coefficient. If it is continued to increase, the porous medium will no longer be able to keep enough heat for the reaction front to sustain and finally the reaction front extinguishes at a critical heat transfer rate. This finding was numerically observed by Leach et al. [16, 17]. It should be mentioned that although Leach et al. [16] employed equation (3.8) for the heat transfer coefficient, but they didn't

confirm it that extinction was predicted using equation (3.8). For the present investigation, the heat transfer coefficient was increased by using equation (3.8) and decreasing the pore diameter of the porous medium. As the pore diameter decreases, internal surface area of the porous medium and the convective heat transfer increases with the fixed gas flow velocity. On the other hand, net heat production remains constant due to the fixed amount of oxidizer, fuel and gas flow velocity. Consequently, the increasing of heat transfer coefficient reduces the temperature of the porous medium so that it fails to retain enough heat to sustain the reaction front and eventually the reaction front extinguishes. To this end, the critical value of heat transfer rate for which the reaction front extinguishes is seen to be higher when the radiation-conduction parameter decreases. Evidently, the radiative heat loss from the porous medium becomes lower as the radiation-conduction parameter decreases and as a result the critical value of heat transfer rate for the extinction becomes higher.

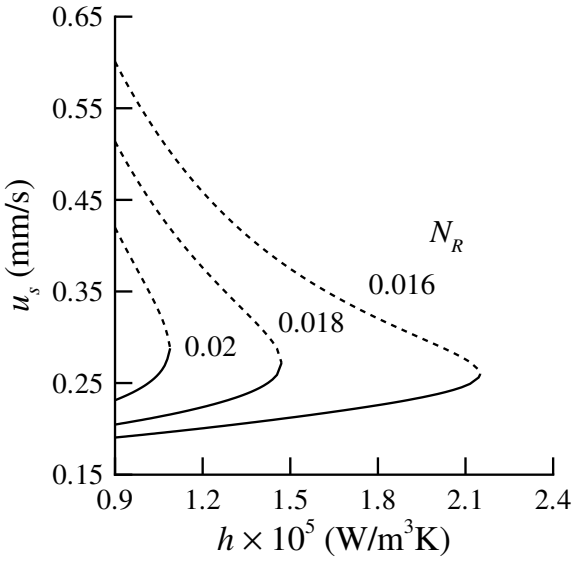

Figure 3.10: Moving speed of the reaction front as a function of volumetric heat transfer coefficient, h, for $\lambda_m = 0.4$ W/(mK), $\varepsilon = 0.8$, $Y_{F,u} = 0.3$, $u_g = 0.40$ m/s and $h_{ex} = 10^4$ W/(m^{3}K).

3.5.6 Effect of heat loss coefficient

The effect of heat loss coefficient on the moving speed of the reaction front, for different values of the gas flow velocity, is shown in Figure 3.11. It is seen from the figure that the moving speed of the reaction front decreases with the increase of heat loss coefficient. Due to increase of heat loss

coefficient, more heat is lost from the porous medium that induces to decrease the moving speed of the reaction front. With further increase of heat loss coefficient, the net heat released by the exothermic reaction fails to increase the temperature of the fresh fuel high enough for the propagation of the reaction front and eventually the reaction front extinguishes at a critical heat loss coefficient. This finding obviously corroborates the previous result that the heat loss rate must not exceed the heat generation rate for the self-sustained propagation of the reaction front [22, 98, 99]. Moreover, this critical value increases with an increase of the gas flow velocity. The reason is that the production of heat increases owing to the increase of the gas flow velocity.

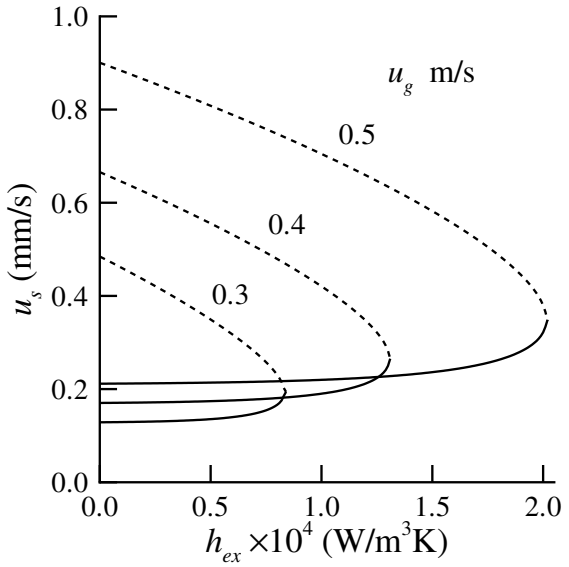

Figure 3.11: Moving speed of the reaction front as a function of heat loss coefficient, h_{ex}, for $\lambda_m = 0.4$ W/(mK), $\varepsilon = 0.8$, $Y_{F,u} = 0.3$ and $N_R = 0.01$.

3.5.7 Effect of Knudsen diffusion

A comparison of the effect of the inclusion of Knudsen diffusion and tortuosity on the effective diffusivity, D_{eff}, and the molecular diffusivity, D, on the temperature and species profiles is shown in Figures 3.12(a) and (b), respectively. It is found from Figure 3.12(a) that the temperatures of gas and porous medium for molecular diffusivity are higher than that for effective diffusivity. This is due to the fact that the molecular diffusivity is smaller than the effective diffusivity and hence the gas remains longer time in the reaction zone during the molecular diffusivity relative to effective

diffusivity. On the other hand, Figure 3.12(b) exhibits that the mass fraction of gas for the molecular diffusivity starts to decrease earlier than the mass fraction of gas for the effective diffusivity and the amount of fuel leakage through the reaction front for the effective diffusivity is higher than that for molecular diffusivity.

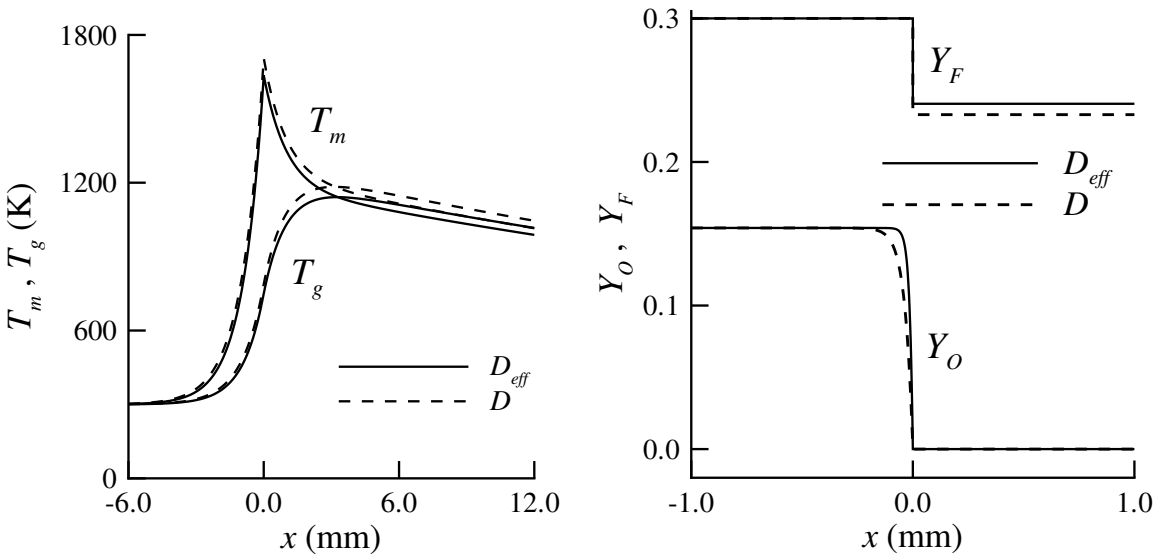

Figure 3.12: Temperature and species profiles for the effect of including Knudsen diffusion with molecular diffusion for λ_m = 0.4 W/(mK), ε = 0.8, $Y_{F,u}$ = 0.3, u_g = 0.6 m/s, h_{ex} = 2×10^4 W/(m^{3}K) and N_R = 0.005 while D_{eff} with Knudsen and molecular diffusion and D with molecular diffusion only.

3.5.8 Extinction limit diagram

In Figure 3.13, the extinction limit is presented in terms of radiation-conduction parameter and gas flow velocity. The figure shows that the extinction limit in terms of heat loss decreases owing to the increase of the radiation-conduction parameter while it increases with the increase of gas flow velocity. Evidently, as heat lost by radiation increases then it is expected that the reaction front will be extinguished at a lower heat loss to the environment. On the other hand, it is well-known that heat production increases when the gas flow velocity is increased. So the extinction limit in terms of heat loss becomes higher for larger gas flow velocity. Additionally, a comparison between the effects of the effective diffusivity, D_{eff}, and the molecular diffusivity, D is presented on the extinction limit of the

reaction front. Although the reaction front cannot be extinguished due to effective diffusivity, but it broadens the extinction limit compared to molecular diffusivity.

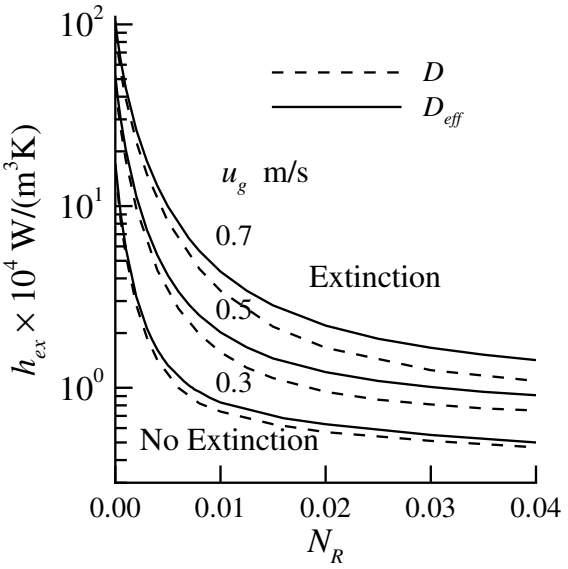

Figure 3.13: Extinction limit diagram as a function of radiation-conduction parameter and gas flow velocity for λ_m = 0.4 W/(mK), ε = 0.8 and $Y_{F,u}$ = 0.3.

3.5.9 Summary of the quantitative studies

The quantitative interactions among the physical parameters over a wide range of conditions are demonstrated above which reveal the following characteristics of combustion wave:

(i) the moving speed of the reaction front increases with the increase of porosity of the porous medium and the initial mass fraction of fuel and the decrease of the heat transfer rate from the porous medium to the gas, the heat loss coefficient and the radiation-conduction parameter;

(ii) the amount of fuel leakage through the reaction front decreases with an increase of radiative heat transfer and the decrease of the gas flow velocity and mass transfer coefficient;

(iii) extinction occurs due to lower porosity of the porous medium, higher volumetric heat transfer from the porous medium to the gas, higher radiative heat transfer from the porous medium and higher heat losses from the porous medium to the environment; and

(iv) the extinction limit in terms of heat loss coefficient decreases due to the increase of the radiation-conduction parameter and the decrease of gas flow velocity while it becomes higher due to effective diffusivity compared to molecular diffusivity.

So the current study can quantify the effect of various transport mechanisms that control the propagation and extinction of combustion wave of the present phenomena. From practical point of view, since the focus of investigation of smoldering combustion, DPF regeneration process and SHS is to control the propagation of combustion wave, thus the observations presented above could be applied for the development of new technology. Before going to apply them, one should keep in mind that the present theoretical analysis has been performed for oxygen-limited opposed flow combustion with single-step reaction. On the contrary, there are a variety of possibilities to occur within these processes, e.g., forward flow, fuel-limited and multi-step reaction mechanisms. Therefore, it might be required further study to investigate these phenomena.

3.6 Conclusions

A one-dimensional model for the combustion of solid fuel deposited over an inert porous medium has been investigated using large activation energy asymptotic. Analytical expressions for the moving speed of the reaction front as well as temperature and species distributions are derived. From the validation of the solution of present model, it is found that the current model predicts correctly the qualitative trend of smolder propagation with the variation of the gas flow velocity. The effect of radiation on the reaction front structure and peak temperature of the porous medium shows the similar tendency as observed in smoldering combustion. Furthermore, the behavior of the moving speed of the reaction front with the variation of the heat transfer coefficient, the mass transfer coefficient and the heat loss coefficient have been justified by the previous findings available in the literature of smoldering combustion. Therefore, it is anticipated that the present model could be applicable and adaptable for predicting the characteristics of smoldering combustion and hence SHS process. In this regard, the features of combustion wave of the present phenomena observed over a wide range of conditions can also be used in the other processes. As the present model is developed taking into

account all of the transport mechanisms controlling the combustion wave of smoldering combustion, DPF regeneration process and SHS, the analytical expressions derived here can be readily and suitably used to examine the behavior of combustion wave so that the acquired knowledge is utilized for the development of new technology. Despite having the consequence of simplifications, the present study is also able to quantify the effect of physical parameters (such as, the heat transfer coefficient, the radiation heat transfer, the porosity and the effective diffusivity) at any point that are not possible by the studies available to date due to numerical solution or the lack of mechanisms considered in them. In this sense, the present work is valuable in academia as well as for practical applications.

Chapter 4

Forward and Opposed Combustion of Solid Fuel over an Inert Porous Medium

4.1 Introduction

One-dimensional propagation of a combustion wave is characterized as two modes: forward and opposed. In forward mode, the combustion wave propagates in the same direction as the oxidizer flow while in opposed mode it propagates in the opposite direction of oxidizer flow. This relative direction of oxidizer flow and the propagation of a combustion wave is a very important factor of the combustion of solid fuel which is rather unclear in many realistic configurations [116]. So the forward and opposed modes have been the focus of research to date in the fire safety context or technological point of view.

Purely forward and purely opposed mode are quite rare in fire safety problems, because the real-world fire-safety problems are deemed as coupled-forward and -opposed modes [22]. Yet, most of the studies in the field of fire safety (e.g., [13, 14, 16-19, 117]) focused on forward and opposed modes separately; while both of these modes comparatively studied in [20, 109, 118, 119]. The qualitative and quantitative differences between the two modes are identified experimentally in [109, 118, 119]. However, experiments have some limitations to investigate the responses of these modes to the important mechanisms of the process. Also their focus was to explore only the steady except unsteady features of the combustion wave.

On the other hand, there are some noticeable numerical studies [16-20] that mainly concentrated on finding the conditions of steady propagation of forward and opposed modes for the purpose of fire safety control. Among them, Rein et al. [20] only examined both modes in microgravity conditions considering the heat loss but neglecting the buoyancy effect. They found that the inclusion of the

external heat loss to the exterior makes a significant difference in the combustion wave characteristics. But the model was solved numerically that is relatively time-consuming and difficult for anybody to be carried out for a physical parameter if required. Even they conceded that modifications in the ignition protocol significantly affect the results.

Apart from fire safety context, the necessity of identifying the insights of different features of forward and opposed modes of the propagation of a combustion wave is also highly admired in technological applications. Very recently, both forward and opposed modes have been recognized in diesel particulate filter (DPF) regeneration process [120, 121] by which solid particulate matters trapped in the porous channel walls of a DPF are burnt out at a steady state. Due to unknown aspects of the combustion of solid matters in the DPF, uncontrolled and unsteady combustion occurs during the DPF regeneration process. Consequently, the DPF may encounter a loss of its mechanical integrity and sometimes it undergoes complete damage and so fails to trap particulate matters from the exhaust gas. Thus the regeneration process poses a major technological challenge. So it has attracted much attention to reveal the unsteady conditions as well as the underlying insights of the combustion of solid particulate matters in the DPF.

Therefore, it is evident that both forward and opposed modes of a combustion wave are jointly observed in fire-safety problems and in technological applications and the reasons of their steady and unsteady characteristics are not fully uncovered to the scientific community. In particular, unsteady conditions needs to be found out because most hazardous circumstances and technological problems are often brought about by unsteady behaviors of the combustion wave. So the motivation for comparative study of two modes is to provide the line of demarcation of their unsteady behaviors beyond which the combustion wave might demonstrate uncontrolled and unpredictable characteristics so that one can control fire-hazard or protect a system from technological failure.

In this chapter, the upgraded model developed in Chapter 3 is used to study both forward and opposed modes combustion of solid fuel over an inert porous medium. To accomplish this goal, the governing equations formulated in Chapter 3 have been solved here for forward mode with appropriate boundary conditions. Large activation energy asymptotics is employed to obtain analytical expressions of the moving speed of the reaction front, temperature and species profiles. The corresponding

solutions of opposed mode are utilized from the Chapter 3. Then the effects of the thermal conductivity of the porous medium, initial mass fraction of oxidizer, heat transfer coefficient and the gas flow velocity, on the moving speed of the reaction front of forward and opposed modes have been examined with a view to identifying the line of demarcation of unsteady behaviors of reaction fronts that can be applied in fire safety as well as in the development of new technology.

4.2 Mathematical formulation

The model configuration employed here is illustrated in Figure 4.1. The figure represents an infinitely long porous medium over which solid fuels are deposited. Oxidizer enters into the reaction zone from left to right through the porous medium. In the reaction zone, oxidizer reacts with solid fuels and generates heat. Accumulating enough heat from the heterogeneous exothermic oxidation of solid fuel, the reaction front propagates in the direction of fresh fuel and the gas flow velocity. For such type of phenomena, there are some important mechanisms that must be considered into a model have been elucidated in [122]. For simplicity reasons, the reaction mechanism is modeled here using a single-step exothermic heterogeneous reaction and so it is assumed that solid fuel is converted (oxidized) directly to the gaseous product:

1 g (unburned solid fuel) + n O_2 → (1+ n) (gaseous product),

where n is the mass of oxygen per mass of fuel ratio.

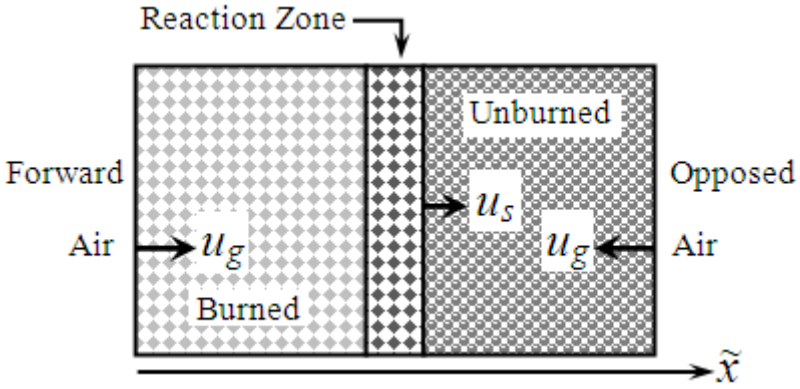

Figure 4.1: Physical configuration of the model.

The model used here was developed by Roy et al. [122]; and according to this, the volume-averaged energy equations for porous material and gas, and species equation for gas and fuel are

$$(1-\varepsilon)\rho_m c_m \frac{\partial T_m}{\partial \tilde{t}} = (1-\varepsilon)\lambda_m \frac{\partial^2 T_m}{\partial \tilde{x}^2} + QW - h\left(T_m - T_g\right) - \frac{\partial q_r}{\partial \tilde{x}} - h_{ex}\left(T_m - T_u\right), \tag{4.1}$$

$$\varepsilon\rho_g c_g \frac{\partial T_g}{\partial \tilde{t}} + \varepsilon\rho_g c_g u_g \frac{\partial T_g}{\partial \tilde{x}} = \varepsilon\lambda_g \frac{\partial^2 T_g}{\partial \tilde{x}^2} + h\left(T_m - T_g\right), \tag{4.2}$$

$$\varepsilon\rho_g \frac{\partial Y_O}{\partial \tilde{t}} + \varepsilon\rho_g u_g \frac{\partial Y_O}{\partial \tilde{x}} = \varepsilon\rho_g \frac{\partial}{\partial \tilde{x}}\left(D_{eff} \frac{\partial Y_O}{\partial \tilde{x}}\right) - nW - \frac{h_m \rho_g}{d}\left(Y_O - Y_{O,u}\right), \tag{4.3}$$

$$\varepsilon\rho_f \frac{\partial Y_F}{\partial \tilde{t}} = -W. \tag{4.4}$$

Here T_m, ρ_m and T_g, ρ_g are the volume-averaged temperature and the density of the porous medium and gas, respectively, ε is the porosity of the porous medium, ρ_f is the density of fuel, Y_O and Y_F are the volume-averaged oxidizer and fuel mass fractions, u_g is the gas flow velocity, Q is the fuel mass based heat of reaction, h is the volumetric heat transfer coefficient from the porous medium to gas, q_r represents the radiative heat flux from the porous medium, h_{ex} is the heat loss coefficient from the porous medium to the environment and h_m is the mass transfer coefficient from the gas stream to the surface of fuel, d is the pore diameter and W is the rate of the chemical reaction, given by an Arrhenius law

$$W = \varepsilon(1-\varepsilon) A \rho_f \rho_g Y_O Y_F \exp\left[-E / RT_m\right], \tag{4.5}$$

where A is a pre-exponential factor, taken to be constant, R is the universal gas constant, and E is the activation energy.

For forward mode, the appropriate boundary conditions to be satisfied by Eqs. (4.1)–(4.4) are

$$\tilde{x} = -\tilde{L}_2 : \; T_m = T_u, \; T_g = T_u, \; Y_O = Y_{O,u}, \; Y_F' = 0, \tag{4.6}$$

$$\tilde{x} = \tilde{L}_1 : \; T_m = T_u, \; T_g = T_u, \quad Y_O' = 0, \; Y_F = Y_{F,u}. \tag{4.7}$$

For opposed mode, the boundary conditions to be satisfied by Eqs. (4.1)–(4.4) are

$$\tilde{x} = -\tilde{L}_2 : \; T_m = T_u, \; T_g = T_u, \; Y_O = Y_{O,u}, \; Y_F = Y_{F,u}, \tag{4.8}$$

$$\tilde{x} = \tilde{L}_1 : \; T_m = T_u, \; T_g = T_u, \quad Y_O^{'} = 0, \; Y_F^{'} = 0. \tag{4.9}$$

As in [118], the volumetric heat transfer coefficient, h, used in Eqs. (4.1) and (4.2) is determined by Fatehi and Kaviany [62] as,

$$h = \frac{6(1-\varepsilon) Nu \lambda_g}{d^2}. \tag{4.10}$$

In Eq. (4.10), the interfacial solid-gas surface area of the porous medium $A_{sg}/V = 6(1-\varepsilon)/d$, where A_{sg} is the solid-gas surface area and d is the pore diameter; the correlation for the interstitial Nusselt number, Nu, is given by Wakao and Kaguei [87] as,

$$Nu = 2 + 1.1 \mathrm{Pr}^{1/3} \mathrm{Re}^{0.6}, \quad 15 < \mathrm{Re} < 8500. \tag{4.11}$$

Here, the Prandtl and Reynolds numbers are defined as $\mathrm{Pr} = \nu_g/\kappa$ and $\mathrm{Re} = \varepsilon u_g d/\nu_g$, respectively, and ν_g and κ are respectively the kinematic viscosity and the thermal diffusivity of the gas.

The solid-gas mass transfer coefficient, h_m, appeared in Eq. (4.3) indicates the mass diffusion of oxygen from the gas stream to the surface of fuel and is included in the model according to [20]. It is defined by Fatehi and Kaviany [62] as,

$$h_m = \frac{6(1-\varepsilon) ShD}{\varepsilon d}, \tag{4.12}$$

where the interstitial mass transfer Sherwood number is correlated by Wakao and Kaguei [87],

$$h_m = \frac{6(1-\varepsilon) ShD}{\varepsilon d}, \tag{4.13}$$

The Schmidt number Sc is defined as $Sc = \nu_g/D$.

Gas phase radiation is neglected here while the radiation heat transfer from the solid has been included. It is because the temperature of the porous medium is quite high owing to exothermic reaction between the gas and solid fuel on the porous medium. The radiant heat flux term which is valid for an optical thick medium is expressed by the Rosseland diffusion approximation [102]:

$$q_r = -\frac{4\sigma}{3a}\frac{\partial T_m^4}{\partial x}, \tag{4.14}$$

where σ is the Stefan-Boltzmann constant and a is the Rosseland extinction coefficient.

The effective diffusivity, D_{eff}, introduced in Eq. (4.3) is defined by [103] as

$$\frac{1}{D_{eff}} = \left(\frac{\Omega}{\varepsilon}\right)\left(\frac{1}{D} + \frac{1}{D_K}\right), \tag{4.15}$$

where the Knudsen diffusion coefficient, D_K, is given by [104] as

$$D_K = \frac{4}{3} d \sqrt{\frac{RT_g}{2\pi M}}. \tag{4.16}$$

Here M is the molar mass of the gas. In Eq. (4.15), Ω is a tortuosity factor which accounts for the extension of the path that a gas must pass through the porous medium. The tortuosity factor typically depends on the structure of the porous medium and it is normally determined experimentally. The value of Ω is assumed here to be 2 [105].

4.3 Forward mode

The detailed derivation of the analytical expressions of the moving speed of the reaction front, temperature and species profiles of forward mode will be described. With a view to achieving this target, the following group of dimensionless variables and parameters are introduced:

$$\begin{aligned}
&\hat{x} = \frac{\tilde{x}}{x_*},\ \hat{t} = \frac{\tilde{t}}{t_*},\ u_* = \frac{x_*}{t_*},\ x_* = \sqrt{\frac{t_*\lambda_m}{\rho_m c_m}},\ t_* = \frac{\beta^2 \exp\left[E/RT_{ad}\right]}{A\rho_g Y_{O,u}},\\
&y_O = \frac{Y_O}{Y_{O,u}},\ y_F = \frac{Y_F}{Y_{F,u}},\ S = \frac{T_m - T_u}{T_{ad} - T_u},\ \theta = \frac{T_g - T_u}{T_{ad} - T_u},\\
&\delta = \frac{T_{ad} - T_u}{T_u},\ N_R = \frac{16\sigma T_u^3}{3\lambda_m a},\ \alpha = \frac{T_{ad} - T_u}{T_{ad}},\ \beta = \frac{E\left(T_{ad} - T_u\right)}{RT_{ad}^2},\ \gamma = \frac{QY_{F,u}}{c_m\left(T_{ad} - T_u\right)},\\
&\Pi = \frac{4}{3}\frac{d}{D}\sqrt{\frac{RT_u}{2\pi M}},\ \Omega_{st} = \frac{Y_{F,u}}{Y_{O,u}},\ K^f = \frac{ht_*}{\rho_m c_m},\ K_{ex}^f = \frac{h_{ex}t_*}{\rho_m c_m},\ K_m^f = \frac{h_m t_*}{d},\\
&c = \frac{c_g}{c_m},\ r_g = \frac{\rho_g}{\rho_m},\ l = \frac{\lambda_g}{\lambda_m},\ u = \frac{u_g}{u_*},\ r_f = \frac{\rho_f}{\rho_m},\ Le = \frac{\lambda_g}{\rho_g D c_g} = 1.
\end{aligned} \tag{4.17}$$

Therefore, the system of Eqs. (4.1)–(4.4) becomes

$$\frac{\partial S}{\partial \hat{t}}=\frac{\partial}{\partial \hat{x}}\left[\left\{1+\frac{N_R}{1-\varepsilon}\left(1+\delta S\right)^3\right\}\frac{\partial S}{\partial \hat{x}}\right]+\beta^2 r_f \varepsilon\gamma w-\frac{K^f}{1-\varepsilon}\left(S-\theta\right)-\frac{K_{ex}^f S}{1-\varepsilon}, \tag{4.18}$$

$$r_g c\frac{\partial \theta}{\partial \hat{t}}+r_g cu\frac{\partial \theta}{\partial \hat{x}}=l\frac{\partial^2 \theta}{\partial \hat{x}^2}+\frac{K^f}{\varepsilon}\left(S-\theta\right), \tag{4.19}$$

$$\begin{aligned}&\frac{Ler_g c}{l}\frac{\partial y_O}{\partial \hat{t}}+\left[\frac{Ler_g cu}{l}-\frac{\varepsilon\Pi\delta}{2\Omega\sqrt{1+\delta\theta}\left(1+\Pi\sqrt{1+\delta\theta}\right)^2}\frac{\partial \theta}{\partial \hat{x}}\right]\frac{\partial y_O}{\partial \hat{x}}\\&=\frac{\varepsilon\Pi\sqrt{1+\delta\theta}}{\Omega\left(1+\Pi\sqrt{1+\delta\theta}\right)}\frac{\partial^2 y_O}{\partial \hat{x}^2}-\frac{\beta^2 Ler_f cn\Omega_{st}\left(1-\varepsilon\right)}{l}w-\frac{LeK_m^f r_g c}{\varepsilon l}\left(y_O-1\right),\end{aligned} \tag{4.20}$$

$$\frac{\partial y_F}{\partial \hat{t}}=-\beta^2\left(1-\varepsilon\right)w, \tag{4.21}$$

where

$$w=y_O y_F\exp\left[\frac{-\beta\left(1-S\right)}{1-\alpha\left(1-S\right)}\right]. \tag{4.22}$$

Again using the transformations $x=\hat{x}+f\left(t\right)$ and $t=\hat{t}$ for the moving coordinate attached to the reaction front, Eqs. (4.18)–(4.21) reduce to

$$\frac{\partial S}{\partial t}+f_t\frac{\partial S}{\partial x}=\frac{\partial}{\partial x}\left[\left\{1+\frac{N_R}{1-\varepsilon}\left(1+\delta S\right)^3\right\}\frac{\partial S}{\partial x}\right]+\beta^2 r_f \varepsilon\gamma w-\frac{K^f}{1-\varepsilon}\left(S-\theta\right)-\frac{K_{ex}^f S}{1-\varepsilon}, \tag{4.23}$$

$$r_g c\frac{\partial \theta}{\partial t}+r_g c\left(u+f_t\right)\frac{\partial \theta}{\partial x}=l\frac{\partial^2 \theta}{\partial x^2}+\frac{K^f}{\varepsilon}\left(S-\theta\right), \tag{4.24}$$

$$\begin{aligned}&\frac{Ler_g c}{l}\frac{\partial y_O}{\partial t}+\left[\frac{Ler_g c\left(u+f_t\right)}{l}-\frac{\varepsilon\Pi\delta}{2\Omega\sqrt{1+\delta\theta}\left(1+\Pi\sqrt{1+\delta\theta}\right)^2}\frac{\partial \theta}{\partial x}\right]\frac{\partial y_O}{\partial x}\\&=\frac{\varepsilon\Pi\sqrt{1+\delta\theta}}{\Omega\left(1+\Pi\sqrt{1+\delta\theta}\right)}\frac{\partial^2 y_O}{\partial x^2}-\frac{\beta^2 Ler_f cn\Omega_{st}\left(1-\varepsilon\right)}{l}w-\frac{LeK_m^f r_g c}{\varepsilon l}\left(y_O-1\right),\end{aligned} \tag{4.25}$$

$$\frac{\partial y_F}{\partial t} + f_t \frac{\partial y_F}{\partial x} = -\beta^2 (1-\varepsilon) w, \tag{4.26}$$

The corresponding boundary conditions (4.6)–(4.7) become

$$x = -L_2 + f(t): \quad S = 0, \quad \theta = 0, \quad y_O = 1, \quad y_F' = 0, \tag{4.27}$$

$$x = L_1 + f(t): \quad S = 0, \quad \theta = 0, \quad y_O' = 0, \quad y_F = 1. \tag{4.28}$$

4.3.1 Asymptotic analysis

4.3.1.1 Combustion zone

In the preheat region $x > 0$, the source term in the conservation equations is exponentially small and in the burned region $x < 0$, all the chemical reaction has gone to completion due to the assumed complete oxygen consumption. So the source terms are negligible in these regions.

To analyze the problem theoretically, the difficulty arises due to the coefficient $1 + N_R(1+\delta S)^3/(1-\varepsilon)$ of Eq. (4.23). In [122], it was assumed approximately to Γ, where

$$\Gamma = \begin{cases} 1 + N_R (1+\delta)^3 / (1-\varepsilon), & x \le 0 \\ 1 + N_R \left\{1 + (1+\delta)^3\right\} / 2(1-\varepsilon), & x > 0 \end{cases}. \tag{4.29}$$

Moreover, Eq. (4.25) cannot be solved analytically because of the variable coefficients of y_O' and y_O'' of the equation. But this difficulty was circumvented in [122] by taking the coefficients of y_O'' and y_O' as $B_1 = \varepsilon\Pi\sqrt{1+\delta\theta_f} \Big/ \Omega\left(1+\Pi\sqrt{1+\delta\theta_f}\right)$ and $B_2 = \varepsilon\delta\left(\partial\theta/\partial x\right)_{x=x_f^+} \Big/ 2\Omega\Pi$, respectively, where θ_f is the maximum temperature of gas at $x = x_f$.

Therefore, for large time i.e., the steady-state combustion front, the system of equations (4.23)–(4.26) in the outer regions become

$$f_t \frac{\partial S}{\partial x} = \frac{\partial}{\partial x}\left[\left\{1 + \frac{N_R}{1-\varepsilon}(1+\delta S)^3\right\}\frac{\partial S}{\partial x}\right] - \frac{K^f}{1-\varepsilon}(S-\theta) - \frac{K_{ex}^f S}{1-\varepsilon}, \tag{4.30}$$

$$r_g c\left(u+f_t\right)\frac{\partial\theta}{\partial x}=l\frac{\partial^2\theta}{\partial x^2}+\frac{K^f}{\varepsilon}\left(S-\theta\right), \tag{4.31}$$

$$\left[\frac{Ler_g c\left(u+f_t\right)}{l}-B_2\right]\frac{\partial y_O}{\partial x}=B_1\frac{\partial^2 y_O}{\partial x^2}-\frac{LeK_m^f r_g c}{\varepsilon l}\left(y_O-1\right), \tag{4.32}$$

$$f_t\frac{\partial y_F}{\partial x}=0 \tag{4.33}$$

Now it is often observed that oxidizer is fully consumed at the reaction front (i.e., $y_O = 0$ at $x = 0$) [12, 109] suggesting that the system is controlled by oxidizer. Thus the solutions of (4.32) in this zone become

$$y_O=\begin{cases}1-\exp\left[\mu_1 x\right], & x<0\\ 0, & x>0\end{cases} \tag{4.34}$$

where

$$\mu_{1,2}=\frac{1}{2}\left\{B\pm\left(B^2+4C\right)^{1/2}\right\},\ B=\frac{Ler_g c\left(u+f_t\right)}{lB_1}-\frac{B_2}{B_1}\quad\text{and}\ C=\frac{LeK_m^f r_g c}{\varepsilon l B_1}. \tag{4.35}$$

Also, if y_F^* is the remained fuel mass fraction at the reaction front (i.e., at $x = 0$), then the solutions of Eq. (4.33) can be written as

$$y_F\left(x<0\right)=y_F^*\quad\text{and}\quad y_F\left(x>0\right)=1. \tag{4.36}$$

Now, from Eq. (4.31) one can find

$$S=\theta+\frac{\varepsilon r_g c\left(u+f_t\right)}{K^f}\frac{\partial\theta}{\partial x}-\frac{\varepsilon l}{K^f}\frac{\partial^2\theta}{\partial x^2}. \tag{4.37}$$

Substitution of Eq. (4.37) into (4.30) gives

$$\begin{aligned}&\frac{\partial^4\theta}{\partial x^4}-\left[\frac{r_g c}{l}\left(u+f_t\right)+\frac{f_t}{\Gamma}\right]\frac{\partial^3\theta}{\partial x^3}-\left[\frac{K^f}{\varepsilon l}+\frac{K^f+K_{ex}^f}{\left(1-\varepsilon\right)\Gamma}-\frac{r_g cf_t}{l\Gamma}\left(u+f_t\right)\right]\frac{\partial^2\theta}{\partial x^2}\\&+\left[\frac{r_g c\left(K^f+K_{ex}^f\right)}{l\left(1-\varepsilon\right)\Gamma}\left(u+f_t\right)+\frac{K^f f_t}{l\varepsilon\Gamma}\right]\theta'+\frac{K^f K_{ex}^f}{l\varepsilon\left(1-\varepsilon\right)\Gamma}\theta=0.\end{aligned} \tag{4.38}$$

To obtain the solutions of Eq. (4.38), it is necessary to find the solutions of the corresponding characteristic polynomial:

$$m^4 - \left[\frac{r_g c}{l}(u+f_t)+\frac{f_t}{\Gamma}\right]m^3 - \left[\frac{K^f}{\varepsilon l}+\frac{K^f+K^f_{ex}}{(1-\varepsilon)\Gamma}-\frac{r_g c f_t}{l\Gamma}(u+f_t)\right]m^2 + \left[\frac{r_g c\left(K^f+K^f_{ex}\right)}{l(1-\varepsilon)\Gamma}(u+f_t)+\frac{K^f f_t}{l\varepsilon\Gamma}\right]m+\frac{K^f K^f_{ex}}{l\varepsilon(1-\varepsilon)\Gamma}=0. \tag{4.39}$$

Considering the appropriate values of the parameters, it can be shown that the characteristic polynomial must have two positive roots, m_1 and m_2 and two negative roots, m_3 and m_4, to define the finite solutions of the Eq. (4.38).

Once Eq. (4.38) is solved, the temperature of the porous material, S, is determined from (4.37). Then the temperatures of the porous material and gas are given by

$$S(x)=\begin{cases} p_1 a_1 \exp[m_1 x]+p_2 a_2 \exp[m_2 x], & x<0 \\ p_3 a_3 \exp[m_3 x]+p_4 a_4 \exp[m_4 x], & x>0 \end{cases} \tag{4.40}$$

$$\theta(x)=\begin{cases} a_1 \exp[m_1 x]+a_2 \exp[m_2 x], & x<0 \\ a_3 \exp[m_3 x]+a_4 \exp[m_4 x], & x>0 \end{cases} \tag{4.41}$$

where

$$p_i = 1+\frac{\varepsilon r_g c(u+f_t)m_i}{K^f}-\frac{\varepsilon l m_i^2}{K^f}, \quad i=1,2,3,4;$$

and the constants a_1, a_2, a_3 and a_4 are found later.

Thus the temperature of the porous medium at the reaction front (i.e., $x = 0$) can be expressed as $s_f = S(0) = p_1 a_1 + p_2 a_2$.

4.3.1.2 Reaction zone

As the activation energy is assumed to be very large, the reaction zone becomes very thin. So the reaction zone is elongated introducing $\xi = \beta x$ in order to obtain the jump conditions of the temperature and species profiles. It should be mentioned that temperature and oxygen mass fraction will be

spatially independent to leading order. Thus the quantities S, θ, y_O and y_F are sought in asymptotic series in β^{-1} as

$$S \sim s_f(\tau) + \beta^{-1} S^1(\xi,\tau) + \cdots, \tag{4.42}$$

$$\theta \sim \theta_f(\tau) + \beta^{-1} \theta^1(\xi,\tau) + \cdots, \tag{4.43}$$

$$y_O \sim \beta^{-1} y_O^1(\xi,\tau) + \cdots, \tag{4.44}$$

$$y_F \sim y_F^0(\xi,\tau) + \cdots . \tag{4.45}$$

Substituting (4.42)–(4.45) into (4.23)–(4.26), the following equations are found

$$\Gamma^{in} \frac{\partial^2 S^1}{\partial \xi^2} + r_f \varepsilon \gamma \omega = 0, \tag{4.46}$$

$$\frac{\partial^2 \theta^1}{\partial \xi^2} = 0, \tag{4.47}$$

$$B_1 \frac{\partial^2 y_O^1}{\partial \xi^2} - \frac{Lenr_f c\Omega_{st}}{l}(1-\varepsilon)\omega = 0, \tag{4.48}$$

$$f_\tau \frac{\partial y_F^0}{\partial \xi} + (1-\varepsilon)\omega = 0, \tag{4.49}$$

where

$$\omega = y_O^1 y_F^0 \exp\left[-\frac{\beta(1-s_f)}{1-\alpha(1-s_f)}\right] \exp\left[\frac{S^1}{\left\{1-\alpha(1-s_f)\right\}^2}\right]. \tag{4.50}$$

Therefore, matching the solutions of the outer variables yields the following jump conditions

$$[S]_-^+ = 0, \quad [\theta]_-^+ = 0, \quad [y_O]_-^+ = 0, \quad [y_F]_-^+ = 1 - y_F^*, \tag{4.51}$$

$$\left[\frac{\partial S}{\partial x}\right]_{0^-}^{0^+} = \frac{\varepsilon\gamma r_f f_\tau (1-y_F^*)}{(1-\varepsilon)\Gamma^{in}}, \quad \left[\frac{\partial \theta}{\partial x}\right]_-^+ = 0, \quad \left[\frac{\partial y_O}{\partial x}\right]_-^+ = -\frac{nLer_f c\Omega_{st} f_\tau}{lB_1}(1-y_F^*). \tag{4.52}$$

From the last equality of (4.52), the amount of remained fuel mass fraction at the reaction front is obtained as

$$y_F^* = 1 + \frac{lB_1\mu_1}{nLer_f c\Omega_{st} f_\tau}. \tag{4.53}$$

Again, Eqs. (4.46) and (4.48) give the similarity solution

$$y_O^1 = -\frac{(1-\varepsilon)\Gamma^{in} nLec\Omega_{st}}{\varepsilon\gamma lB_1} S^1 \tag{4.54}$$

Now, from (4.46) and (4.49) one can easily find

$$y_F^0 = 1 + \frac{(1-\varepsilon)\Gamma^{in}}{\varepsilon\gamma r_f f_t}\frac{\partial S^1}{\partial \xi} \tag{4.55}$$

Upon substitution of (4.54) and (4.55) into (4.46) give

$$\frac{\partial^2 S^1}{\partial \xi^2}\Bigg/\left\{1 + \frac{(1-\varepsilon)\Gamma^{in}}{\varepsilon\gamma r_f f_t}\frac{\partial S^1}{\partial \xi}\right\} = \frac{(1-\varepsilon) nLer_f c\Omega_{st}}{lB_1\Gamma^{in}} \exp\left[-\frac{\beta(1-s_f)}{1-\alpha(1-s_f)}\right]$$
$$\times S^1 \exp\left[\frac{S^1}{\left\{1-\alpha(1-s_f)\right\}^2}\right]. \tag{4.56}$$

Integrating Eq. (4.56) from 0 to +∞, the following relation is obtained

$$Log\left[1 + \frac{(1-\varepsilon)\Gamma^{in}}{\varepsilon\gamma r_f f_t}\left(\frac{\partial S}{\partial x}\right)_{x=0}\right] = \frac{(1-\varepsilon)^2 nLec\Omega_{st}\left\{1-\alpha(1-s_f)\right\}^2}{\varepsilon\gamma f_t lB_1} \exp\left[-\frac{\beta(1-s_f)}{1-\alpha(1-s_f)}\right]$$
$$\times\left[S(0) - \left\{1-\alpha(1-s_f)\right\}^2\right] \exp\left[\frac{S[0]}{\left\{1-\alpha(1-s_f)\right\}^2}\right]. \tag{4.57}$$

Thus the dimensionless moving speed of the reaction front, f_t, is implicitly related to the other parameters by the expression (4.57). Having obtained f_t from (4.57), one can readily find the dimensional moving speed of the reaction front, $u_s = x_* f_t / t_*$, using the relations given in (4.17).

4.4 A brief of solutions of opposed mode

Details of the analysis have been presented in [122]. The important expression of the analysis is the implicit relation of determining the moving speed of the reaction front, u_s, as given below:

$$2\left[\frac{nLec\left(1-\varepsilon\right)\Omega_{st}\Gamma^{in}\left\{1-\alpha\left(1-s_f\right)\right\}^2}{\varepsilon\gamma lB_1\mu_1}\right]^2\frac{nLec\left(1-\varepsilon\right)\Omega_{st}f_0^*A\lambda_m\rho_g\rho_fY_{O,u}e^{-\beta/\alpha}}{lB_1\rho_m^2u_s^2c_m\beta^2}$$
$$=\exp\left[\frac{\beta\left(1-s_f\right)}{1-\alpha\left(1-s_f\right)}-\psi\chi\right], \tag{4.58}$$

in which $\psi\chi = 1.344\psi - 4\psi^2(1-\psi)/(1-2\psi) + 3\psi^3 - \ln[1-4\psi^2]$ for $-0.2 < \psi < 0.5$.

The value of ψ can also be found from the definition $\psi = S'(0^+)/\{S'(0^+) - S'(0^-)\}$.

The temperature and species profiles are similar to Eqs. (4.40), (4.41), (4.34) and (4.36). In this case, m_1, m_2, m_3, m_4 are the solutions of

$$m^4-\left\{\frac{1}{\Gamma}+\frac{r_gc\left(1-U\right)}{lU}\right\}m^3-\left\{\frac{K}{\varepsilon l}+\frac{K+K_{ex}}{\left(1-\varepsilon\right)\Gamma}-\frac{r_gc\left(1-U\right)}{lU\Gamma}\right\}m^2$$
$$+\frac{1}{\Gamma}\left\{\frac{K}{\varepsilon l}+\frac{\left(K+K_{ex}\right)r_gc\left(1-U\right)}{l\left(1-\varepsilon\right)U}\right\}m+\frac{KK_{ex}}{\varepsilon\left(1-\varepsilon\right)l\Gamma}=0, \tag{4.59}$$

where $K = h\lambda_m/\rho_m^2u_s^2c_m^2$, $K_{ex} = h_{ex}\lambda_m/\rho_m^2u_s^2c_m^2$, $U = u_s/u_g$ and other constants are same as the present analysis.

The following is the detail of the effects of various physical parameters on the moving speed of the reaction front of both forward and opposed combustion using the relations (4.57) and (4.58), respectively.

4.5 Results and discussion

For the validation of the solutions of forward mode, a comparison of the present solutions with the experimental data of Torero and Fernandez-Pello [123] and the numerical data of Leach et al. [18] is shown in Figure 4.2. All of the parameters are taken from Torero and Fernandez-Pello [123] except Q = 32300 kJ/kg [124], $A = 3.92\times10^{11}$ m^3/(kg s) [12] and others required data are T_{ad} = 1800 K, $Y_{F,u}$ =

0.30 as assumed in the present study. Since Leach et al. [18] made a comparison between their computational results and the experimental data of Torero and Fernandez-Pello [123], hence both of these two data are presented here. It is seen from the figure that the present solutions agree very well with the experimental data of Torero and Fernandez-Pello [123] and numerical data of Leach et al. [18].

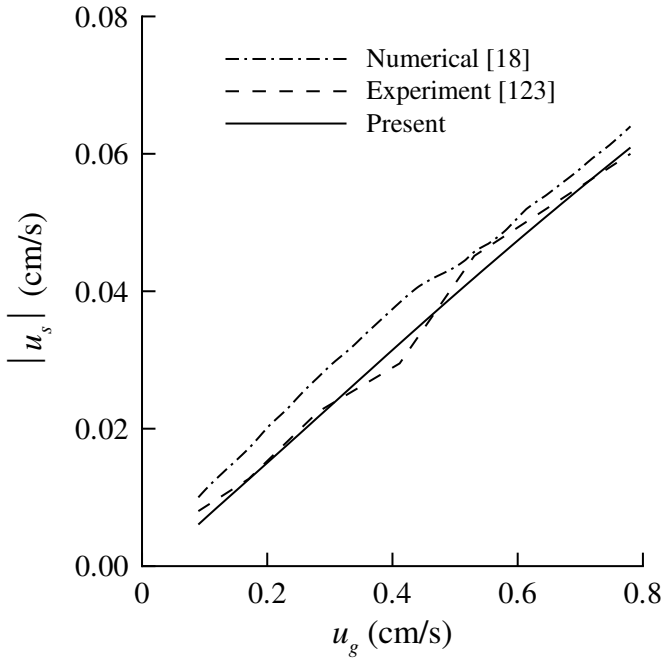

Figure 4.2: Variation of the moving speed of the reaction front with the gas flow velocity. Experimental data are taken from Torero and Fernandez-Pello [123] and numerical data are from Leach et al. [18].

In Figure 4.3, the temperature profiles of forward and opposed modes are presented. In this study, the thermophysical properties of the porous medium and gas are taken from [83] and [21], respectively; while others are $\rho_f = 550$ kg/m^3, $Y_{O,u} = 0.154$ [41], $A = 1.0\times10^{10}$ m^3/kg s [13], $\lambda_m = 0.40$ W/(mK), $\varepsilon = 0.80$, $d = 1.0\times10^{-3}$ m, $\beta = 15$ and $T_0 = 300$ K [122]. From the figure it is found that the reaction front temperature of forward mode is higher than that of opposed mode. This is because in forward mode, the gas is being preheated by the hot porous medium as it enters into the reaction zone passing over the burned region. On the other hand, the hot product gas flows over the fresh fuel

resulting in increasing the temperature of preheat region. For the same reasons, the preheat region of forward mode is wider compared to that of opposed mode. It is also observed that for opposed mode the gas temperature in the preheat zone is lower than the porous medium temperature when its opposite scenario is found in forward mode. Furthermore, the difference between the temperatures of gas and porous medium of opposed mode is larger than that of forward mode.

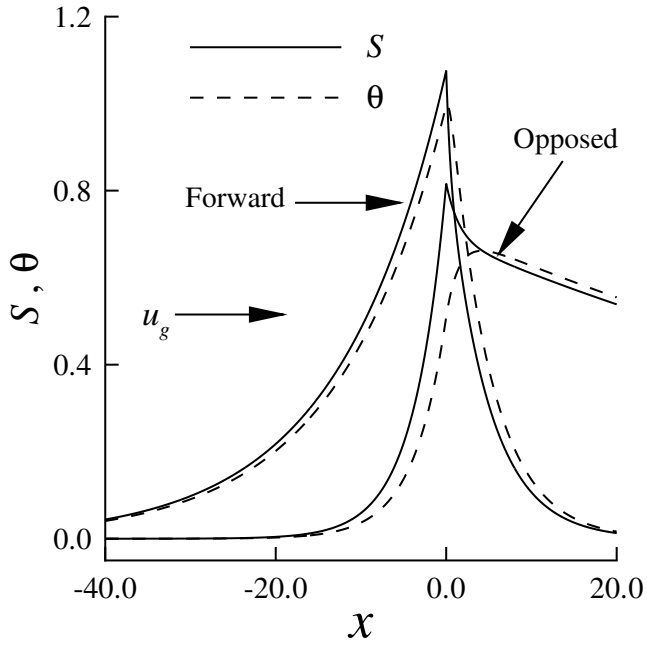

Figure 4.3: Temperature profiles of forward and opposed modes while h_{ex} = 10^4 W/(m^3K), N_R = 0.01 and u_g = 0.4 m/s.

The responses of the moving speed of the reaction front of forward and opposed modes to the thermal conductivity of the porous medium are presented in Figure 4.4. In the figure, the upper branch of the curves lying above the turning point corresponds to stable solutions while the lower branch of the curves corresponds to unstable solutions. As the unstable solutions are not of great physical interest, the main concern of this study will be concentrated on stable solutions. Now, it is well-known that when the thermal conductivity of the porous medium is gradually decreased, the rate of heat conduction through the porous medium also slows down and hence the heat loss from it. Accordingly, with decreasing the thermal conductivity of the porous medium the reaction front temperatures of both

forward and opposed modes continue to increase that make high temperature gradient along the porous medium together with the adjacent fresh fuel. Thus the moving speed of the reaction front of both forward and opposed modes is increased owing to the decrease of the thermal conductivity of the porous medium. However, the steepness of decreasing behavior of forward mode due to the increase of the thermal conductivity of the porous medium is lower than the opposed mode. It is because in forward mode, gas becomes preheated over the burned region before it enters into the reaction front; hot product gas flows over the fresh fuel and there also occurs heat recirculation from the burned region to the preheat region, while in opposed mode there are no such type of supportive conditions. Moreover, it can be inferred that the opposed mode shows unsteady behavior when $\lambda_m > 0.306$, while both modes will exhibit unsteady behaviors if $\lambda_m > 0.572$.

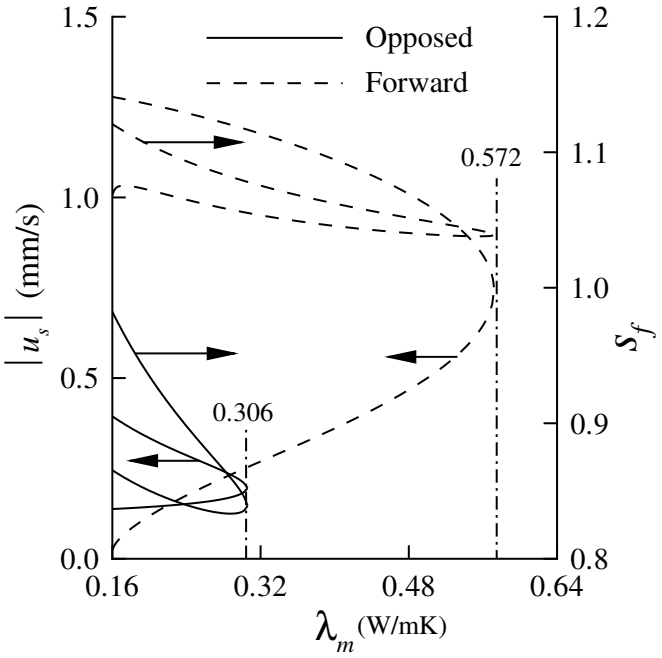

Figure 4.4: Moving speed of the reaction front as a function of thermal conductivity of the porous medium, λ_m, while $h_{ex} = 10^4$ W/(m^{3}K), $u_g = 0.3$ m/s and $N_R = 0.01$.

The effects of the initial mass fraction of oxygen on the moving speed of the reaction front of forward and opposed modes are shown in Figure 4.5. With an increase of $Y_{O,u}$, the moving speed of the reaction front of forward and opposed modes increases linearly away from the boundary of steady

moving of the reaction front. But the rate of increase of the moving speed of opposed mode is steeper than the forward mode. To be clear about this trend, it should be recalled here that the analysis has been performed presuming complete consumption of oxygen at the reaction front. Under this assumption, in opposed mode the larger amount of oxygen relating to higher $Y_{O,u}$ directly attacks the fresh fuel within the regions of preheat as well as the reaction thickness, while in forward mode gas only reacts with that of the reaction thickness. In addition to, it can be deduced from the figure that the opposed mode demonstrates unsteady behavior when $Y_{O,u} < 0.1472$, while both modes will exhibit unsteady behaviors if $Y_{O,u} < 0.116$.

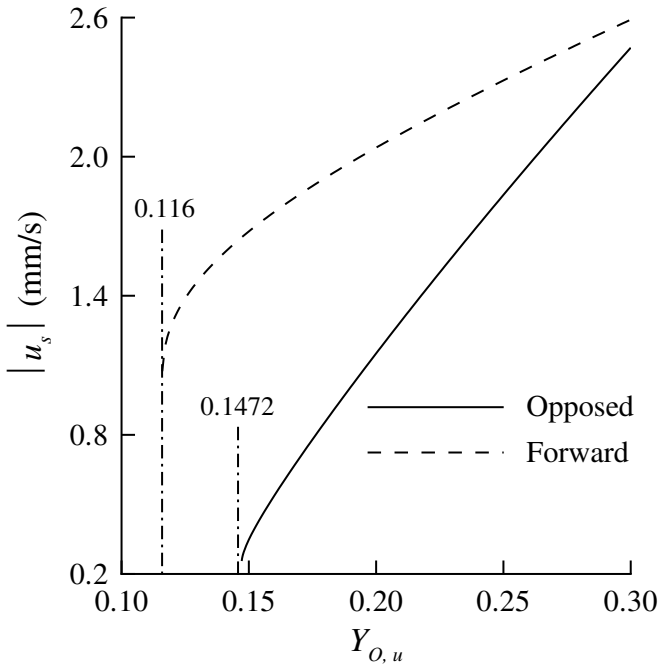

Figure 4.5: Moving speed of the reaction front as a function of initial oxygen mass fraction, $Y_{O,u}$, while $h_{ex} = 10^4$ W/(m^{3}K), $u_g = 0.4$ m/s and $N_R = 0.01$.

The effects of heat transfer coefficient on the moving speed of the reaction front of forward and opposed modes are shown in Figure 4.6. It is seen from the figure that the moving speed of the reaction front of forward mode increases with an increase of the heat transfer coefficient. But the rate of increment of the moving speed of the reaction front gradually slows down owing to the increase of heat transfer coefficient. This is due to the fact that the heat transfer coefficient increases

approximately to $1/d^2$ with the decrease of d. With the increase of heat transfer coefficient, the heat transfer layer of forward mode within which the fresh fuel being heated up decreases. Moreover, the temperature of gas rises through the heat transfer from the porous medium during its flow through the pores of smaller diameter and over the burned region. So, it is understandable that the moving speed of the reaction front of forward mode increases as like as the trend of increasing the heat transfer coefficient when d is decreased. Contrary to this, it decreases owing to the decrease of heat transfer coefficient and eventually the reaction front shows unsteady behavior at a smaller heat transfer rate. The reason is that the heat transfer layer becomes very large for smaller heat transfer coefficient and the reaction front requires a large amount of heat to sustain. As long as the energy required to heat the fresh fuel becomes lower than the generation of heat by the exothermic reaction, the reaction front quenches immediately. But for opposed mode, it is seen that the moving speed of the reaction front monotonically decreases with an increase of heat transfer coefficient. If it is continued to increase, the porous medium will no longer be able to keep enough heat for the reaction front to sustain and finally it exhibits unsteady features at a critical heat transfer rate. Thus the responses to increasing heat transfer coefficient of the moving speed of the reaction front of forward and opposed modes are completely opposite. Furthermore, it is worthy of mentioning that there is an "unsteady solution region" (as shown in the figure for condition (i)) in between of the critical heat transfer coefficients of forward and opposed modes in which the reaction front could demonstrate uncontrolled and unpredictable characteristics.

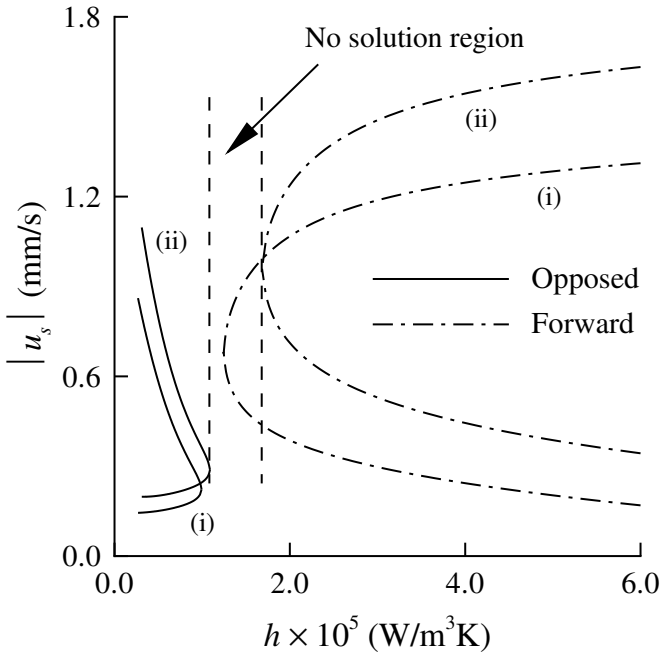

Figure 4.6: Moving speed of the reaction front as a function of volumetric heat transfer coefficient, h, for $h_{ex} = 10^4$ W/(m^{3}K) when (i) $u_g = 0.30$ m/s, $N_R = 0.01$ and (ii) $u_g = 0.40$ m/s, $N_R = 0.02$.

The moving speed of the reaction front of forward and opposed modes varying the inlet gas flow velocity is depicted in Figure 4.7. The figure shows that the moving speed of the reaction front increases linearly with the increase of the gas flow velocity except near the boundary of steady moving. This tendency is similar to as observed in [12]. Also, it is seen that for a given set of parameters, the reaction front becomes unsteady for $u_g < 0.255$ m/s and $u_g < 0.332$ m/s of forward and opposed modes, respectively. It implies that the reaction front of forward mode can sustain at a lower gas flow velocity than the opposed mode. This is obviously due to the fact that in forward mode, the reaction front requires relatively lower energy to heat the adjacent fresh fuel to the reaction temperature as the gas is already preheated during its flow over the burned region. Furthermore, it can be concluded that the moving speed of the reaction front of forward mode is about 3 times higher than that of opposed. Above all, it can be inferred that the reaction fronts of both forward and opposed modes will be unsteady when $u_g < 0.255$ m/s and the opposed mode might show unsteady features if $u_g < 0.332$ m/s.

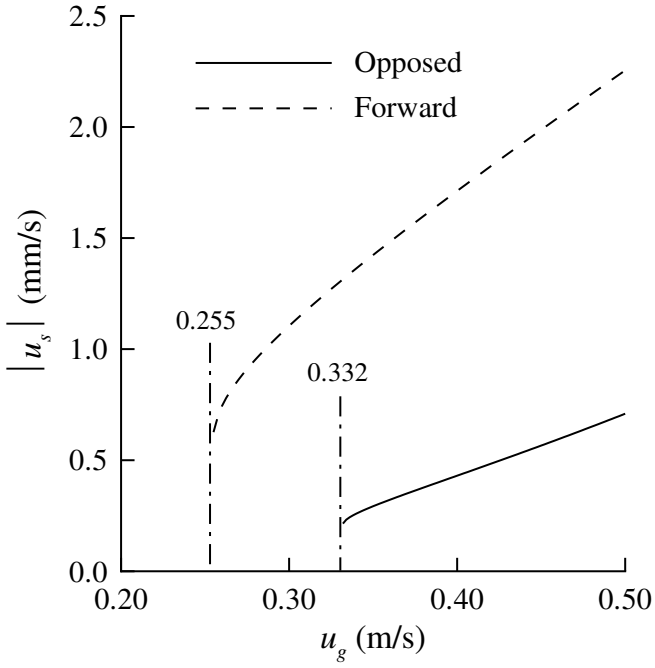

Figure 4.7: Moving speed of the reaction front as a function of gas flow velocity while $h_{ex} = 10^4$ W/(m^{3}K) and $N_R = 0.01$.

4.6 Conclusions

Analytical expressions of forward and opposed combustion behaviors of solid fuel deposited over an inert porous medium are obtained utilizing large activation energy asymptotics. It is found that the reaction fronts of both modes demonstrate unsteady behaviors for higher thermal conductivity porous medium, lower initial mass fraction of oxidizer and lower gas flow velocity. The response of the moving speed of the reaction front of forward mode to increasing heat transfer coefficient is completely opposite to that of opposed mode. In between of the critical heat transfer coefficients of forward and opposed modes, an "unsteady solution region" has been recognized in which the reaction fronts of both modes could be uncontrolled and unpredictable. This comparative study exposes the insights behind the distinguished features of the forward and opposed modes as well as the line of demarcation beyond which the reaction fronts of both modes will be unsteady. In this regard, it will help to make a bridge between these two modes. Also, from practical point of view, this understanding could be used for preventing unwanted fire hazards or, for the development of new technology by utilizing any of the two modes or by combining them that is suitable for a system.

Chapter 5

Combustion of Solid Fuel over an Inert Porous Medium ignited around the Middle

5.1 Introduction

A diesel engine is widely used over the world ranging from light to heavy-duty vehicles because of its higher efficiency and longer durability. The major drawback of the diesel engine is its harmful emissions, especially for particulate matters (PMs)/soot. At present, a variety of ceramic and sintered metal-based diesel particulate filters (DPFs) have been adopted in order to remove emissions from the exhaust gas. Most efficient are the so-called wall flow filters, where the exhaust gas is forced to pass through the porous walls of successive channels. PMs are trapped accordingly over the surface of the channel walls. After the relatively long run, accumulation of PMs could lead to increase a considerable pressure-drop across the filter, resulting in decreasing engine performance. For this reason, the trapped PMs have to be removed to regenerate the DPF, either periodically or continuously, during the regular engine operation. The on-vehicle filter regeneration is most commonly done by oxidizing (burning) of solid PMs in the filter. During the regeneration of the DPF, a high temperature combustion wave is generated by the exothermic heterogeneous reaction between solid PMs and oxygen. Sometimes, the temperature of the combustion wave becomes higher than the melting temperature of the DPF material that causes significant structural damage to the DPF. As a result, the DPF fails to trap the PMs efficiently.

To date, the efficient combustion of PMs is deemed to be the major obstacle of the PM removal technolgy. Numerous modeling works have been studied to understand the regeneration process. A detailed mathematical formulation of the regeneration process of PM layer was first described by Bissett and Shadman [40]. This was a zero-dimensional model dealing with PM combustion in one

point of a filter channel which was then extended to one-dimensional accounting for the axial heat conduction, and the PM layer and flow distribution along the channel [41]. In addition to, Bissett [42] made an attempt to describe the process in a somewhat general setting with an aim to provide the interesting physical and mathematical features of the process. However, the majority of the models in use today could be considered as an extension of Bisset and Shadman [40] and Bisset [41] (see [84]). All models have considered only one mode of propagation and investigated the characteristics of regeneration process based on steady-state propagation of the reaction front. Recently, both forward and opposed modes have been jointly recognized experimentally in DPF regeneration process [121, 125, 126]. These studies only examined the influences of inlet gas temperature and velocity, and the oxygen concentration on the moving velocity of the reaction front and temperature profile. Moreover, Chen et. al [126] reported the effects of oxygen concentration on one or more ignited locations. When conducting experiment they obseved that the heat loss from the reactor wall affects the temperature profiles and the location at which the ignition occurred. Nevertheless, they tried to pass this effect off by heating the sides and bottom of the reactor with an electrical ceramic fibre heater.

Therefore, the combustion behaviors of two reaction fronts propagating in the upstream and downstream directions from the ignition point have not been completely studied yet. Because the influences of heat loss from the DPF to the environment, radiative heat transfer from the DPF, heat transfer from the DPF material to the gas and the mass tansfer from the gas stream to the surface of solid PMs must be investigated, but it is very difficult to reveal these effects by an experiment. On the other hand, no study has taken an attempt to formulate a model illustrating this application. Thus the objective of this chapter is to develop a model for the combustion of solid fuel over an inert porous medium while it is ignited around the middle, and to provide a body of knowledge of identifying an efficient regeneration process.

To formulate the model of the present problem, the governing equations developed by Roy et al. [122] are used first. Then the required boundary conditions are imposed at the ends of the DPF and also at the ignition point. Analytical expressions of the moving speeds of the reaction fronts and temperature profiles are obtained utilizing the theoretical concepts of Chapter 3 and Chapter 4. Using

these expressions, the effects of the heat transfer coefficient on the moving speeds of the reaction fronts as well as the temperature profiles of both forward and opposed modes are presented.

5. 2 Mathematical formulation

The physical configuration of the problem is shown in Figure 5.1. The sample is an infinitely long porous medium over which solid fuel are attached. Oxidizer (gas) is flowing from left to right over the porous medium. It is ignited crosswise (as shown in Figure 5.1) somewhere around the middle. Due to fuel availability on both sides of the ignition source line and under necessary conditions, it can be presumed that the single reaction front propagates with sufficient heat to the opposite ends of the sample and the thickness of the reaction zone gradually broadens. After a short period of time, the single reaction front is separated as two reaction fronts. Since oxidizer flows from left to right, hence one reaction front propagates against the gas which is referred to as opposed mode, while the other reaction front moves in the same direction of the gas which is referred to as forward mode.

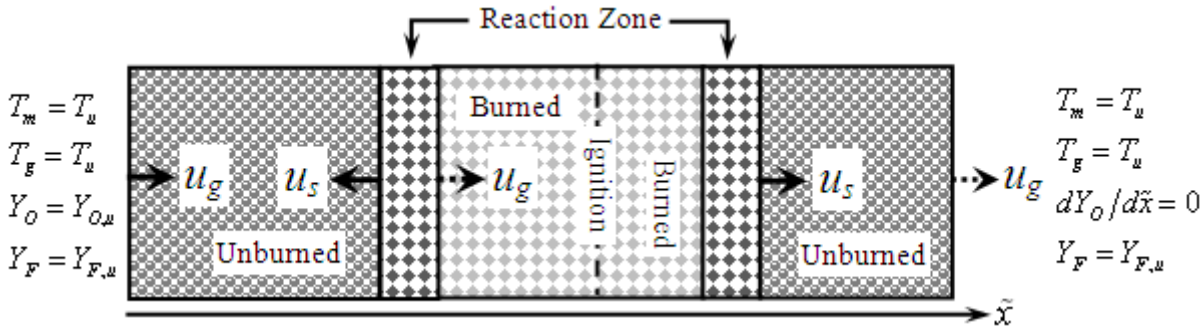

Figure 5.1: Physical configuration of ignition at the middle.

To formulate the above described problem, the governing equations developed by Roy et al. [122] are utilized here. The volume-averaged energy equations for porous material and gas, and species equation for gas and fuel are

$$(1-\varepsilon)\rho_m c_m \frac{\partial T_m}{\partial \tilde{t}} = (1-\varepsilon)\lambda_m \frac{\partial^2 T_m}{\partial \tilde{x}^2} + QW - h(T_m - T_g) - \frac{\partial q_r}{\partial \tilde{x}} - h_{ex}(T_m - T_u), \tag{5.1}$$

$$\varepsilon\rho_g c_g \frac{\partial T_g}{\partial \tilde{t}} + \varepsilon\rho_g c_g u_g \frac{\partial T_g}{\partial \tilde{x}} = \varepsilon\lambda_g \frac{\partial^2 T_g}{\partial \tilde{x}^2} + h\left(T_m - T_g\right), \tag{5.2}$$

$$\varepsilon\rho_g \frac{\partial Y_O}{\partial \tilde{t}} + \varepsilon\rho_g u_g \frac{\partial Y_O}{\partial \tilde{x}} = \varepsilon\rho_g \frac{\partial}{\partial \tilde{x}}\left(D_{eff} \frac{\partial Y_O}{\partial \tilde{x}}\right) - nW - \frac{h_m \rho_g}{d}\left(Y_O - Y_{O,u}\right), \tag{5.3}$$

$$\varepsilon\rho_f \frac{\partial Y_F}{\partial \tilde{t}} = -W. \tag{5.4}$$

Here T_m, ρ_m and T_g, ρ_g are the volume-averaged temperature and the density of the porous medium and gas, respectively, ε is the porosity of the porous medium, ρ_f is the density of fuel, Y_O and Y_F are the volume-averaged oxidizer and fuel mass fractions, u_g is the gas flow velocity, Q is the fuel mass based heat of reaction, h is the volumetric heat transfer coefficient from the porous medium to gas, q_r represents the radiative heat flux from the porous medium, h_{ex} is the heat loss coefficient from the porous medium to the environment and h_m is the mass transfer coefficient from the gas stream to the surface of fuel, d is the pore diameter and W is the rate of the chemical reaction, given by an Arrhenius law

$$W = \varepsilon\left(1-\varepsilon\right) A \rho_f \rho_g Y_O Y_F \exp\left[-E / RT_m\right], \tag{5.5}$$

where A is a pre-exponential factor, taken to be constant, R is the universal gas constant, and E is the activation energy.

The appropriate boundary conditions for the present problem are

Case 1:

$$\tilde{x} = 0: \ T_m = T_u, \ T_g = T_u, \ Y_O = Y_{O,u}, \ Y_F = Y_{F,u}, \tag{5.6}$$

$$\tilde{x} = \tilde{x}_{ig}: \ T_m = T_u, \ T_g = T_u, \ Y_O = Y_O^*, \ \frac{\partial Y_F}{\partial \tilde{x}} = 0, \tag{5.7}$$

$$\tilde{x} = \tilde{L}_1: \ T_m = T_u, \ T_g = T_u, \ \frac{\partial Y_O}{\partial \tilde{x}} = 0, \ Y_F = Y_{F,u}. \tag{5.8}$$

Case 2:

$$\tilde{x} = 0: \ T_m = T_u, \ T_g = T_u, \ Y_O = Y_{O,u}, \ Y_F = Y_{F,u}, \tag{5.9}$$

$$\tilde{x}=\tilde{x}_{ig}:\ \frac{\partial T_m}{\partial \tilde{x}}=0,\ \ \frac{\partial T_g}{\partial \tilde{x}}=0,\ \ Y_O=Y_O^*,\ \frac{\partial Y_F}{\partial \tilde{x}}=0, \tag{5.10}$$

$$\tilde{x}=\tilde{L}_1:\ T_m=T_u,\ \ T_g=T_u,\ \ \frac{\partial Y_O}{\partial \tilde{x}}=0,\ \ Y_F=Y_{F,u}. \tag{5.11}$$

5.3 Asymptotic analysis

5.3.1 Opposed Mode $\left(0<\tilde{x}<\tilde{x}_{ig}\right)$:

The main interest of the present problem is to examine how the reaction fronts propagate towards the opposite ends from the ignition source line. Therefore, the moving speed of the reaction front, u_s, has been taken as a right choice of characteristic speed. To render the governing equations into dimensionless form, the following group of dimensionless variables is utilized:

$$\xi=\frac{\rho_m c_m u_s}{\lambda_m}\tilde{x},\ \ \tau=\frac{\rho_m c_m u_s^2}{\lambda_m}\tilde{t},\ \ y_O=\frac{Y_O}{Y_{O,u}},\ y_F=\frac{Y_F}{Y_{F,u}},\ \ S=\frac{T_m-T_u}{T_{ad}-T_u},\ \ \theta=\frac{T_g-T_u}{T_{ad}-T_u}. \tag{5.12}$$

Thus the conservation equations (5.1)–(5.4) reduce to

$$\frac{\partial S}{\partial \tau}=\frac{\partial}{\partial \xi}\left[\left\{1+\frac{N_R}{1-\varepsilon}\left(1+\delta S\right)^3\right\}\frac{\partial S}{\partial \xi}\right]+\Lambda\varepsilon\gamma\omega-\frac{K}{1-\varepsilon}\left(S-\theta\right)-\frac{K_{ex}}{1-\varepsilon}S, \tag{5.13}$$

$$\frac{r_g c}{l}\frac{\partial \theta}{\partial \tau}+\frac{r_g c}{lu}\frac{\partial \theta}{\partial \xi}=\frac{\partial^2 \theta}{\partial \xi^2}+\frac{K}{\varepsilon l}\left(S-\theta\right), \tag{5.14}$$

$$\begin{aligned}&\frac{Ler_g c}{l}\frac{\partial y_O}{\partial \tau}+\left[\frac{Ler_g c}{lu}-\frac{\varepsilon\Pi\delta}{2\Omega\sqrt{1+\delta\theta}\left(1+\Pi\sqrt{1+\delta\theta}\right)^2}\frac{\partial \theta}{\partial \xi}\right]\frac{\partial y_O}{\partial \xi}\\&=\frac{\varepsilon\Pi\sqrt{1+\delta\theta}}{\Omega\left(1+\Pi\sqrt{1+\delta\theta}\right)}\frac{\partial^2 y_O}{\partial \xi^2}-\frac{\left(1-\varepsilon\right)\Lambda n Lec\Omega_{st}}{l}\omega-\frac{Ler_g cK_m}{\varepsilon l}\left(y_O-1\right),\end{aligned} \tag{5.15}$$

$$\frac{\partial y_F}{\partial \tau}=-\frac{\Lambda\left(1-\varepsilon\right)}{r_f}\omega. \tag{5.16}$$

The associated boundary conditions become

Case 1:

$$\xi = 0:\ S = 0, \quad \theta = 0, \quad y_O = 1, \quad y_F = 1, \tag{5.17}$$

$$\xi = X_{ig}:\ S = 0, \quad \theta = 0, \quad y_O = g_0, \quad \frac{\partial y_F}{\partial \xi} = 0. \tag{5.18}$$

Case 2:

$$\xi = 0:\ S = 0, \quad \theta = 0, \quad y_O = 1, \quad y_F = 1, \tag{5.19}$$

$$\xi = X_{ig}:\ S' = 0, \quad \theta' = 0, \quad y_O = g_0, \quad \frac{\partial y_F}{\partial \xi} = 0. \tag{5.20}$$

Here the nondimensional parameters

$$\begin{gathered}
\gamma \equiv \frac{QY_{F,u}}{c_m\left(T_{ad} - T_u\right)}, \quad \delta \equiv \frac{T_{ad} - T_u}{T_u}, \quad K \equiv \frac{h\lambda_m}{\rho_m^2 u_s^2 c_m^2}, \quad N_R \equiv \frac{16\sigma T_u^3}{3\lambda_m a}, \\
\Pi \equiv \frac{4}{3}\frac{d}{D}\sqrt{\frac{RT_u}{2\pi M}}, \quad K_{ex} \equiv \frac{h_{ex}\lambda_m}{\rho_m^2 u_s^2 c_m^2}, \quad K_m \equiv \frac{h_m \lambda_m}{\rho_m u_s^2 c_m d}, \quad \Omega_{st} \equiv \frac{Y_{F,u}}{Y_{O,u}}, \\
Le \equiv \frac{\lambda_g}{\rho_g D c_g}, \quad \Lambda \equiv \frac{A\lambda_m \rho_g \rho_f Y_{O,u} e^{-\beta/\alpha}}{\rho_m^2 u_s^2 c_m}, \quad g_0 \equiv \frac{Y_O^*}{Y_{O,u}}, \quad X_{ig} = \frac{\rho_m c_m u_s \tilde{x}_{ig}}{\lambda_m},
\end{gathered} \tag{5.21}$$

where γ is the dimensionless heat release, δ represents the thermal excursion during the burning process, K is the heat transfer parameter, N_R is the radiation-conduction parameter, K_{ex} is the heat loss parameter, K_m is the mass transfer parameter, Le is a Lewis number which is assumed to be unity and Λ is the burning rate eigenvalue, the determination of which will yield the dimensional moving speed of the burning front, u_s, according to its definition.

The nondimensional reaction rate, ω, is given by

$$\omega \equiv y_O y_F \exp\left[-\frac{\beta(1-S)}{1-\alpha(1-S)}\right], \tag{5.22}$$

where

$$\alpha \equiv \frac{T_{ad} - T_u}{T_{ad}} \quad \text{and} \quad \beta \equiv \frac{E\left(T_{ad} - T_u\right)}{RT_{ad}^2}, \tag{5.23}$$

are the dimensionless heat of combustion and the Zel'dovich number, respectively. The other additional parameters are defined by

$$r_g \equiv \frac{\rho_g}{\rho_m},\ r_f \equiv \frac{\rho_f}{\rho_m},\ l \equiv \frac{\lambda_g}{\lambda_m},\ U \equiv \frac{u_s}{u_g} \text{ and } c \equiv \frac{c_g}{c_m}. \tag{5.24}$$

With the definitions of the aforementioned quantities, the nondimensional moving speed of the reaction front is equal to unity. Thus, the transformation of the moving coordinate attached to the reaction front is $X = \xi - \tau$. In this case, the moving speed of the reaction front becomes time-independent. Therefore, the system of equations (5.13)–(5.16) along with this transformation takes the form

$$\frac{dS}{dX} = \frac{d}{dX}\left[\left\{1+\frac{N_R}{1-\varepsilon}\left(1+\delta S\right)^3\right\}\frac{dS}{dX}\right] + \Lambda\varepsilon\gamma\omega - \frac{K}{1-\varepsilon}\left(S-\theta\right) - \frac{K_{ex}}{1-\varepsilon}S, \tag{5.25}$$

$$\frac{r_g c\left(1-U\right)}{lU}\frac{d\theta}{dX} = \frac{d^2\theta}{dX^2} + \frac{K}{\varepsilon l}\left(S-\theta\right), \tag{5.26}$$

$$\begin{aligned}&\left[\frac{Ler_g c\left(1-U\right)}{lU} - \frac{\varepsilon\Pi\delta}{2\Omega\sqrt{1+\delta\theta}\left(1+\Pi\sqrt{1+\delta\theta}\right)^2}\frac{d\theta}{dX}\right]\frac{dy_O}{dX}\\ &= \frac{\varepsilon\Pi\sqrt{1+\delta\theta}}{\Omega\left(1+\Pi\sqrt{1+\delta\theta}\right)}\frac{d^2y_O}{dX^2} - \frac{\left(1-\varepsilon\right)\Lambda nLec\Omega_{st}}{l}\omega - \frac{Ler_g cK_m}{\varepsilon l}\left(y_O-1\right),\end{aligned} \tag{5.27}$$

$$\frac{dy_F}{dX} = -\frac{\left(1-\varepsilon\right)\Lambda}{r_f}\omega. \tag{5.28}$$

The corresponding boundary conditions become

Case 1:

$$X=0:\ S=\theta=0,\ y_O=1,\ y_F=1, \tag{5.29}$$

$$X=X_{ig}:\ S=\theta=0,\ y_O=g_0,\ y_F'=0. \tag{5.30}$$

Case 2:

$$X = 0: \;\; S = \theta = 0, \;\; y_O = 1, \;\; y_F = 1, \tag{5.31}$$

$$X = X_{ig}: \;\; S' = \theta' = 0, \;\; y_O = g_0, \;\; y_F' = 0. \tag{5.32}$$

Our purpose is to solve the steady problem given by equations (5.25)–(5.28) subject to the boundary conditions (5.29)–(5.30) for Case 1 and (5.31)–(5.32) for Case 2, and thus to determine the burning rate eigenvalue Λ by carrying out an asymptotic analysis. This can then be used to find the dimensional moving speed of the reaction front u_s, according to its definition (5.21).

5.3.1.1 Outer solutions

At first, the reaction front of opposed mode is assumed at $X = X_O$. As the nondimensional activation energy, β, is large, then the reaction is concentrated to a thin $O(\beta^{-1})$ reaction zone. In this regard, the source terms in the conservation equations are exponentially small in the preheat region $X < X_O$ and all the chemical reaction has gone to completion in the burned region $X > X_O$. Thus the reaction terms can be neglected in these regions.

According to [122],

$$1 + \frac{N_R}{1-\varepsilon}\left(1+\delta S\right)^3 \approx \Gamma, \tag{5.33}$$

where

$$\Gamma = \begin{cases} 1 + \dfrac{N_R}{1-\varepsilon}\left(1+\delta\right)^3, & X \le X_O \\ 1 + \dfrac{N_R}{2\left(1-\varepsilon\right)}\left\{1+\left(1+\delta\right)^3\right\}, & X > X_O \end{cases}. \tag{5.34}$$

Again, the coefficients of y_O' and y_O'' of the Eq. (5.27) are presumed as follows in [122]:

$$\frac{\varepsilon\Pi\sqrt{1+\delta\theta}}{\left\{\Omega\left(1+\Pi\sqrt{1+\delta\theta}\right)\right\}} \approx \frac{\varepsilon\Pi\sqrt{1+\delta\theta_f^*}}{\Omega\left(1+\Pi\sqrt{1+\delta\theta_f^*}\right)} = B_1, \tag{5.35}$$

and

$$\frac{\varepsilon\Pi\delta}{2\Omega\sqrt{1+\delta\theta}\left(1+\Pi\sqrt{1+\delta\theta}\right)^2}\frac{d\theta}{dx}\approx\frac{\varepsilon\delta}{2\Omega\Pi}\left(\frac{d\theta}{dX}\right)_{X=X_f^{\pm}}=B_2, \tag{5.36}$$

where $\theta_f^*=\theta\left(X_f\right)$.

Therefore, the equations to be solved for the outer regions are

$$\frac{dS}{dX}=\Gamma\frac{d^2S}{dX^2}-\frac{K}{1-\varepsilon}\left(S-\theta\right)-\frac{K_{ex}}{1-\varepsilon}S, \tag{5.37}$$

$$\frac{r_g c\left(1-U\right)}{lU}\frac{d\theta}{dX}=\frac{d^2\theta}{dX^2}+\frac{K}{\varepsilon l}\left(S-\theta\right), \tag{5.38}$$

$$\left[\frac{Ler_g c\left(1-U\right)}{lU}-B_2\right]\frac{dy_O}{dX}=B_1\frac{d^2y_O}{dX^2}-\frac{Ler_g cK_m}{\varepsilon l}\left(y_O-1\right), \tag{5.39}$$

$$\frac{dy_F}{dX}=0, \tag{5.40}$$

with the boundary conditions

Case 1:

$$X=0:\ \ S=\theta=0,\ \ y_O=y_F=1, \tag{5.41}$$

$$X=X_{ig}:\ \ S=\theta=0,\ \ \ y_O=g_0,\ \ \ y_F'=0. \tag{5.42}$$

Case 2:

$$X=0:\ \ S=\theta=0,\ \ y_O=y_F=1, \tag{5.43}$$

$$X=X_{ig}:\ \ S'=\theta'=0,\ \ \ y_O=g_0,\ \ \ y_F'=0. \tag{5.44}$$

Now Eq. (5.38) implies

$$S=\theta+\frac{\varepsilon r_g c\left(1-U\right)}{UK}\theta'-\frac{\varepsilon l}{K}\theta''. \tag{5.45}$$

Using (5.45) into (5.37), one can find the following equation

$$\theta^{(iv)} - \left\{\frac{1}{\Gamma} + \frac{r_g c(1-U)}{lu}\right\}\theta''' - \left\{\frac{K}{\varepsilon l} + \frac{K+K_{ex}}{(1-\varepsilon)\Gamma} - \frac{r_g c(1-U)}{lU\Gamma}\right\}\theta'' + \frac{1}{\Gamma}\left\{\frac{K}{\varepsilon l} + \frac{r_g c(1-U)(K+K_{ex})}{(1-\varepsilon)lU}\right\}\theta' + \frac{KK_{ex}}{\varepsilon(1-\varepsilon)l\Gamma}\theta = 0. \tag{5.46}$$

Obtaining the solutions of Eq. (5.46), it needs to find the solutions of the corresponding characteristic polynomial:

$$m^4 - \left\{\frac{1}{\Gamma} + \frac{r_g c(1-U)}{lu}\right\}m^3 - \left\{\frac{K}{\varepsilon l} + \frac{K+K_{ex}}{(1-\varepsilon)\Gamma} - \frac{r_g c(1-U)}{lU\Gamma}\right\}m^2 + \frac{1}{\Gamma}\left\{\frac{K}{\varepsilon l} + \frac{r_g c(1-U)(K+K_{ex})}{(1-\varepsilon)lU}\right\}m + \frac{KK_{ex}}{\varepsilon(1-\varepsilon)l\Gamma} = 0. \tag{5.47}$$

Considering the appropriate values of the parameters, it can be shown by Descartes' rule of signs that Eq. (5.47) must have two positive roots, m_1 and m_2; and two negative roots, m_3 and m_4, to define the finite solutions of the Eq. (5.46).

Once Eq. (5.46) is solved, the temperature of the porous medium, S, is determined from Eq. (5.45). Then the temperatures of the porous medium and gas are given by

Case 1:

$$S(X) = \begin{cases} p_1 a_1 \exp\left[m_1(X - X_O)\right] + p_2 a_2 \exp\left[m_2(X - X_O)\right], & X < X_O \\ p_3 a_3 \exp\left[m_3(X - X_O)\right] + p_4 a_4 \exp\left[m_4(X - X_O)\right], & X > X_O \end{cases} \tag{5.48}$$

$$\theta(X) = \begin{cases} a_1 \exp\left[m_1(X - X_O)\right] + a_2 \exp\left[m_2(X - X_O)\right], & X < X_O \\ a_3 \exp\left[m_3(X - X_O)\right] + a_4 \exp\left[m_4(X - X_O)\right], & X > X_O \end{cases}. \tag{5.49}$$

Case 2:

$$S(X) = \begin{cases} p_1 a_1 \exp\left[m_1(X - X_O)\right] + p_2 a_2 \exp\left[m_2(X - X_O)\right], & X < X_O \\ S_{down} + p_3 a_3 \exp\left[m_3(X - X_O)\right] + p_4 a_4 \exp\left[m_4(X - X_O)\right], & X > X_O \end{cases} \tag{5.50}$$

$$\theta(X) = \begin{cases} a_1 \exp\left[m_1(X - X_O)\right] + a_2 \exp\left[m_2(X - X_O)\right], & X < X_O \\ S_{down} + a_3 \exp\left[m_3(X - X_O)\right] + a_4 \exp\left[m_4(X - X_O)\right], & X > X_O \end{cases}. \tag{5.51}$$

where

$$p_i = 1 - \frac{\varepsilon l}{K} m_i^2 + \frac{\varepsilon r_g c (1-U)}{UK} m_i, \quad i = 1, 2, 3, 4, \tag{5.52}$$

and the constants a_1, a_2, a_3 and a_4 are found later.

Thus the temperature of the porous medium at the reaction front (i.e., $X = X_O$) can be expressed as follows:

$$S(0) = s_f^* = p_1 a_1 + p_2 a_2. \tag{5.53}$$

As the activation energy is assumed to be large, the reaction front temperature will be very high. Consequently, one of the reactants (fuel and oxidizer) must be depleted after passing through the reaction front. Here it is considered that fuel is fully consumed at the reaction front (i.e., at $X = X_O$), then the solutions of (5.40) can be written as

$$y_F (X < X_O) = 1 \quad \text{and} \quad y_F (X > X_O) = 0. \tag{5.54}$$

Now the solutions of Eq. (5.39) become

$$y_O (X < X_O) = 1 - (1 - g_0) \exp\left[\nu_1 (X - X_O)\right] \quad \text{and} \quad y_O (X > X_O) = g_0. \tag{5.55}$$

where

$$\nu_{1,2} = \left[\frac{Ler_g c (1-U)}{lUB_1} - \frac{B_2}{B_1} \pm \sqrt{\left\{ \frac{Ler_g c (1-U)}{lUB_1} - \frac{B_2}{B_1} \right\}^2 + \frac{4Ler_g cK_m}{\varepsilon l B_1}} \right] \Big/ 2.$$

5.3.1.2 Reaction zone

In the asymptotic limit $\beta \to \infty$, the reaction zone becomes very thin which acts as a heat source and a sink of oxygen that cause jumps in the heat flux as well as oxygen. For this reason, it is required to introduce a stretched inner variable $\eta = \beta X$ for measuring the jumps of temperature and oxygen across the reaction front. Inner solutions for the dependent variables S, θ and y, and the burning rate eigenvalue Λ are now sought as expansions of the form:

$$S = s_f^* + \beta^{-1} S_1^{in} + \cdots, \tag{5.56}$$

$$\theta = \theta_f^* + \beta^{-1} \Theta_1^{in} + \cdots, \tag{5.57}$$

$$y_O = g_0 + \beta^{-1} G_1^{in} + \cdots, \tag{5.58}$$

$$y_F = F_0^{in} + \beta^{-1} F_1^{in} + \cdots, \tag{5.59}$$

$$\Lambda = \beta\left(\Lambda_0 + \beta^{-1}\Lambda_1 + \cdots\right), \tag{5.60}$$

$$\eta = \beta X. \tag{5.61}$$

Thus the governing equations for the reaction zone problem become

$$\Gamma^{in} \frac{d^2 S_1^{in}}{d\eta^2} + \varepsilon\gamma\Lambda_0 F_0^{in} g_0 \exp\left[-\frac{\beta\left(1-s_f^*\right)}{1-\alpha\left(1-s_f^*\right)}\right] \exp\left[\frac{S_1}{\left\{1-\alpha\left(1-s_f^*\right)\right\}^2}\right] = 0, \tag{5.62}$$

$$\frac{d^2 \Theta_1^{in}}{d\eta^2} = 0, \tag{5.63}$$

$$B_1 \frac{d^2 G_1^{in}}{d\eta^2} - \frac{nLec\Omega_{st}}{l}\left(1-\varepsilon\right)\Lambda_0 F_0^{in} g_0 \exp\left[-\frac{\beta\left(1-s_f^*\right)}{1-\alpha\left(1-s_f^*\right)}\right] \exp\left[\frac{S_1^{in}}{\left\{1-\alpha\left(1-s_f^*\right)\right\}^2}\right] = 0, \tag{5.64}$$

$$\frac{dF_0^{in}}{d\eta} + \frac{\Lambda_0\left(1-\varepsilon\right)}{r_f} F_0^{in} g_0 \exp\left[-\frac{\beta\left(1-s_f^*\right)}{1-\alpha\left(1-s_f^*\right)}\right] \exp\left[\frac{S_1^{in}}{\left\{1-\alpha\left(1-s_f^*\right)\right\}^2}\right] = 0. \tag{5.65}$$

The matching conditions are:

as $\eta \to -\infty$,

$$\frac{dS_1^{in}}{d\eta} \to \left(\frac{dS}{dX}\right)_{X=X_O^-}, \tag{5.66}$$

$$\frac{d\Theta_1^{in}}{d\eta} \to \left(\frac{d\theta}{dX}\right)_{X=X_O^-}, \tag{5.67}$$

$$\frac{dG_1^{in}}{d\eta} \to \left(\frac{dy_O}{dX}\right)_{X=X_O^-} = -(1-g_0)\nu_1, \tag{5.68}$$

$$\frac{dF_0^{in}}{d\eta} \to \frac{1}{\beta}\left(\frac{dy_F}{dX}\right)_{X=X_O^-} = 0, \tag{5.69}$$

as $\eta \to +\infty$,

$$\frac{dS_1^{in}}{d\eta} \to \left(\frac{dS}{dX}\right)_{X=X_O^+}, \tag{5.70}$$

$$\frac{d\Theta_1^{in}}{d\eta} \to \left(\frac{d\theta}{dX}\right)_{X=X_O^+}, \tag{5.71}$$

$$\frac{dG_1^{in}}{d\eta} \to 0, \tag{5.72}$$

$$\frac{dF_0^{in}}{d\eta} \to 0. \tag{5.73}$$

Combining Eqs. (5.64) and (5.65) and using the matching conditions yield

$$\left[y_F\right]_{X_O^-}^{X_O^+} = -\frac{lB_1}{nLecr_f\Omega_{st}}\left[\frac{dy_O}{dX}\right]_{X_O^-}^{X_O^+},$$

which implies

$$g_0 = 1 - \frac{nLecr_f\Omega_{st}}{lB_1\nu_1}. \tag{5.74}$$

Adding Eqs. (5.62) and (5.64),

$$\frac{\Gamma^{in}}{\varepsilon\gamma}\frac{d^2S_1^{in}}{d\eta^2} + \frac{lB_1}{nLec(1-\varepsilon)\Omega_{st}}\frac{d^2G_1^{in}}{d\eta^2} = 0. \tag{5.75}$$

Integrating the Eq. (5.75) and matching yields the energy balance

$$\left(\frac{dS_1^{in}}{d\eta}\right)_{\eta\to-\infty} - \left(\frac{dS_1^{in}}{d\eta}\right)_{\eta\to+\infty} = -\frac{\varepsilon\gamma lB_1}{nLec(1-\varepsilon)\Omega_{st}\Gamma^{in}}\left[\left(\frac{dG_1^{in}}{d\eta}\right)_{\eta\to-\infty} - \left(\frac{dG_1^{in}}{d\eta}\right)_{\eta\to+\infty}\right],$$

That is, $$\left(\frac{dS}{dX}\right)_{X=X_O^-} - \left(\frac{dS}{dX}\right)_{X=X_O^+} = \frac{\varepsilon\gamma l B_1 (1-g_0)\nu_1}{nLec\Omega_{st}(1-\varepsilon)\Gamma^{in}}. \tag{5.76}$$

Similarly, the jump relation obtained from Eq. (5.63) and matching conditions at the reaction front (i.e., $X = X_O$) gives the following three constraints:

$$\theta'(X_O^-) = \theta'(X_O^+),\ S(X_O^-) = S(X_O^+) \ \text{ and } \ \theta(X_O^-) = \theta(X_O^+). \tag{5.77}$$

Now using Eqs. (5.48)–(5.49) into (5.76) and (5.77), the constants a_1, a_2, a_3 and a_4 can be determined easily.

Again, Eqs. (5.62) and (5.65) provide the similarity solution

$$y_F = \frac{(1-\varepsilon)\Gamma^{in}}{\varepsilon\gamma r_f}\frac{dS_1^{in}}{d\eta}. \tag{5.78}$$

Therefore, Eq. (5.62) takes the form

$$\frac{d^2 S_1^{in}}{d\eta^2} = -\frac{(1-\varepsilon)\Lambda_0 g_0}{r_f}\exp\left[-\frac{\beta(1-s_f^*)}{1-\alpha(1-s_f^*)}\right]\frac{dS_1^{in}}{d\eta}\exp\left[\frac{S_1^{in}}{\left\{1-\alpha(1-s_f^*)\right\}^2}\right]. \tag{5.79}$$

Equation (5.79) is solved by Liñán [92]. According to the relation between Λ and Λ_0 given by (5.60) along with the definition of Λ given in Eq. (5.21), the moving speed of the reaction front is implicitly related to the other parameters by the expression

$$\begin{aligned} S'(X_O^+) &= -\frac{2(1-\varepsilon)A\lambda_m\rho_g\rho_f Y_{O,u}e^{-\beta/\alpha}g_0}{r_f\rho_m^2 u_s^2 c_m\beta} \\ &\times\left\{1-\alpha(1-s_f^*)\right\}^2\exp\left[-\frac{\beta(1-s_f^*)}{1-\alpha(1-s_f^*)}\right]\left[\frac{S(X_O^+)}{\left\{1-\alpha(1-s_f^*)\right\}^2}\right]. \end{aligned} \tag{5.80}$$

Having obtained the maximum temperature of the porous medium s_f^* by Eq. (5.53), one can readily determine the moving speed of the reaction front u_s from (5.80).

5.3.2 Forward Mode $\left(\tilde{x}_{ig} < \tilde{x} < \tilde{L}_1\right)$:

Let us now introduce the following group of dimensionless variables along with them as defined in Eq. (5.12)

$$\hat{x} \equiv \frac{\tilde{x}}{x_*},\ \hat{t} \equiv \frac{\tilde{t}}{t_*},\ u_* \equiv \frac{x_*}{t_*},\ x_* \equiv \sqrt{\frac{t_* \lambda_m}{\rho_m c_m}},\ t_* \equiv \frac{\beta^2 \exp\left[E/RT_{ad}\right]}{A\rho_g Y_{O,u}}. \tag{5.81}$$

Thus the Eqs. (5.1)–(5.4) reduce to

$$\frac{\partial S}{\partial \hat{t}} = \frac{\partial}{\partial \hat{x}}\left[\left\{1+\frac{N_R}{1-\varepsilon}\left(1+\delta S\right)^3\right\}\frac{\partial S}{\partial \hat{x}}\right] + \beta^2 r_f \varepsilon \gamma y_O y_F \exp\left[-\frac{\beta(1-S)}{1-\alpha(1-S)}\right] - \frac{K^f}{1-\varepsilon}(S-\theta) - \frac{K_{ex}^f S}{1-\varepsilon}, \tag{5.82}$$

$$r_g c \frac{\partial \theta}{\partial \hat{t}} + r_g cu \frac{\partial \theta}{\partial \hat{x}} = l \frac{\partial^2 \theta}{\partial \hat{x}^2} + \frac{K^f}{\varepsilon}(S-\theta), \tag{5.83}$$

$$\frac{Ler_g c}{l}\frac{\partial y_O}{\partial \hat{t}} + \left[\frac{Ler_g cu}{l} - \frac{\varepsilon\Pi\delta}{2\Omega\sqrt{1+\delta\theta}\left(1+\Pi\sqrt{1+\delta\theta}\right)^2}\frac{\partial \theta}{\partial \hat{x}}\right]\frac{\partial y_O}{\partial \hat{x}} = \frac{\varepsilon\Pi\sqrt{1+\delta\theta}}{\Omega\left(1+\Pi\sqrt{1+\delta\theta}\right)}\frac{\partial^2 y_O}{\partial \hat{x}^2} - \frac{\beta^2 Ler_f c\nu\Omega_{st}(1-\varepsilon)}{l} y_O y_F \exp\left[-\frac{\beta(1-S)}{1-\alpha(1-S)}\right] - \frac{LeK_m^f r_g c}{\varepsilon l}(y_O - 1), \tag{5.84}$$

$$\frac{\partial y_F}{\partial \hat{t}} = -\beta^2 (1-\varepsilon) y_O y_F \exp\left[-\frac{\beta(1-S)}{1-\alpha(1-S)}\right]. \tag{5.85}$$

Here the dimensionless parameters

$$K^f = \frac{ht_*}{\rho_m c_m},\ K_{ex}^f = \frac{h_{ex} t_*}{\rho_m c_m},\ K_m^f = \frac{h_m t_*}{d},\ u = \frac{u_g}{u_*},\ x_{ig} = \frac{\tilde{x}_{ig}}{x_*}, \tag{5.86}$$

where K^f is the heat transfer parameter, K_{ex}^f is the heat loss parameter and K_m^f is the mass transfer parameter.

The remaining dimensionless parameters used in Eqs. (5.82)–(5.85) are defined in Eqs. (5.21), (5.23) and (5.24).

The corresponding boundary conditions are

Case 1:

$$\hat{x} = x_{ig}: \quad S = 0, \quad \theta = 0, \quad y_O = g_0, \quad y_F' = 0, \tag{5.87}$$

$$\hat{x} = L: \quad S = 0, \quad \theta = 0, \quad y_O' = 0, \quad y_F = 1. \tag{5.88}$$

Case 2:

$$\hat{x} = x_{ig}: \quad S' = 0, \quad \theta' = 0, \quad y_O = g_0, \quad y_F' = 0, \tag{5.89}$$

$$\hat{x} = L: \quad S = 0, \quad \theta = 0, \quad y_O' = 0, \quad y_F = 1. \tag{5.90}$$

Now the use of the transformation $x = \hat{x} + f(t)$ and $t = \hat{t}$ for the moving coordinate attached to the reaction front transforms the Eqs. (5.82)–(5.85) to

$$\frac{\partial S}{\partial t} + f_t \frac{\partial S}{\partial x} = \frac{\partial}{\partial x}\left[\left\{1 + \frac{N_R}{1-\varepsilon}(1+\delta S)^3\right\}\frac{\partial S}{\partial x}\right] + \beta^2 r_f \varepsilon\gamma y_O y_F \exp\left[-\frac{\beta(1-S)}{1-\alpha(1-S)}\right] - \frac{K^f}{1-\varepsilon}(S-\theta) - \frac{K_{ex}^f S}{1-\varepsilon}, \tag{5.91}$$

$$r_g c \frac{\partial \theta}{\partial t} + r_g c(u + f_t)\frac{\partial \theta}{\partial x} = l\frac{\partial^2 \theta}{\partial x^2} + \frac{K^f}{\varepsilon}(S-\theta), \tag{5.92}$$

$$\frac{Ler_g c}{l}\frac{\partial y_O}{\partial t} + \left[\frac{Ler_g c(u+f_t)}{l} - \frac{\varepsilon\Pi\delta}{2\Omega\sqrt{1+\delta\theta}\left(1+\Pi\sqrt{1+\delta\theta}\right)^2}\frac{\partial \theta}{\partial x}\right]\frac{\partial y_O}{\partial x} = \frac{\varepsilon\Pi\sqrt{1+\delta\theta}}{\Omega\left(1+\Pi\sqrt{1+\delta\theta}\right)}\frac{\partial^2 y_O}{\partial x^2} - \frac{\beta^2 Ler_f cn\Omega_{st}(1-\varepsilon)}{l} y_O y_F \exp\left[-\frac{\beta(1-S)}{1-\alpha(1-S)}\right] - \frac{LeK_m^f r_g c}{\varepsilon l}(y_O - 1), \tag{5.93}$$

$$\frac{\partial y_F}{\partial t} + f_t \frac{\partial y_F}{\partial x} = -\beta^2(1-\varepsilon) y_O y_F \exp\left[-\frac{\beta(1-S)}{1-\alpha(1-S)}\right]. \tag{5.94}$$

Then the boundary conditions become

Case 1:

$$x = x_{ig} + f(t): \quad S = 0, \quad \theta = 0, \quad y_O = g_0, \quad y_F' = 0, \tag{5.95}$$

$$x = L + f(t): \quad S = 0, \quad \theta = 0, \quad y_O' = 0, \quad y_F = 1. \tag{5.96}$$

Case 2:

$$x = x_{ig} + f(t): \quad S' = 0, \quad \theta' = 0, \quad y_O = g_0, \quad y_F' = 0, \tag{5.97}$$

$$x = L + f(t): \quad S = 0, \quad \theta = 0, \quad y_O' = 0, \quad y_F = 1. \tag{5.98}$$

5.3.2.1 Combustion Zone

Since it is assumed that the activation energy is very high, hence in the preheat region $x > x_{ig} + x_f$, the source term in the conservation equations is exponentially small and in the burned region $x < x_{ig} + x_f$, all the chemical reaction has gone to completion due to the assumed complete oxygen consumption. So the source terms are set to zero in these regions. At large time i.e., for the steady-state combustion front, the equations to be solved are

$$f_t \frac{\partial S}{\partial x} = \frac{\partial}{\partial x}\left[\left\{1 + \frac{N_R}{1-\varepsilon}(1+\delta S)^3\right\}\frac{\partial S}{\partial x}\right] - \frac{K^f}{1-\varepsilon}(S-\theta) - \frac{K_{ex}^f S}{1-\varepsilon}, \tag{5.99}$$

$$r_g c(u + f_t)\frac{\partial \theta}{\partial x} = l\frac{\partial^2 \theta}{\partial x^2} + \frac{K^f}{\varepsilon}(S-\theta), \tag{5.100}$$

$$\left[\frac{Ler_g c(u+f_t)}{l} - \frac{\varepsilon \Pi \delta}{2\Omega\sqrt{1+\delta\theta}\left(1+\Pi\sqrt{1+\delta\theta}\right)^2}\frac{\partial \theta}{\partial x}\right]\frac{\partial y_O}{\partial x} = \frac{\varepsilon\Pi\sqrt{1+\delta\theta}}{\Omega\left(1+\Pi\sqrt{1+\delta\theta}\right)}\frac{\partial^2 y_O}{\partial x^2} - \frac{LeK_m^f r_g c}{\varepsilon l}(y_O - 1), \tag{5.101}$$

$$f_t \frac{\partial y_F}{\partial x} = 0. \tag{5.102}$$

To analyze the problem theoretically, the difficulty arises due to the coefficient $1 + N_R(1+\delta S)^3/(1-\varepsilon)$ of Eq. (5.99). In the previous study [122], it was simplified as follows

$$1+\frac{N_R}{1-\varepsilon}\left(1+\delta S\right)^3 \approx \Gamma, \tag{5.103}$$

where

$$\Gamma=\begin{cases}1+\dfrac{N_R}{1-\varepsilon}\left(1+\delta\right)^3, & x \le x_{ig}+x_f \\ 1+\dfrac{N_R}{2\left(1-\varepsilon\right)}\left\{1+\left(1+\delta\right)^3\right\}, & x > x_{ig}+x_f\end{cases}. \tag{5.104}$$

Moreover, Eq. (5.101) cannot be solved analytically because of the variable coefficients of y_O' and y_O'' of the equation. But this difficulty was circumvented in [122] by taking the coefficients of y_O'' and y_O' as $B_1=\varepsilon\Pi\sqrt{1+\delta\theta_f}\Big/\Omega\left(1+\Pi\sqrt{1+\delta\theta_f}\right)$ and $B_2=\varepsilon\delta\left(\partial\theta/\partial x\right)_{x=x_m^{\pm}}\Big/2\Omega\Pi$, respectively, where θ_f is the maximum temperature of gas at $x = x_m$. Therefore, the equations to be solved for the outer regions are

$$f_t\frac{\partial S}{\partial x}=\Gamma\frac{\partial^2 S}{\partial x^2}-\frac{K^f}{1-\varepsilon}\left(S-\theta\right)-\frac{K_{ex}^f S}{1-\varepsilon}, \tag{5.105}$$

$$r_g c\left(u+f_t\right)\frac{\partial\theta}{\partial x}=l\frac{\partial^2\theta}{\partial x^2}+\frac{K^f}{\varepsilon}\left(S-\theta\right), \tag{5.106}$$

$$\left[\frac{Ler_g c\left(u+f_t\right)}{l}-B_2\right]\frac{\partial y_O}{\partial x}=B_1\frac{\partial^2 y_O}{\partial x^2}-\frac{LeK_m^f r_g c}{\varepsilon l}\left(y_O-1\right), \tag{5.107}$$

$$f_t\frac{\partial y_F}{\partial x}=0. \tag{5.108}$$

In this study, it is assumed that oxidizer is fully consumed at the flame front (i.e., $y_O = 0$ at $x = x_{ig} + x_f$) suggesting that the system is controlled by oxidizer. Thus the solutions of (5.107) becomes

$$y_O\left(x\right)=\begin{cases}g_0\left(1-\exp\left[\mu_1\left(x-x_{ig}-x_f\right)\right]\right), & x < x_{ig}+x_f \\ 0, & x > x_{ig}+x_f\end{cases} \tag{5.109}$$

where

$$\mu_{1,2}=\left[\left\{\frac{Ler_g c\left(u+f_t\right)}{lB_1}-\frac{B_2}{B_1}\right\}\pm\sqrt{\left\{\frac{Ler_g c\left(u+f_t\right)}{lB_1}-\frac{B_2}{B_1}\right\}^2+\frac{4LeK_m^f r_g c}{\varepsilon lB_1}}\right]\Big/2.$$

Also, if y_F^* is the remained fuel mass fraction at the reaction front (i.e., at $x = x_{ig} + x_f$), then the solutions of Eq. (5.108) can be written as

$$y_F\left(x<x_{ig}+x_f\right)=y_F^* \quad \text{and} \quad y_F\left(x>x_{ig}+x_f\right)=1. \tag{5.110}$$

From Eq. (5.106), one can find

$$S=\theta+\frac{\varepsilon r_g c\left(u+f_t\right)}{K}\frac{\partial\theta}{\partial x}-\frac{\varepsilon l}{K}\frac{\partial^2\theta}{\partial x^2}. \tag{5.111}$$

Using Eq. (5.111) into (5.105), the following equation is obtained

$$\begin{aligned}&\frac{\partial^4\theta}{\partial x^4}-\left[\frac{r_g c}{l}\left(u+f_t\right)+\frac{f_t}{\Gamma}\right]\frac{\partial^3\theta}{\partial x^3}-\left[\frac{K^f}{\varepsilon l}+\frac{K^f+K_{ex}^f}{(1-\varepsilon)\Gamma}-\frac{r_g c f_t}{l\Gamma}\left(u+f_t\right)\right]\frac{\partial^2\theta}{\partial x^2}\\&+\left[\frac{r_g c\left(K^f+K_{ex}^f\right)}{l(1-\varepsilon)\Gamma}\left(u+f_t\right)+\frac{K^f f_t}{l\varepsilon\Gamma}\right]\theta'+\frac{K^f K_{ex}^f}{l\varepsilon(1-\varepsilon)\Gamma}\theta=0.\end{aligned} \tag{5.112}$$

To get the solutions of Eq. (5.112), the solutions of the corresponding characteristic polynomial have to be found. Considering the appropriate values of the parameters, it can be shown by Descartes' rule of signs that the characteristic polynomial must have two positive roots, n_1 and n_2 and two negative roots, n_3 and n_4, to define the finite solutions of the Eq. (5.112).

Once Eq. (5.112) is solved, the temperature of the porous material, S, is determined from Eq. (5.111). Then the temperatures of the porous material and gas are given by

Case 1:

$$S(x)=\begin{cases}l_1b_1\exp\left[n_1\left(x-x_{ig}-x_f\right)\right]+l_2b_2\exp\left[n_2\left(x-x_{ig}-x_f\right)\right], & x<x_{ig}+x_f\\ l_3b_3\exp\left[n_3\left(x-x_{ig}-x_f\right)\right]+l_4b_4\exp\left[n_4\left(x-x_{ig}-x_f\right)\right], & x>x_{ig}+x_f\end{cases} \tag{5.113}$$

$$\theta(x)=\begin{cases}b_1\exp\left[n_1\left(x-x_{ig}-x_f\right)\right]+b_2\exp\left[n_2\left(x-x_{ig}-x_f\right)\right], & x<x_{ig}+x_f\\ b_3\exp\left[n_3\left(x-x_{ig}-x_f\right)\right]+b_4\exp\left[n_4\left(x-x_{ig}-x_f\right)\right], & x>x_{ig}+x_f\end{cases}. \tag{5.114}$$

Case 2:

$$S(x)=\begin{cases} S_{down}+l_1b_1\exp\left[n_1\left(x-x_{ig}-x_f\right)\right]+l_2b_2\exp\left[n_2\left(x-x_{ig}-x_f\right)\right], & x<x_{ig}+x_f \\ l_3b_3\exp\left[n_3\left(x-x_{ig}-x_f\right)\right]+l_4b_4\exp\left[n_4\left(x-x_{ig}-x_f\right)\right], & x>x_{ig}+x_f \end{cases} \tag{5.115}$$

$$\theta(x)=\begin{cases} S_{down}+b_1\exp\left[n_1\left(x-x_{ig}-x_f\right)\right]+b_2\exp\left[n_2\left(x-x_{ig}-x_f\right)\right], & x<x_{ig}+x_f \\ b_3\exp\left[n_3\left(x-x_{ig}-x_f\right)\right]+b_4\exp\left[n_4\left(x-x_{ig}-x_f\right)\right], & x>x_{ig}+x_f \end{cases}. \tag{5.116}$$

where

$$l_i=1+\frac{\varepsilon r_g c}{K^f}\left(u+f_t\right)n_i-\frac{\varepsilon l}{K^f}n_i^2, \qquad i=1,2,3,4. \tag{5.117}$$

The constants b_1, b_2, b_3 and b_4 are found later.

Thus the temperature of the porous medium at the flame front (i.e., $x = x_{ig} + x_f$) can be expressed as $s_f = S(x_{ig} + x_f) = l_1b_1 + l_2b_2$.

5.3.2.2 Reaction zone

With a view to solving the reaction zone problem, the spatial coordinate x is made wider by introducing the transformation $\xi = \beta x$. It is noted that the temperature and oxygen mass fraction will be spatially independent to leading order. Thus the following asymptotic series in β^{-1} are used for the quantities S, θ, y_O and y_F:

$$S \sim s_f(\tau)+\beta^{-1}S^1(\xi,\tau)+\cdots, \tag{5.118}$$

$$\theta \sim \theta_f(\tau)+\beta^{-1}\theta^1(\xi,\tau)+\cdots, \tag{5.119}$$

$$y_O \sim \beta^{-1}y_O^1(\xi,\tau)+\cdots, \tag{5.120}$$

$$y_F \sim y_F^0(\xi,\tau)+\cdots\ . \tag{5.121}$$

Upon substitution of (5.118)–(5.121) into (5.91)–(5.94) implies

$$\Gamma^{in}\frac{\partial^2 S^1}{\partial\xi^2}+r_f\varepsilon\gamma y_O^1 y_F^0\exp\left[-\frac{\beta\left(1-s_f\right)}{1-\alpha\left(1-s_f\right)}\right]\exp\left[\frac{S^1}{\left\{1-\alpha\left(1-s_f\right)\right\}^2}\right]=0, \tag{5.122}$$

$$\frac{\partial^2\theta^1}{\partial\xi^2}=0, \tag{5.123}$$

$$B_1\frac{\partial^2 y_O^1}{\partial\xi^2}-\frac{Lenr_f c\Omega_{st}}{l}\left(1-\varepsilon\right)y_O^1 y_F^0\exp\left[-\frac{\beta\left(1-s_f\right)}{1-\alpha\left(1-s_f\right)}\right]\exp\left[\frac{S^1}{\left\{1-\alpha\left(1-s_f\right)\right\}^2}\right]=0, \tag{5.124}$$

$$f_\tau\frac{\partial y_F^0}{\partial\xi}+\left(1-\varepsilon\right)y_O^1 y_F^0\exp\left[-\frac{\beta\left(1-s_f\right)}{1-\alpha\left(1-s_f\right)}\right]\exp\left[\frac{S^1}{\left\{1-\alpha\left(1-s_f\right)\right\}^2}\right]=0. \tag{5.125}$$

Equations (5.122), (5.124) and (5.125) give

$$\begin{aligned}&-\frac{\Gamma^{in}}{\varepsilon\gamma r_f}\frac{\partial^2 S^1}{\partial\xi^2}=\frac{lB_1}{\left(1-\varepsilon\right)nLer_f c\Omega_{st}}\frac{\partial^2 y_O^1}{\partial\xi^2}=-\frac{f_\tau}{1-\varepsilon}\frac{\partial y_F^0}{\partial\xi}\\&=y_O^1 y_F^0\exp\left[-\frac{\beta\left(1-s_f\right)}{1-\alpha\left(1-s_f\right)}\right]\exp\left[\frac{S^1}{\left\{1-\alpha\left(1-s_f\right)\right\}^2}\right].\end{aligned} \tag{5.126}$$

From the first and second equalities of Eq. (5.126), one obtains

$$-\frac{\Gamma^{in}}{\varepsilon\gamma r_f}\frac{\partial^2 S^1}{\partial\xi^2}=\frac{lB_1}{\left(1-\varepsilon\right)nLer_f c\Omega_{st}}\frac{\partial^2 y_O^1}{\partial\xi^2}. \tag{5.127}$$

Integrating the Eq. (5.127) and matching yields

$$\left[\frac{\partial S}{\partial x}\right]_-^+=-\frac{\varepsilon\gamma lB_1 g_0\mu_1}{\left(1-\varepsilon\right)\Gamma^{in}nLec\Omega_{st}}. \tag{5.128}$$

Again, the second and third equalities of Eq. (5.126) provide

$$\frac{lB_1}{\left(1-\varepsilon\right)nLer_f c\Omega_{st}}\frac{\partial^2 y_O^1}{\partial\xi^2}=-\frac{f_\tau}{1-\varepsilon}\frac{\partial y_F^0}{\partial\xi}. \tag{5.129}$$

Integrating Eq. (5.129) and using the matching conditions, the remained fuel mass fraction at the reaction front can be found as

$$y_F^* = 1 + \frac{lB_1 g_0 \mu_1}{nLer_f c\Omega_{st} f_\tau}. \tag{5.130}$$

Similarly, the jump relation obtained from Eq. (5.123) and matching conditions at the reaction front (i.e., $x = x_{ig} + x_f$) give the following three constraints:

$$\left[\theta'\right]_-^+ = 0,\ \left[S\right]_-^+ = 0 \ \text{ and } \ \left[\theta\right]_-^+ = 0. \tag{5.131}$$

The definition that is used in the above equations is $\left[P\right]_-^+ = P\left(x_{igf}^+\right) - P\left(x_{igf}^-\right)$ with $x_{igf} = x_{ig} + x_f$.

Now, Eqs. (5.127) and (5.126) give the similarity solutions

$$y_O^1 = -\frac{(1-\varepsilon)\Gamma^{in} nLec\Omega_{st}}{\varepsilon\gamma lB_1} S^1, \tag{5.132}$$

$$y_F^0 = 1 + \frac{(1-\varepsilon)\Gamma^{in}}{\varepsilon\gamma r_f f_t}\frac{\partial S^1}{\partial \xi}. \tag{5.133}$$

Upon substitution of (5.132) and (5.133) into (5.122), following equation is obtained

$$\frac{\dfrac{\partial^2 S^1}{\partial \xi^2}}{1 + \dfrac{(1-\varepsilon)\Gamma^{in}}{\varepsilon\gamma r_f f_t}\dfrac{\partial S^1}{\partial \xi}} = \frac{(1-\varepsilon) nLer_f c\Omega_{st}}{lB_1\Gamma^{in}} \exp\left[-\frac{\beta\left(1-s_f\right)}{1-\alpha\left(1-s_f\right)}\right] S^1 \exp\left[\frac{S^1}{\left\{1-\alpha\left(1-s_f\right)\right\}^2}\right]. \tag{5.134}$$

Integrating Eq. (5.134) from 0 to $+\infty$, one can easily find

$$\begin{aligned} Log\left[1 + \frac{(1-\varepsilon)\Gamma^{in}}{\varepsilon\gamma r_f f_t}\left(\frac{\partial S}{\partial x}\right)_{x=0}\right] &= \frac{(1-\varepsilon)^2 nLec\Omega_{st}\left\{1-\alpha\left(1-s_f\right)\right\}^2}{\varepsilon\gamma f_t lB_1} \exp\left[-\frac{\beta\left(1-s_f\right)}{1-\alpha\left(1-s_f\right)}\right] \\ &\times\left[S(0) - \left\{1-\alpha\left(1-s_f\right)\right\}^2\right] \exp\left[\frac{S[0]}{\left\{1-\alpha\left(1-s_f\right)\right\}^2}\right]. \end{aligned} \tag{5.135}$$

Thus the dimensionless moving speed of the flame front, f_t, is implicitly related to the other parameters by the expression (5.135). Having obtained f_t from (5.135), one can readily find the dimensional moving speed of the flame front, $u_s = x_* f_t / t_*$, using the relations given in (5.81).

For Case 1, the problem is closed when the positions of the reaction fronts of opposed and forward mode x_O and x_f, respectively are chosen arbitrarily, the unknown constants b_1, b_2, b_3 and b_4 are found using Eqs. (5.128) and (5.131) and the point x_{ig} is determined by the matching condition

$$S\left(x_{ig}^{-}\right) = S\left(x_{ig}^{+}\right). \tag{5.136}$$

Now for Case 2, the unknown constants are b_1, b_2, b_3, b_4, S_{down} and x_{ig}, when the positions of the reaction fronts of opposed and forward mode x_O and x_f, respectively are taken arbitrarily. To close the problem, the following two matching conditions have to be used with the others in Eqs. (5.128) and (5.131):

$$S\left(x_{ig}^{-}\right) = S\left(x_{ig}^{+}\right) \quad \text{and} \quad \theta\left(x_{ig}^{-}\right) = \theta\left(x_{ig}^{+}\right). \tag{5.137}$$

5.4 Results and discussion

The temperature profiles of the porous medium and gas for Case 1 and Case 2 are shown in Figure 5.2 and Figure 5.3, respectively. The thermophysical properties use in this study are listed in Table 3.1 except $d = 2.0\times10^{-3}$ m, $Y_{F,u} = 0.30$ and $Y_{O,u} = 0.23$. Figure 5.2 shows that for opposed mode, the gas temperature is higher than the porous medium temperature in the downstream region while in forward mode, the same scenario is seen in the preheat region. The reasons are that in opposed mode, porous medium temperature gradually goes down in the downstream region because of the heat loss from the porous medium and so the gas temperature decreases through the heat transfer mechanism between the gas and the porous medium; on the other hand, in forward mode the temperature of the gas becomes higher when it passes over the burned region, and it remains higher in the preheat region as long as the gas temperature is equal to the porous medium temperature. When the heat flux at the ignition point is imposed as zero (Case 2), in opposed mode the gas temperature slowly increases to the porous

medium temperature and at the ignition point, the temperatures of the porous medium and the gas equilibrate at a higher temperature than the ambient. The temperature profiles of forward mode are same as Case 1 except the initial temperatures that are the final temperatures of opposed mode of Case 2. Moreover, the reaction front temperature of forward mode of any of the cases is always higher than that of opposed.

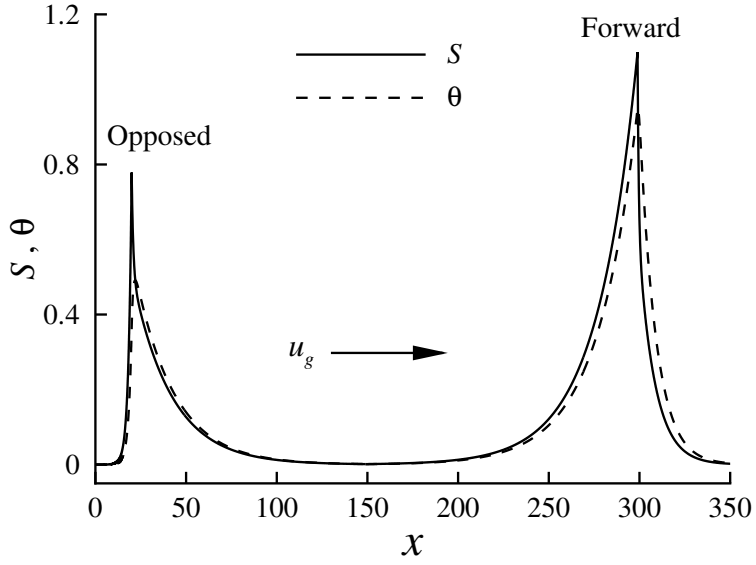

Figure 5.2: Temperature profiles of forward and opposed modes of Case 1 while h_{ex} = 10^4 W/(m^3K), N_R = 0.01, d = 2×10^{-3} m and u_g = 0.4 m/s.

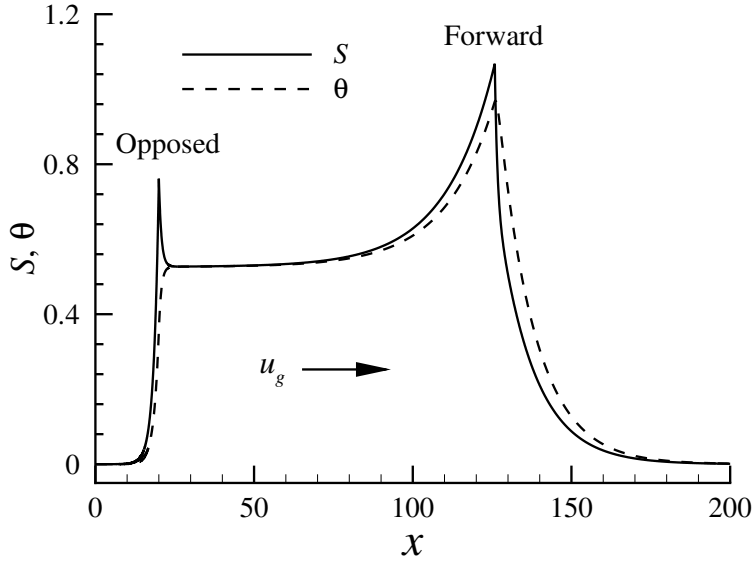

Figure 5.3: Temperature profiles of forward and opposed modes of Case 2 while h_{ex} = 10^4 W/(m^3K), N_R = 0.01, d = 2×10^{-3} m and u_g = 0.4 m/s.

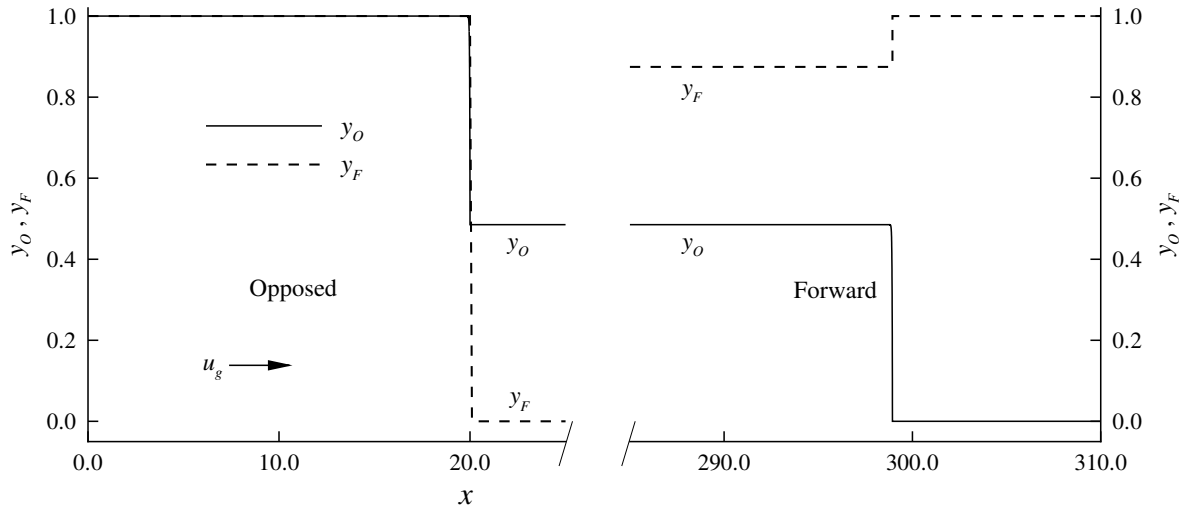

Figure 5.4: Species profiles of forward and opposed modes of Case 1 while $h_{ex} = 10^4$ W/(m^{3}K), $N_R = 0.01$, $d = 2\times10^{-3}$ m and $u_g = 0.4$ m/s.

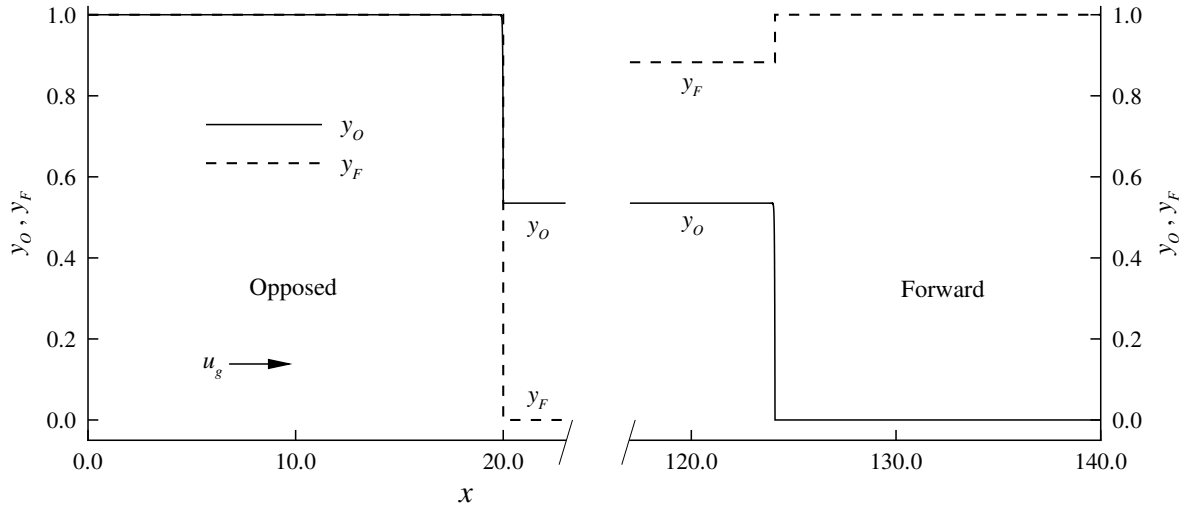

Figure 5.5: Temperature profiles of forward and opposed modes of Case 2 while $h_{ex} = 10^4$ W/(m^{3}K), $N_R = 0.01$, $d = 2\times10^{-3}$ m and $u_g = 0.4$ m/s.

The species profiles of fuel and oxidizer of Case 1 and Case 2 are shown in Figure 5.4 and Figure 5.5, respectively. As the reaction fronts generated somewhere around the middle propagate in the upstream and downstream regions, so there are fresh fuel at the opposite ends. Here it is assumed that oxidizer is flowing from left to right. Consequently, it is seen in the opposed mode that the level of

ambient oxidizer decreases at the reaction front and fuel is fully consumed; there remains excess oxidizer in opposed mode. Eventually, this excess oxidizer reaches into the reaction front of forward mode passing over the burned region of it and reacts with the fresh fuel. Contrary to the opposed mode, oxidizer is fully depleted at the reaction front and unburned fuel remains behind the reaction front.

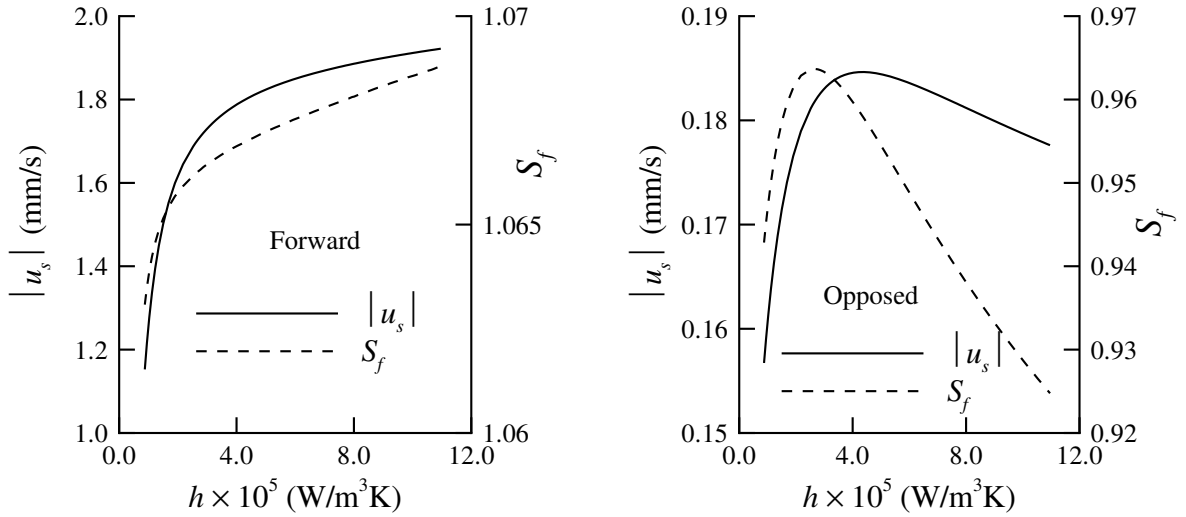

Figure 5.6: Moving speed of the reaction front of forward and opposed modes of Case 1as a function of the heat transfer coefficient, h, for $h_{ex} = 10^4$ W/(m^{3}K), $u_g = 0.40$ m/s and $N_R = 0.01$.

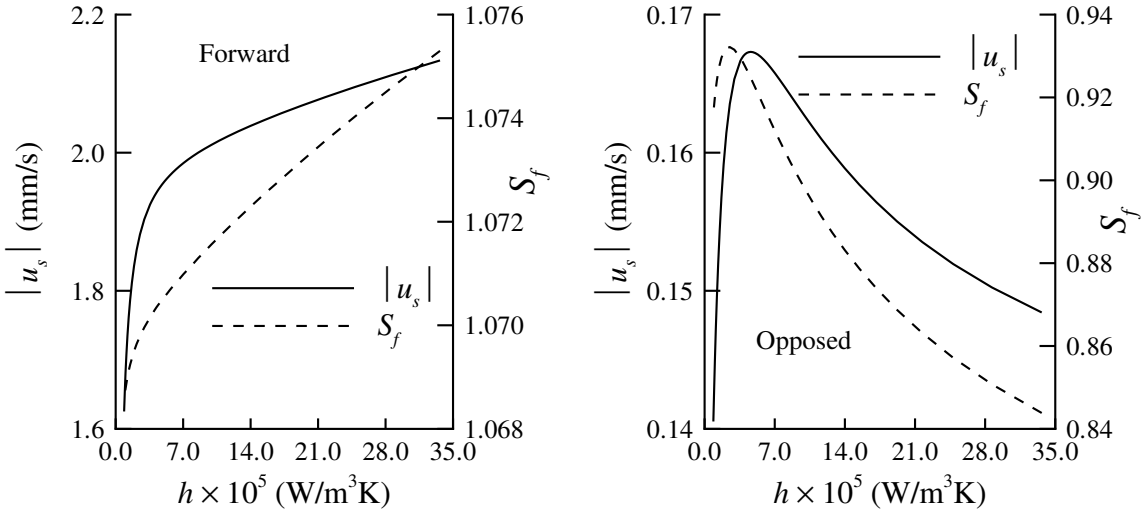

Figure 5.7: Moving speed of the reaction front of opposed mode of Case 1 and Case 2 as a function of the heat transfer coefficient, h, for $h_{ex} = 10^4$ W/(m^{3}K), $u_g = 0.40$ m/s and $N_R = 0.01$.

The effects of the heat transfer coefficient on the moving seeds of the reaction fronts of forward and opposed modes are presented in Figures 5.6 and 5.7, respectively, for the Case 1 and Case 2. At first, the focus of attention is on forward and opposed modes of the Case 1. When the heat transfer coefficient is increased from low to high value, at the very beginning the moving speed of the reaction front of forward mode increases swiftly and then it gradually increases (Figure 5.6) but in opposed mode, the moving speed of the reaction front drastically increases first and later on it slowly decreases (Figure 5.7). The same trend is seen for Case 2. It is well-known that the moving speed of the reaction front and the reaction front temperature always maintain the similar tendency. Accordingly, the same features are also observed here. In addition to, the turning points of the Case 1 that are found in changing the gradients of the moving speed of the reaction front are lower in heat transfer coefficient compared to that of the Case 2.

5.5 Conclusions

In this chapter, a model has been formulated to study the combustion of solid fuel over an inert porous medium ignited around the middle. Analytical expressions of the combustion behaviors of solid combustible are derived using large activation energy asymptotics. It is found that the moving speed of the reaction front of forward mode is monotonically increases owing to the increase of heat transfer coefficient but in opposed mode, it first increases and then decreases as the heat transfer increases. In addition, the reaction front of forward mode always shows higher temperature than the opposed mode.

Chapter 6

Concluding Remarks and Future Works

6.1 Concluding remarks

Stringent regulations to reduce the diesel particulate emissions are introducing day by day. For this reason, the major challenges of the present PM trap system and the efficient combustion of PM have gained much attention of international research community to develop a new technology for reducing the PM emissions from the exhaust gas of diesel engine. To give a new dimension to the ongoing researches on this engineering problem, a mathematical model has been developed for understanding the combustion of solid fuel over an inert porous medium. The step-by-step advancement in formulating a universal model and justifying its applicability, and the contributing findings are summarized below:

In Chapter 2, a simple mathematical model is proposed to study the combustion behavior of solid fuel over an inert porous medium that can be used for the development of particulate matter trap design and in the engineering of the regeneration process. Analytical expressions of the temperature profiles of porous medium and gas, species profile of gas and the moving speed of the reaction front are obtained using large activation energy asymptotics. Also the numerical simulation of the governing equations was carried out to determine the sensitivity of the asymptotic analysis for variation of each of the parameters and to give a clear concept about the deviation of the asymptotic analysis from the numerical solution. The following results are concluded that may provide in-depth knowledge about the focusing problem of this thesis:

(i) The moving speed of the reaction front first increases while the thermal conductivity of the porous medium is slightly increased from that of the gas; and then it decreases for further increase of the thermal conductivity.

(ii) The moving speed of the reaction front almost linearly decreases due to the increase of

deposition of solid fuel.

The simple model developed in Chapter 2 possesses some limitations. It could not be used for determining the fuel distribution and to examine the forward flow combustion of solid fuel over an inert porous medium as well as it is lack of some key transport mechanisms. As a result, an upgraded model for the combustion of solid fuel over an inert porous medium was formulated in Chapter 3 that could be applicable and adaptable for predicting the characteristics of DPF regeneration process, smoldering combustion and SHS process. The model equations are solved theoretically for opposed flow configuration and it provides analytical expressions of the combustion characters of solid combustible over the inert porous medium. Analytical solutions are then validated for smoldering combustion. Below, the major contributions of this chapter that reveal the important characteristics of the reaction front have been summarized:

(i) The moving speed of the reaction front increases with the increase of porosity of the porous medium and the initial mass fraction of fuel and the decrease of the heat transfer rate from the porous medium to the gas, the heat loss coefficient and the radiation-conduction parameter.

(ii) The amount of fuel leakage through the reaction front decreases with an increase of radiative heat transfer and the decrease of the gas flow velocity and mass transfer coefficient;

(iii) Extinction occurs due to lower porosity of the porous medium, higher volumetric heat transfer from the porous medium to the gas, higher radiative heat transfer from the porous medium and higher heat losses from the porous medium to the environment.

(iv) The extinction limit in terms of heat loss coefficient decreases due to the increase of the radiation-conduction parameter and the decrease of gas flow velocity while it becomes higher due to effective diffusivity compared to molecular diffusivity.

In Chapter 4, the upgraded model developed in Chapter 3 is used to analyze the forward flow combustion of solid fuel over an inert porous medium. The detailed derivation of the analytical expressions of temperature profiles of the porous medium and the gas, species profiles of the fuel and the gas, and the moving speed of the reaction front has been carried out in this chapter. It is observed that for any of the physical parameters, the moving speed of the reaction front of forward mode is always higher than that of opposed mode. Moreover, the effects of various parameters demonstrate

similar trends as opposed mode without some exception. As a result, in spite of examining the forward mode separately, there has been presented a comparative study between the forward and opposed modes. From this chapter, the following conclusions can be inferred:

(i) The reaction fronts of both modes demonstrate unsteady behaviors for higher thermal conductivity porous medium and lower initial mass fraction of oxidizer.

(ii) The response of the moving speed of the reaction front of forward mode to increasing heat transfer coefficient is completely opposite to that of opposed mode. In between of the critical heat transfer coefficients of forward and opposed modes, an "unsteady solution region" has been recognized in which the reaction fronts of both modes could be uncontrolled and unpredictable.

In Chapter 5, a practical application of forward and opposed modes has been imitated by presuming a process in which two reaction fronts generated from the ignition source somewhere around the middle of a sample propagate towards the ends of the sample. Although the problem has been solved, the results are not analyzed yet. So, the detailed study of the effects of various parameters has not been presented here. In this chapter, it was concluded that the moving speed of the reaction front of forward mode is monotonically increases with an increase of the heat transfer coefficient but in opposed mode, it first increases and then decreases as the heat transfer increases. Furthermore, the reaction front of forward mode always shows higher temperature than the opposed mode.

6.2 Future works

In this dissertation, an upgraded model has been developed for understanding the combustion characteristics of solid fuel over an inert porous medium. Finally, an attempt was made to formulate a model of a practical technological problem. However, after the formulation, the problem is somewhat solved but not investigated completely. So, a further study can be done on this problem.

It is worthwhile to note that although the present upgraded model of the combustion of solid fuel over an inert porous medium is very simple in regard to its input data and analytical solutions but the analytical solutions of the present model cannot be directly validated for the DPF regeneration process.

It is possible if the available data is changed as like as in this model.

Moreover, a single-step reaction mechanism is used here for the simplicity reasons. So, detailed reaction kinetics can be considered. In that case, the theoretical investigation may not be possible and the modified model must be solved numerically. Then it can be examined that how much accurately the present analytical solutions can predict the actual phenomena.

References

[1] H. –G. Neumann, Health risk of combustion products: toxicological considerations, Chemosphere, 42, pp. 473–479 (2001).

[2] A. G. Konstandopoulos, M. Kostoglou, Theory and practice of soot particle trap operation, Proceedings of the Global Powertrain Congress, 9, pp. 89–98 (1999).

[3] A. Liati, P. D. Eggenschwiler, Characterization of particulate matter deposited in diesel particulate filters: Visual and analytical approach in macro-, micro- and nano-scales, Combustion and Flame, 157, pp. 1658–1670 (2010).

[4] K. S. Martirosyan, K. Chen, D. Luss, Behavior features of soot combustion in diesel particulate filter, Chemical Engineering Science, 65, pp. 42–46 (2010).

[5] B. A. A. L. van Setten, M. Makkee, J. A. Moulijn, Science and technology of catalytic diesel particulate filters, Catalysis Reviews, 43(4), pp. 489–564 (2001).

[6] G. C. Koltsakis, A. M. Stamatelos, Modeling thermal regeneration of wall-flow diesel particulate traps, American Institute of Chemical Engineers Journal, 42, pp. 1662–1672 (1996).

[7] K. N. Pattas, C. C. Michalopoulou, Catalytic Activity in the regeneration of the ceramic diesel particulate trap, SAE paper 926362 (1992).

[8] U. Hoffman, J. Ma, Study on regeneration of diesel particulate filter using a laboratory reactor, Chemical Engineering Technology, 13, pp. 251–258 (1990).

[9] C. W. Wahle, B. J. Matkowsky, Rapid, upward buoyant filtration combustion waves driven by convection, Combustion and Flame, 124 (2001), pp. 14–34.

[10] C. W. Wahle, B. J. Matkowsky, A. P. Aldushin, Effects of gas-solid nonequilibrium infiltration combustion, Combustion Science and Technology, 175, pp. 1389–1499 (2003).

[11] G. Rein, Smouldering combustion phenomena in science and technology, International Review of Chemical Engineering, 1, pp. 3–18 (2009).

[12] T. J. Ohlemiller, J. Bellan, F. Rogers, A model of smoldering combustion applied to flexible polyurethane foams, Combustion and Flame, 36, pp. 197–215 (1979).

[13] S. S. Dosanjh, P. J. Pagni, A. C. Fernandez-Pello, Forced cocurrent smoldering combustion, Combustion and Flame, 68, pp. 131–142 (1987).

[14] D. A. Schult, B. J. Matkowsky, V. A. Volpert, Propagation and extinction of forced opposed flow smolder waves, Combustion and Flame, 101, pp. 471–490 (1995).

[15] M. A. Mujeebu, M. Z. Abdullah, A. A. Mohammad, M. Z. A. Bakar, Trends in modeling of porous media combustion, Progress in Energy Combustion Science, 36, pp. 627–650 (2010).

[16] S. V. Leach, J. L. Ellzey, O. A. Ezekoye, Convection, pyrolysis, and Damköhler number effects on extinction of reverse smoldering combustion, Proceedings of the Combustion Institute, 27, pp. 2873–2880 (1998).

[17] S. V. Leach, J. L. Ellzey, O. A. Ezekoye, A numerical study of reverse smoldering, Combustion Science and Technology, 130, pp. 247–267 (1997).

[18] S. V. Leach, G. Rein, J. L. Ellzey, O. A. Ezekoye, J. L. Torero, Kinetic and fuel property effects on forward smoldering combustion, Combustion and Flame, 120, pp. 346–358 (2000).

[19] G. Rein, A. Bar-Ilan, A. C. Fernandez-Pello, J. L. Ellzey, J. L. Torero, D. L. Urban, Modeling of one-dimensional smoldering of polyurethane in microgravity conditions, Proceedings of the Combustion Institute, 30, pp. 2327–2334 (2005).

[20] G. Rein, A. C. Fernandez-Pello, D. L. Urban, Computational model of forward and opposed smoldering combustion in microgravity, Proceedings of the Combustion Institute, 31, pp. 2677–2684 (2007).

[21] J. H. Wang, C. Y. H. Chao, W. Kong, Experimental study and asymptotic analysis of horizontally forced forward smoldering combustion, Combustion and Flame 135, pp. 405–419 (2003).

[22] T. J. Ohlemiller, Modeling of smoldering combustion propagation, Progress in Energy Combustion Science, 13, pp. 277–310 (1985).

[23] A. Makino, Fundamental aspects of the heterogeneous flame in the self-propagating high-temperature synthesis (SHS) process, Progress in Energy Combustion Science, 27, pp. 1–74 (2001).

[24] S. B. Margolis, An asymptotic theory of heterogeneous condensed combustion, Combustion Science and Technology, 43, pp. 197–215 (1985).

[25] H. G. Kaper, G.K. Leaf, S. B. Margolis, B. J. Matkowsky, On nonadiabatic condensed phase combustion, Combustion Science and Technology, 53, pp. 289–314 (1987).

[26] A. G. Merzhanov, The theory of stable homogeneous combustion of condensed substances, Combustion and Flame, 13, pp. 143–156 (1969).

[27] A. N. Firsov, K. G. Shkadinskii, Combustion of gasless compositions in the presence of heat losses, Combustion Explosion and Shock Waves, 23, pp. 288–294 (1987).

[28] A. G. Strunina, L. K. Demidova, A. N. Firsov, A. G. Merzhanov, Stability of gasless system combustion in the presence of heat losses, Combustion Explosion and Shock Waves, 23, pp. 294–299 (1987).

[29] Y. S. Naiborodenko, V. I. Itin, Gasless combustion of metal powder mixtures, Combustion Explosion and Shock Waves 11, pp. 293–300 (1975).

[30] Z. A. Munir, J. B. Holt, The combustion synthesis of refractory nitrides, part 1 theoretical analysis, Journal of Materials Science, 22, pp. 710–714 (1987).

[31] Z. A. Munir, U. Anselmi-Tumburini, Self-propagating exothermic reactions: the synthesis of high-temperature materials by combustion, Material Science Reports, 3, pp. 277–365 (1989).

[32] A. Makino, C. K. Law, Propagation and diffusion-limited extinction of nonadiabatic heterogeneous flame in the SHS process, Proceedings of the Combustion Institute, 25, pp. 1659–1667 (1994).

[33] A. Makino, C. K. Law, Pulsating instability in the nonadiabatic heterogeneous SHS flame: theory and experimental comparisons, Proceedings of the Combustion Institute, 26, pp. 1867–1874 (1996).

[34] J. B. Holt, Z. A. Munir, Combustion synthesis of titanium carbide: theory and experiment, Journal of Materials Science, 21, pp. 251–259 (1986).

[35] A. G. Strunina, T. M. Martem'yanova, V. V. Barzykin, V. I. Ermakov, Ignition of gasless systems by a combustion wave, Combustion Explosion and Shock Waves, 10, pp. 449–455 (1974).

[36] A. Makino, C. K. Law, Heterogeneous flame propagation in the self-propagating high-temperature synthesis (SHS) process: theory and experimental comparisons, Proceedings of the Combustion Institute, 24, pp. 1883–1891 (1992).

[37] A. S. Rogachev, F. Baras, Models of SHS: an overview, International Journal of Self-Propagating High-Temperature Synthesis, 16 (3), pp. 141–153 (2007).

[38] A. S. Rogachev, Microheterogeneous mechanism of gasless combustion, Combustion Explosion and Shock Waves, 39(2), pp. 150–158 (2003).

[39] V. K. Smolyakov, "Roughness" of the gasless combustion front, Combustion Explosion and Shock Waves, 37(3), pp. 274–284 (2001).

[40] E. J. Bissett, F. Shadman, Thermal regeneration of diesel-particulate monolithic filters, American Institute of Chemical Engineers Journal, 31(5), pp. 753–765 (1985).

[41] E. J. Bissett, Mathematical model of the thermal regeneration of a wall-flow monolith diesel particulate filter, Chemical Engineering Science, 39, pp. 1233–1244 (1984).

[42] E. J. Bissett, Thermal regeneration of particulate filters with large conduction, Mathematical Modeling, 6, pp. 1–18 (1985).

[43] O. A. Haralampous, G. C. Koltsakis, Back-diffusion modeling of NO_2 in catalyzed diesel particulate filters, Industrial & Engineering Chemistry Research, 43, pp. 875–883 (2004).

[44] K. Chen, K. S. Martirosyan, D. Luss, Hot zones formation during regeneration of diesel particulate filters, American Institute of Chemical Engineers Journal, 57, pp. 497–506 (2011).

[45] M. Schejbal, M. Marek, M. Kubíček, P. Kočí, Modelling of diesel filters for particulates removal, Chemical Engineering Journal, 154, pp. 219–230 (2009).

[46] C. K. Dardiotis, O. A. Haralampous, G. C. Koltsakis, Catalytic oxidation performance of wall-flow versus flow-through monoliths for diesel emissions control, Industrial & Engineering Chemistry Research, 45, pp. 3520–3530 (2006).

[47] P. Tourlonias, G. C. Koltsakis, Model-based comparative study of Euro 6 diesel aftertreatment concepts, focusing on fuel consumption, International Journal of Engine Research, 12, pp. 238–251 (2011).

[48] M. C. Law, M. Clarke, C. P. Garner, The effects of soot properties on the regeneration behaviour of wall-flow diesel particulate filters, Proceedings of the Institute of Mechanical Engineers, Part D: Journal of Automobile Engineering, 218, pp. 1513–1524 (2004).

[49] C. Depcik, A. Assanis, One-dimensional automotive catalyst modeling, Progress in Energy Combustion Science, 31, pp. 308–369 (2005).

[50] M. Flytzani-Stephanopoulos, G. E. Voecks, T. Charng, Modelling of heat transfer in non-adiabatic monolith reactors and experimental comparisons of metal monoliths with packed beds, Chemical Engineering Science, 41(5), pp. 1203–1212 (1986).

[51] O. A. Haralampous and G. C. Koltsakis, Oxygen diffusion modeling in diesel particulate filter regeneration, American Institute of Chemical Engineers Journal, 50(9), pp. 2008–2019 (2004).

[52] G. C. Koltsakis, A. M. Stamatelos, Catalytic automotive exhaust aftertreatment, Progress in Energy Combustion Science, 23, pp. 1–39 (1997).

[53] M. Kostoglou, P. Housiada, A. Konstandopoulos, Multi-channel simulation of regeneration in honeycomb monolithic diesel particulate filters, Chemical Engineering Science, 58, pp. 3273–3283 (2003).

[54] G. C. Koltsakis, A. M. Stamatelos, Modeling catalytic regeneration of diesel articulate traps, Industrial & Engineering Chemistry Research, 35, pp. 2–13 (1996).

[55] G. C. Koltsakis, A. M. Stamatelos, Modes of catalytic regeneration in diesel particulate filters, Industrial & Engineering Chemistry Research, 36, pp. 4155–4165 (1997).

[56] Se H. Oh, J. C. Cavendish, Transients of monolithic catalytic converters: response to step changes in feedstream temperature as related to automobile emissions, Industrial & Engineering Product Chemistry Research and Development, 21, pp. 29–37 (1982).

[57] Se H. Oh, E. J. Bissett, A. Battiston, Mathematical modeling of electrically heated monolith converters: model formulation numerical methods, and experimental validation, Industrial & Engineering Chemistry Research, 32, pp. 1560–1567 (1993).

[58] F. Shadman, E. J. Bissett, Analysis of thermal regeneration of fibrous diesel-particulate filters, Industrial & Engineering Process Design and Development, 22, pp. 203–208 (1983).

[59] A. G. Konstandopoulos, E. Skaperdas, J., Warren, R., Alansson, Optimized filter design and selection criteria for continuously regenerating diesel particulate traps, SAE Technical Paper, Paper No. 1999-01-0468 (1999).

[60] G. Pontikakis, A. Stamatelos, K. Bakasis, N. Aravas, 3-D Catalytic Regeneration and Stress Modeling of Diesel Particulate Filters by ABAQUS FEM Software, SAE Technical Paper, Paper No. 2002-01-1017 (2002).

[61] K. Hanamura, T. Suzuki, T. Tanaka, Y. Miyairi, Visualization of combustion phenomena of diesel particulates in regeneration of diesel particulate filter, SAE Technical Paper, Paper No. 2003-01-0836 (2003).

[62] M. Fatehi, M. Kaviany, Role of gas-phase reaction and gas-solid thermal nonequilibrium in reverse combustion, International Journal of Heat and Mass Transfer, 40, pp. 2607–2620 (1997).

[63] I. Y. Akkutlu, Y. C. Yortsos, The dynamics of in-situ combustion fronts in porous medium, Combustion and Flame, 134, pp. 229–247 (2003).

[64] G. Debenest, V. V. Mourzenko, J. –F. Thovert, Smouldering in fixed beds of oil shale grains. a three-dimensional microscale numerical model, Combustion Theory and Modeling, 9, pp. 113–135 (2005).

[65] G. Debenest, V. V. Mourzenko, J. –F. Thovert, Smouldering in fixed beds of oil shale grains: governing parameters and global regimes, Combustion Theory and Modeling, 9, pp. 301–321 (2005).

[66] G. Debenest, V. V. Mourzenko, J. –F. Thovert, J. –F., Three-dimensional microscale numerical simulation of smoldering process in heterogeneous porous medium, Combustion Science and Technology, 180, pp. 2170–2185 (2008).

[67] R. Venkataramana, S. S. Gupta, P. C. Kapur, N. Ramachandran, Mathematical modelling and simulation of the iron ore sintering process, Tata Search , pp. 50–55 (1998).

[68] W. Yang, C. Ryu, S. Chol, E. Chol, D. W. Ri, W. Huh, Mathematical model of thermal processes in an iron ore sintering bed, Metals Materials International, 10, pp. 493–500 (2004).

[69] W. Yang, C. Ryu, S. Chol, E. Chol, D. W. Ri, W. Huh, Modeling of combustion and heat transfer in an iron ore sintering bed with considerations of multiple solid phases, The Iron and Steel

Institute of Japan International, 44, pp. 492–499 (2004).

[70] W. Yang, C. Ryu, S. Choi, E. Choi, D. W. Ri, S. Kim, Combustion characteristics in an iron ore sintering bed—evaluation of fuel substitution, Combustion and Flame, 145, pp. 447–463 (2006).

[71] H. Kang, S. Choi, W. Yang, B. Cho, Influence of oxygen supply in an iron ore sintering process, The Iron and Steel Institute of Japan International, 51, pp. 1065–1071 (2011).

[72] E. Kasai, S. Komarov, K. Nushiro, M. Nakano, Design of bed structure aiming the control of void structure formed in the sinter cake, The Iron and Steel Institute of Japan International, 45, pp. 538–543 (2005).

[73] N. Hayashi, S. Komarov, E. Kasai, Heat transfer analysis of the mosaic embedding iron ore sintering (MEBIOS) process, The Iron and Steel Institute of Japan International, 49, pp. 681–686 (2009).

[74] D. A. Schult, B. J. Matkowsky, V. A. Volpert, Forced forward smolder combustion, Combustion and Flame, 104, pp. 1–26 (1996).

[75] D. A. Schult, A. Bayliss, B. J. Matkowsky, Traveling waves in natural counterflow filtration combustion and their stability, SIAM Journal of Applied Mathematics, 58, pp. 806–852 (1998).

[76] O. S. Rabinovich, I. G. Gurevich, Effect of heat losses on propagation of stationary low-temperature filtration combustion waves with forced filtration of the gas-oxidizer, Combustion Explosion and Shock Waves, 20, pp. 29–35 (1984).

[77] A. P. Aldushin, B. J. Matkowsky, Rapid filtration combustion waves driven by convection, Combustion Science and Technology, 140, pp. 259–293 (1998).

[78] H. Zheng, J. M. Keith, Ignition analysis of wall-flow monolith diesel particulate filters, Catalysis Today, 98, pp. 403–412 (2004).

[79] L. Boshoff-Mostert H. J. Viljoen, Analysis of homogeneous combustion in monolithic structures, Chemical Engineering Science, 51, pp. 1107–1111 (1996).

[80] C. N. Opris, J. H. Johnson, A 2-D computational model describing the flow and filtration characteristics of a ceramic diesel particulate trap, SAE Paper No. 980545 (1998).

[81] C. N. Opris, J. H. Johnson, A 2-D computational model describing the heat transfer, reaction kinetics and regeneration characteristics of a ceramic diesel particulate trap, SAE Paper No.

980546 (1998).

[82] A. G. Konstandopoulos, M. Kostoglou, Reciprocating flow regeneration of soot filters, Combustion and Flame, 121, pp. 488–500 (2000).

[83] O. Haralampous, G. C. Koltsakis, Intra-layer temperature gradients during regeneration of diesel particulate filters, Chemical Engineering Science, 57, pp. 2345–2355 (2002).

[84] G. Pontikakis, A. Stamatelos, Three-dimensional catalytic regeneration modeling of SiC diesel particulate filters, Journal of Engineering for Gas Turbines and Power, 128, pp. 421–433 (2006).

[85] S. Bensaid, D. L. Marchisio, D. Fino, Numerical simulation of soot filtration and combustion within diesel particulate filters, Chemical Engineering Science, 65, pp. 357–363 (2010).

[86] D. A. Nield, A. Bejan, Convection in Porous Media, Second ed., Springer-Verlag, New York, 1992.

[87] N. Wakao, S. Kaguei, Heat and Mass Transfer in Packed Beds, Gordon and Breach Science Publications, New York, 1982.

[88] A. M. Telengator, F. A. Williams, S. B. Margolis, Finite-rate interphase heat-transfer effects on multiphase burning in confined porous propellants, Combustion Science and Technology, 178, pp. 1685–1720 (2006).

[89] B. Deshaies, G. Joulin, Asymptotic study of an excess-enthalpy flame, Combustion Science and Technology, 22, pp. 281–285 (1980).

[90] W. B. Bush, F. E. Fendell, Asymptotic analysis of laminar flame propagation for general Lewis number, Combustion Science and Technology, 1, pp. 421–428 (1970).

[91] J. Buckmaster, The quenching of deflagration waves, Combustion and Flame, 26, pp. 151–162 (1976).

[92] A. Liñán, The asymptotic structure of counter flow diffusion flames for large activation energies, Acta Astronautica, 1, pp. 1007–1039 (1974).

[93] D. Lozinski, J. Buckmaster, Quenching of reverse smolder, Combustion and Flame, 102, pp. 87–100 (1995).

[94] F. M. Pereira, A. A. M. Oliveira, F. F. Fachini, Asymptotic analysis of stationary adiabatic premixed flames in porous inert medium, Combustion and Flame, 156, pp. 152–165 (2009).

[95] V. N. Kurdyumov, E. Fernández, A. Liñán, Flame flashback and propagation of premixed flames near a wall, Proceedings of the Combustion Institute, 28, pp. 1883–1889 (2000).

[96] J. F. Qiu, J. T. Li, K. L. Smirnov, Combustion synthesis of high porosity sic foam with nanosized grains, Ceramics International, 36, pp. 1901–1904 (2010).

[97] J. Adler, Ceramic diesel particulate filters, International Journal of Applied Ceramic Technology, 2, pp. 429–439 (2005).

[98] A. Bar-Ilan, G. Rein, D. C. Walther, A. C. Fernandez-Pello, J. L. Torero, D. L. Urban, The effect of buoyancy on opposed smoldering, Combustion Science and Technology, 176, pp. 2027–2055 (2004).

[99] T. J. Ohlemiller, Smoldering combustion, SFPE Handbook of Fire Protection Engineering, 3rd ed., Massachusetts, pp. 2.200–2.210 (2002).

[100] N. C. Roy, Y. Nakamura, Modeling and asymptotic analysis of combustion of solid fuel deposited over an inert porous medium, Journal of Thermal Science and Technology, 7(4), pp. 723–739 (2012).

[101] P. H. Bouma, L. P. H. D. Goey, Premixed combustion on ceramic foam burners, Combustion and Flame, 119, pp. 133–143 (1999).

[102] R. Siegel, J. R. Howell, Thermal Radiation Heat Transfer, McGraw-Hill, New York, 1972.

[103] G. R. Youngquist, Diffusion and flow of gases, Industrial & Engineering Chemistry, 62(8), pp. 52–63 (1970).

[104] A. Wheeler, Reacion Rates and Selectivity of Catalyst Pores, Advances in Catalysis, Vol. III, Academic Press, New York, 1951, p. 249.

[105] N. M. Laurendeau, Heterogeneous kinetics of coal char gasification and combustion, Progress in Energy Combustion Science, 4, pp. 221–270 (1978).

[106] J.-R. Shi, M.-Z. Xie, H. Liu, G. Li, L. Zhou, Numerical simulation and theoretical analysis of premixed low-velocity filtration combustion, International Journal of Heat and Mass Transfer, 51, pp. 1818–1829 (2008).

[107] S. Zhdanok, L. A. Kennedy, G. Koester, Superadiabatic combustion of methane air mixtures under filtration in a packed bed, Combustion and Flame, 100, pp. 221–231 (1995).

[108] S. I. Foutko, S. I. Shabunya, S. A. Zhdanok, L. A. Kennedy, Proceedings of the Combustion Institute 26 (1998) 3377–3382.

[109] T. J. Ohlemiller, D. A. Lucca, An experimental comparison of forward and reverse smolder propagation in permeable fuel beds, Combustion and Flame, 54, pp. 131-147 (1983).

[110] K. Schnitzlein, A. Löwe, Numerical simulation of the performance of ceramic fiber coil diesel particulate traps, Chemical Engineering Science, 45, pp. 2671–2678 (1990).

[111] U. Hoffmann, T. Rieckmann, J. Ma, Kinetic study and modelling of diesel particulate filter regeneration, Chemical Engineering Science, 46, pp. 1101–1113 (1991).

[112] J. L. Torero, A. C. Fernandez-Pello, M. Kitano, Opposed forced flow smoldering of polyurethane foam, Combustion Science and Technology, 91, pp. 95–117 (1993).

[113] M. Fatehi, M. Kaviany, Adiabatic reverse combustion in a packed bed, Combustion and Flame, 99, pp. 1–17 (1994).

[114] J. Lu, Y. Dong, Fingering instability in forward smolder combustion, Combustion Theory and Modeling, 15(6), pp. 795–815 (2011).

[115] A. Bar-Ilan, G. Rein, A. C. Fernandez-Pello, J. L. Torero, D. L. Urban, Forced forward smoldering experiments in microgravity, Experimental Thermal and Fluid Science, 28, pp. 743–751 (2004).

[116] T. J. Ohlemiller, Smoldering combustion, SFPE Handbook of Fire Protection Engineering, 2nd ed., 1995, 2.171–2.179.

[117] S. S. Dosanjh, P. J. Pagni, Forced countercurrent smoldering combustion, Proceedings of the 1987 ASME/JSME Thermal Engineering Joint Conference, pp. 165–173 (1987).

[118] K. N. Palmer, Smoldering combustion in dusts and fibrous materials, Combustion and Flame, 1, pp. 129–153 (1957).

[119] T. J. Ohlemiller, Forced smolder propagation and the transition to flaming in cellulosic insulation, Combustion and Flame, 81, pp. 354–365 (1990).

[120] K. Chen, K. S. Martirosyan, D. Luss, Temperature excursions during soot combustion in a diesel particulate filter (DPF), Industrial & Engineering Chemistry Research, 49, pp. 10358–10363 (2010).

[121] K. Chen, K. S. Martirosyan, D. Luss, Counter-intuitive temperature excursions during regeneration of a diesel particulate filter, American Institute of Chemical Engineers Journal, 57, pp. 2229–2236 (2011).

[122] N. C. Roy, A. Hossain, Y. Nakamura, A universal model of opposed flow combustion of solid fuel over an inert porous medium, Combustion and Flame, http://dx.doi.org/10.1016/j. combustflame.2013.11.025.

[123] J. L. Torero, A. C. Fernandez-Pello, Forward smolder of polyurethane foam in a forced air flow, Combustion and Flame, 106, pp. 89–109 (1996).

[124] D. C. Walther, A. C. Fernandez-Pello, J. L. Torero, D. L. Urban, Space shuttle based microgravity smoldering combustion experiments, Combust. Flame, 116, pp. 398–414 (1999).

[125] K. Chen, K. S. Martirosyan, D. Luss, Transient temperature rise during regeneration of diesel particulate filters, Chemical Engineering Journal, 176-177, pp. 144–150 (2011).

[126] K. Chen, K. S. Martirosyan, D. Luss, Soot combustion dynamics in a planar diesel particulate filter, Industrial & Engineering Chemistry Research, 48, pp. 3323–3330 (2009).

Appendix

In this appendix, the derivation of some important expressions of the thesis is described in detail. To have the implicit relation given in Eq. (2.50), a lot of analysis has to be done. At first, define the following transformations:

$$-\left\{1-\alpha\left(1-s_f^*\right)\right\}^2 f = S_1^{in} - \left(\frac{dS}{dX}\right)_{X=0^+} \eta, \tag{A.1}$$

$$\xi = \frac{\varepsilon\gamma(1-\phi)(1+u)}{n(1-\varepsilon)ru\left\{1-\alpha\left(1-s_f^*\right)\right\}^2}\eta - \frac{\ln(2p)}{\chi}, \tag{A.2}$$

$$\chi = -\frac{n(1-\varepsilon)ru}{\varepsilon\gamma(1-\phi)(1+u)}\left(\frac{dS}{dX}\right)_{X=0^+}, \tag{A.3}$$

$$q = \left[\frac{n(1-\varepsilon)ru\left\{1-\alpha\left(1-s_f^*\right)\right\}^2}{\varepsilon\gamma(1-\phi)(1+u)}\right]^2 \frac{nLel\phi A\lambda_m e^{-\beta/\alpha}}{(1-\phi)b\rho_m^2 u_s^2 c_m \beta^2} \exp\left[-\frac{\beta\left(1-s_f^*\right)}{1-\alpha\left(1-s_f^*\right)}\right]. \tag{A.4}$$

Substituting Eqs. (A.1)–(A.4) into Eq. (2.49) give

$$-\left\{1-\alpha\left(1-s_f^*\right)\right\}^2 \frac{d^2 f}{d\xi^2} \times \left[\frac{\varepsilon\gamma(1-\phi)(1+u)}{n(1-\varepsilon)ru\left\{1-\alpha\left(1-s_f^*\right)\right\}^2}\right]^2 = \frac{nLel\phi\Lambda_0}{(1-\phi)b}\exp\left[-\frac{\beta\left(1-s_f^*\right)}{1-\alpha\left(1-s_f^*\right)}\right]$$

$$\times -\left\{1-\alpha\left(1-s_f^*\right)\right\}^2 f \times \exp\left[-f + \frac{\left(\frac{dS}{dX}\right)_{X=0^+}}{\left\{1-\alpha\left(1-s_f^*\right)\right\}^2} \times \frac{n(1-\varepsilon)ru\left\{1-\alpha\left(1-s_f^*\right)\right\}^2}{\varepsilon\gamma(1-\phi)(1+u)}\left\{\xi + \frac{\ln(2q)}{\chi}\right\}\right]$$

$$\Rightarrow \left[\frac{\varepsilon\gamma(1-\phi)(1+u)}{n(1-\varepsilon)ru\left\{1-\alpha\left(1-s_f^*\right)\right\}^2}\right]^2 \frac{d^2 f}{d\xi^2} = \frac{nLel\phi\Lambda_0}{(1-\phi)b}\exp\left[-\frac{\beta\left(1-s_f^*\right)}{1-\alpha\left(1-s_f^*\right)}\right]$$

$$\times f \exp\left[-f + \frac{n(1-\varepsilon)ru}{\varepsilon\gamma(1-\phi)(1+u)}\left(\frac{dS}{dX}\right)_{X=0^+}\left\{\xi + \frac{\ln(2q)}{\chi}\right\}\right]$$

$$\Rightarrow \frac{d^2 f}{d\xi^2} = \left[\frac{n(1-\varepsilon) ru \left\{ 1-\alpha\left(1-s_f^*\right) \right\}^2}{\varepsilon\gamma(1-\phi)(1+u)} \right]^2 \frac{nLel\phi\Lambda_0}{(1-\phi)b} \exp\left[-\frac{\beta\left(1-s_f^*\right)}{1-\alpha\left(1-s_f^*\right)} \right]$$

$$\times f \exp\left[-f - \chi\left\{ \xi + \frac{\ln(2q)}{\chi} \right\} \right]$$

$$\Rightarrow \frac{d^2 f}{d\xi^2} = p \times f \exp\left[-f - \chi\xi - \ln(2q) \right]$$

$$\Rightarrow \frac{d^2 f}{d\xi^2} = q \times \frac{1}{2q} \times f \exp\left[-f - \chi\xi \right]$$

That is, $2\frac{d^2 f}{d\xi^2} = f \exp\left[-f - \chi\xi \right].$ (A.5)

Now, differentiating both sides of Eq. (A.1) with respect to η, it is found that

$$-\left\{ 1-\alpha\left(1-s_f^*\right) \right\}^2 \frac{df}{d\xi} \times \frac{\varepsilon\gamma(1-\phi)(1+u)}{n(1-\varepsilon) ru \left\{ 1-\alpha\left(1-s_f^*\right) \right\}^2} = \frac{dS_1^{in}}{d\eta} - \left(\frac{dS}{dX} \right)_{X=0^+}. \quad \text{(A.6)}$$

As $\xi \to -\infty$, Eq. (A.6) along with matching condition implies

$$\frac{df}{d\xi} = -\frac{n(1-\varepsilon) ru}{\varepsilon\gamma(1-\phi)(1+u)} \left\{ \left(\frac{dS}{dX} \right)_{X=0^-} - \left(\frac{dS}{dX} \right)_{X=0^+} \right\}.$$

Therefore, using Eq. (2.47) the above relation results in

$$\lim_{\xi \to -\infty} \frac{df}{d\xi} = -1. \quad \text{(A.7)}$$

Similarly when $\xi \to +\infty$, Eq. (A.6) gives

$$\lim_{\xi \to +\infty} \frac{df}{d\xi} = 0. \quad \text{(A.8)}$$

Again, as $\xi \to -\infty$, the value of $f + \xi$ is determined as

$$\lim_{\xi \to -\infty} \left(f + \xi \right)$$

$$= \lim_{\xi\to-\infty}\left[-\frac{1}{\left\{1-\alpha\left(1-s_f^*\right)\right\}^2}\left\{S_1^{in}-\left(\frac{dS}{dX}\right)_{X=0^+}\eta\right\}+\frac{\varepsilon\gamma(1-\phi)(1+u)}{n(1-\varepsilon)ru\left\{1-\alpha\left(1-s_f^*\right)\right\}^2}\eta-\frac{\ln(2q)}{\chi}\right]$$

$$= \frac{1}{\left\{1-\alpha\left(1-s_f^*\right)\right\}^2}\times\lim_{\xi\to-\infty}\left[-\left\{S_1^{in}-\left(\frac{dS}{dX}\right)_{X=0^+}\eta\right\}+\frac{\varepsilon\gamma(1-\phi)(1+u)}{n(1-\varepsilon)ru}\eta\right]-\frac{\ln(2q)}{\chi}$$

$$= \frac{1}{\left\{1-\alpha\left(1-s_f^*\right)\right\}^2}\times\lim_{\xi\to-\infty}\left[-\left\{S_1^{in}-\left(\frac{dS}{dX}\right)_{X=0^+}\eta\right\}+\left\{\left(\frac{dS}{dX}\right)_{X=0^-}-\left(\frac{dS}{dX}\right)_{X=0^+}\right\}\eta\right]-\frac{\ln(2q)}{\chi}$$

$$= \frac{-1}{\left\{1-\alpha\left(1-s_f^*\right)\right\}^2}\times\lim_{\xi\to-\infty}\left[S_1^{in}-\left(\frac{dS}{dX}\right)_{X=0^-}\eta\right]-\frac{\ln(2q)}{\chi}$$

$$= \frac{-1}{\left\{1-\alpha\left(1-s_f^*\right)\right\}^2}\times 0-\frac{\ln(2q)}{\chi}$$

Therefore, $\lim_{\xi\to-\infty}\left(f+\xi\right)=-\frac{\ln(2q)}{\chi}$.

If it is assumed that $\lim_{\xi\to-\infty}\left(f+\xi\right)=p$ then the above relation can be rewritten as

$$2q=\exp[-p\chi]. \tag{A.9}$$

Using the value of q into the Eq. (A.9) and after some simplifications, one can easily find

$$\left[\frac{n(1-\varepsilon)ru\left\{1-\alpha\left(1-s_f^*\right)\right\}^2}{\varepsilon\gamma(1-\phi)(1+u)}\right]^2\frac{nLel\phi A\lambda_m e^{-\beta/\alpha}}{(1-\phi)b\rho_m^2u_s^2c_m\beta^2}=\exp\left[\frac{\beta\left(1-s_f^*\right)}{1-\alpha\left(1-s_f^*\right)}-p\chi\right]. \tag{A.10}$$

This is the solution of Eq. (A.5) subject to the boundary conditions (A.7) and (A.8). The moving speed of the reaction front is determined from this relation as given in Eq. (2.50). In addition to, Eq. (3.78) is obtained doing the similar analysis as presented above.

Now the value of χ can be found from Eq. (A.3) as

$$\chi = -\frac{n(1-\varepsilon)ru}{\varepsilon\gamma(1-\phi)(1+u)}\left(\frac{dS}{dX}\right)_{X=0^+}$$

$$= -\frac{\left(\frac{dS}{dX}\right)_{X=0^+}}{\left(\frac{dS}{dX}\right)_{X=0^-} - \left(\frac{dS}{dX}\right)_{X=0^+}}$$

That is, $\chi = \dfrac{S'(0^+)}{S'(0^+) - S'(0^-)}.$ (A.11)

When the expressions of the temperature of the porous medium given in Eqs. (2.31) and (2.33) and the values of $a_1,\ a_2,\ a_3$ determined by the matching conditions are used in Eq. (A.11), it is seen that

$$\chi = \frac{p_1(m_2 - m_3)}{p_1(m_2 - m_3) + p_2(m_3 - m_1) + p_3(m_1 - m_2)}.$$ (A.12)

Equation (2.52) of the Chapter 2 is derived as like as Eq. (A.12). It should be mentioned here that since the values of $a_1,\ a_2,\ a_3,\ a_4$ cannot be explicitly determined from the matching conditions, hence the expression given in Eq. (A.11) is the value of χ which is same as of Eq. (3.80) of the Chapter 3.

List of Research Accomplishments

1. Journal Papers

(1) N. C. Roy and Y. Nakamura, Modeling and asymptotic analysis of combustion of solid fuel deposited over an inert porous medium, J. Therm. Sci. Technol. 7(4), pp. 723–739 (2012).

(2) Nepal C. Roy, Akter Hossain, Yuji Nakamura, A universal model of opposed flow combustion of solid fuel over an inert porous medium, Combust. Flame, http://dx.doi.org/10.1016/j.combustflame.2013.11.025.

2. Conference Papers

(1) Nepal C. Roy and Yuji Nakamura, Asymptotic Analysis of Combustion of Soot Deposited Over an Inert Porous Media, Paper No. 11F-48, 2011 Fall Technical Meeting of the Western States Section of the Combustion Institute, 16-18 Oct., 2011, University of California, Riverside.

(2) N. C. Roy and Y. Nakamura, Mathematical Modeling for the Regeneration of Diesel Particulate Filter (DPF), International Conference on EcoTopia Science'11, Dec. 9-11, 2011, Nagoya University, Nagoya, Japan.